Photochemistry, Photophysics and Spectroscopy of Redox States of Flavins relevant to Photoactive Flavoproteins

RuiKun Zhao

School of Chemistry

University of East Anglia

Norwich, UK

2012

A thesis submitted in partial fulfillment of the requirements for the degree of Doctor of Philosophy of University of East Anglia.

Declaration

I declare that the work contained in this thesis for the degree of Doctor of Philosophy is my work, except where due reference is made to other authors, and has not been previously submitted for a degree at this or any other university.

RuiKun Zhao

Acknowledgment

To speak of science first, I would like to thank my supervisor: Professor Steve R Meech, who has given me more assistance than I thought was possible, who has taught me more than I realized was knowable, and who has shown more kindness than I believed possible.

I also thank Dr. Andras Lukas who taught me the background of physical chemistry and spectroscopy from the basis and supported my studies through my PhD project. I appreciate Dr. David Russell helping my PhD study as a second supervisor and giving me advices.

I also would like to express my thanks to all members of Meech's group: Andras, Ismale, Jamie, Kamila, Mike, Michael, Minako and Kiri for their hospitality and encouragement for the whole time of my studies and to the group of Prof. Peter J. Tonge in Stony Brook University: Allison and Richard for their cooperation. I thank EPSRC for my research fund, NSF for my scholarship.

To conclude with family, I would like to thank my entire family and especially my wife: Dr Ling Xiao, who has worked tirelessly to give me whatever helps she could, and who have provided more encouragement and love than I can ever describe.

Abstract

There has been a tremendous interest in the study of flavins and their derivatives in order to gain information valuable for designing model compounds that can mimic the functions of flavoenzymes. This thesis aims a) to explore and enhance the knowledge about the behavior of the flavin cofactors in its different redox states b) to further study and develop the mechanism of BLUF domain protein.

To achieve a better understanding of flavin behavior, we conducted a comparative study of excited state dynamics of different redox states of flavin cofactors in both aqueous solutions and protein. In this thesis, we present the systematic study of excited-state dynamics of the common flavin molecule: FAD and its fully reduced hydroquinones: $FADH_2$ and $FADH^-$ together with its radical semiquinones: $FADH^{\bullet}$ and $FAD^{\bullet -}$ with the visible to mid-IR transient absorption spectroscopy. Ground and excited state frequencies of the characteristic carbonyl modes are observed and assigned with the aid of DFT calculations.

Moreover, the stable neutral radical flavin has been prepared for study in aqueous solution, and both neutral and anionic radical states have been stabilized in the protein: flavodoxin and glucose oxidase. Ultrafast transient absorption measurements were performed in the visible and mid infrared region in order to characterize the excited and ground state's dynamics and vibrational spectra, and to probe the effect of the protein matrix on them.

We also report our comprehensive studies of radiationless decay in reduced and radical flavins using ultrafast spectroscopy and temperature dependent fluorescence. Those model results are essential inputs to help us analyzing the flavin photo-kinetics in proteins and thus advance the knowledge of BLUF domain protein.

Contents

Chapter 1 Background and Introduction

It was about 110 years ago that an English chemist named A.Wynter Blyth reported his work on chemical composition of cow milk to the '*Transactions of the Chemical Society'*. One of his remarkable finds was a bright yellow pigment which he called lactochrome (now the compound is known as riboflavin) [1, 2]. Very soon after that, Richard Kuhn in Heidelberg and Paul Karrer in Zurich had managed to detect the structure of this yellow pigment and prove it by chemical synthesis [3]. However, half a century later, this yellow pigment which gave a bright greenish fluorescence had been isolated from a variety sources. Much interest in this compound arose when they were discovered to be a constituent of the vitamin B complex which started the new subject of Flavin chemistry.

Since the 1950s', flavin chemistry has continually attracted much scientific attention because of the discovery of a large number of flavin-containing enzymes, which play significant roles in many crucial biological processes. Flavin adenine dinucleotide (FAD) as the key flavin redox cofactor is involved in mediating either one or two electron transfer processes[4]. More recently they were found to be the key component in photoactive flavoprotein also including the BLUF (Blue light sensing Using Flavin) domain protein we consider below [5].

It is established that sensing blue light is of significance for a diverse range of organisms. For instance, plants, algae, and photosynthetic bacteria all rely on blue light to control development and achieve optimization of photosynthesis, while organisms such as mice and drosophila mediate circadian rhythms also through blue light [6]. It was established in the 1990's that flavoproteins are involved in this blue light sensing mechanism. This thesis describes our study of the underlying photophysics of some flavin molecules, with the objective of supporting an ongoing investigation of the BLUF domain proteins [7].

1.1 Photoactive flavoprotein

1.1.1 Photoreceptor protein and flavoprotein

Photoreceptor proteins are defined as light-sensitive proteins involved in sensing and responding to light in a variety of organisms. They function in nature to mediate light-induced signal transduction. Photoreceptor protein families have been developed to absorb light in different regions of the solar spectrum, ranging from UV to far-red [8]. Some typical examples are rhodopsins, phytochromes and xanthopsins. These are characterised by the ability to undergo large structure changes upon excitation providing the driving force for conformation change in proteins [9].

Flavoproteins are a large group of proteins which have a flavin cofactor bound. There are more than 150 types of flavoproteins, but most of them are light independent, and only a few of them are photoactive which can be grouped among the 'Photoreceptor proteins'. So the overlapped zone between these two groups is the 'photoactive flavoprotein' which is further divided into three groups: Light-Oxygen-Voltage domain proteins (LOV domain such as phototropins), photolyase-like cryptochrome and Blue Light sensing Using Flavin (BLUF) domain proteins which are the key subject of this project (Fig. 1.1) [10, 11]

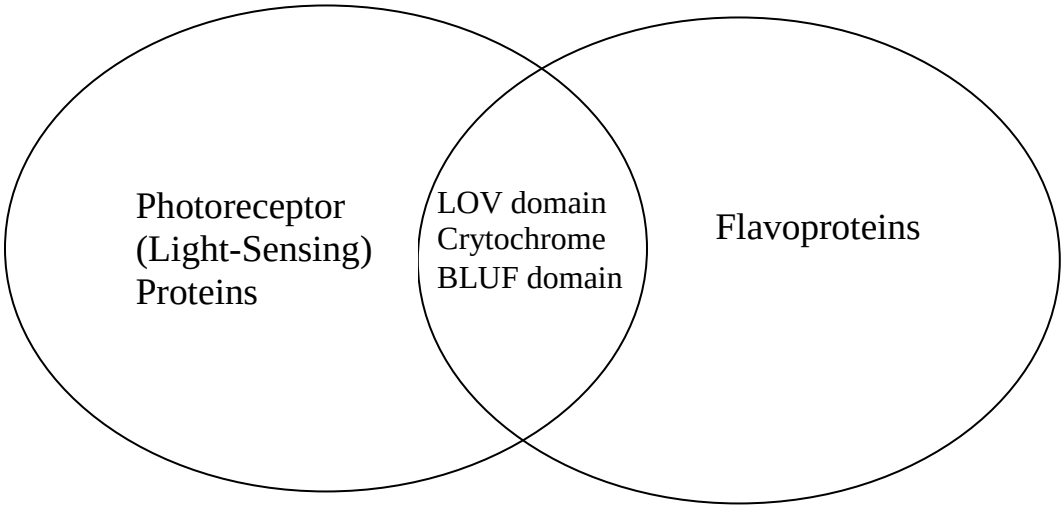

Fig. 1.1. Illustration of Photoreceptor Proteins and Flavoproteins

LOV domain proteins exist in many signal transduction proteins such as the phototropins from plants mediating different light responses. Photolyase-like cryptochrome is a flavoenzyme which repairs the UV-damaged lesions in DNA. Further background on these proteins will be included in the following paragraphs. More recently, the BLUF domain has been established as a third category of flavin-binding, blue light photoreceptors. However, its mechanism is still not fully understood. For this reason our research group has focused on the investigation of BLUF domain proteins and we aimed to have a through understanding of mechanism involved.

1.1.2 LOV domain: light-oxygen-voltage domain protein such as phototropin

The LOV domain is an essential regulatory motif which applies to the light sensing response in plants like phototropism, chloroplast movement, stomata opening and rapid inhibition of hypocotyl growth [12]. LOV domains use the flavin derivative as its light-sensitive chromophore. Moreover, LOV domain also plays a part in mediating protein-protein interactions [13, 14] . The formation of the signalling state in LOV domain is based on light-induced structural change of a metastable covalent adduct between a carbon atom of flavin and the sulphur atom of a conserved cysteine.

1.1.3 Photolyase-like cryptochrome

Photolyase is a flavoenzyme which photochemically repairs DNA damaged by UV light. For this, photolyase performs two processes: photo-repair and photo-reduction. During photo-repair, after excitation with visible light an electron is transferred from the excited flavin to the pyrimidine-pyrimidine bond of the damaged part of DNA resulting in cleavage of the bond, repairing the DNA damage. Subsequently under light excitation again, an electron transfers back to flavin (photoreduction process) to form the enzymatically active, fully reduced, state which is ready for the next repair (i.e. in this process flavin works as catalyst) [13, 14].

1.1.4 BLUF domain-- Blue Light sensing Using Flavin

BLUF domain proteins are a group of flavin-containing blue light photosensory proteins which are found in a variety of bacterial and algal proteins. These proteins are the main focus of our research activity. A photocycle of BLUF domain proteins under light excitation has been proposed, involving different redox state changes of flavin as shown in Fig. 1.2 [15, 16]. There are three different redox states of flavin in this cycle: oxidised FAD, neutral radical semiquinone $FADH^{\bullet}$ and anionic radical semiquinone $FAD^{\bullet -}$. The light absorption by flavin results in a 10 nm red-shift in the absorption spectra (Fig.1.3) [17]. From this some questions arise such as: what gives rise to this shift, and how this apparently small change in spectrum causes the disruption of protein–repressor complex (as described below).

To better understand this proposed photocycle, it is necessary to characterize the different redox states individually. In this project, we investigated the spectroscopy of those intermediates, as well as the other two fully reduced states of flavin $FADH^{-}$ and $FADH_2$. Specifically we measured the electronic and vibrational spectra of these intermediates in solution first and then when bonded to protein. By such characterisation it will be possible to identify these redox states when they appear as intermediates in the BLUF photocycle.

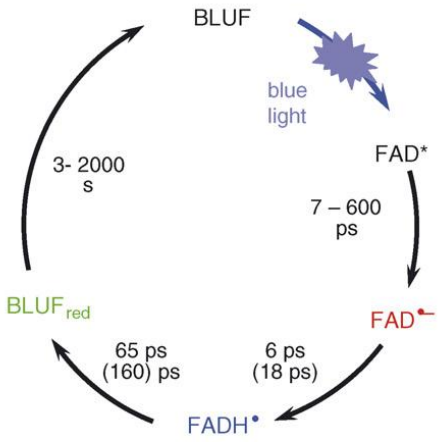

Fig. 1.2. Proposed Photocycle of BLUF Domain Protein [15,16]

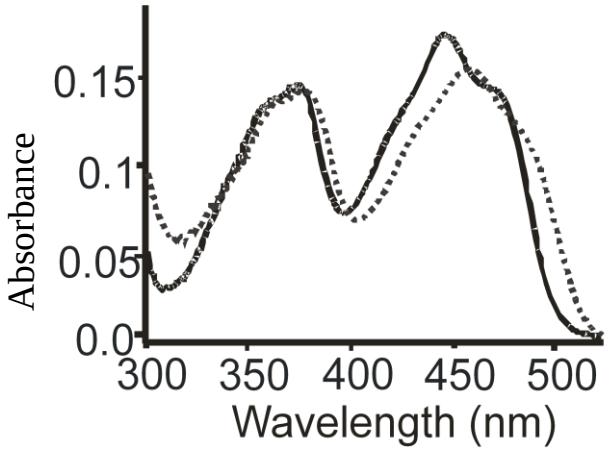

Fig. 1.3. Absorption Spectra Shift of BLUF Domain Protein from dark state (solid line) to light state (dash line) [15,16]

1.2 BLUF domain proteins

1.2.1. The photoactivated adenylylcyclase (PAC) from E. gracilis

Euglena gracilis, a unicellular flagellate, is an interesting example demonstrating how blue light affects organisms. The swimming direction of Euglena Gracilis changes immediately in response to an abrupt change of blue light intensity. This phenomenon has been described by Yoshikawa *et al* [17] as a step up and down photophobic reaction. PAC, which is extracted from the photoreceptor organelle of *Euglena Gracilis*, mediates the step-up photophobic response through a blue-light-dependent activation [18, 19].

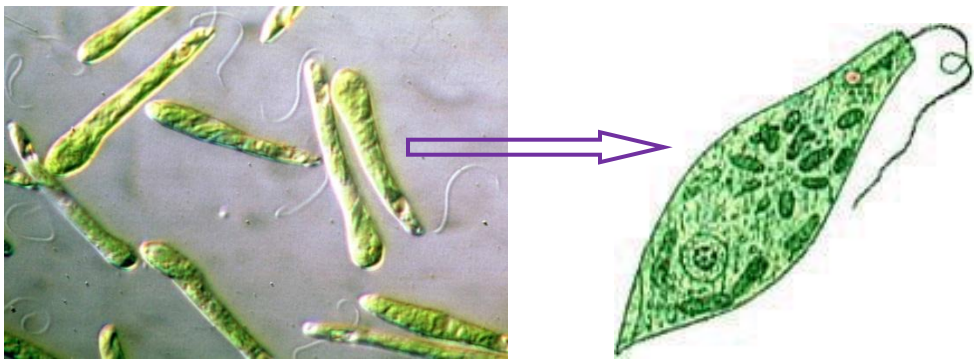

Fig. 1.4. *Euglena Gracilis*

1.2.2. Slr1694 from Synechocystis PCC6803

Synechocystis PCC6803 was identified as a freshwater cyano-bacterium which can photo-lithographically grow under sunlight and heterotrophicly grow during dark periods [19]. The protein Slr1694 was found in the *Synechocystis* PCC6803 has also been classified as a member of the BLUF domain family because of its FAD-binding domain characteristics. Hasegawa *et al* pointed out that upon illumination at different temperatures, Slr1694 presents a small red shift in the UV-visible spectrum and light-introduced changes in the Fourier Transform Infrared (FTIR) which indicated signalling state formation [19-20]. These changes are quite characteristic of BLUF domains.

1.2.3. YcgF from Escherichia Coli

YcgF includes a photosensory BLUF domain which goes through a reversible photocycle under blue light excitation. During such a cycle, the photo-stationary state and kinetics of recovery in the dark state are similar to the BLUF domain of AppA protein and slr1694. YcgF has been shown to be able to modulate the cellular levels of the second messenger cyclic diguanylate (c-di-GMP) in a blue-light-dependent manner [21, 22].

1.2.4. AppA from Rb. Sphaeroides

AppA is a 450 nm absorbing- blue-light photoreceptor protein that was identified by its ability to mediate blue-light repression of bacterial chlorophyll synthesis [23]. It acts as a transcriptional anti-repressor in Rhodobacter sphaeroides that senses both light and oxygen in the cell and alters the photosynthesis gene expression accordingly [24]. The properties and mechanisms of BLUF mediated AppA light activation are the focus of this research project and will be introduced in more details below.

1.3 AppA

AppA is sensitive to light and functions as a transcriptional anti-repressor, controlling the expression of photosynthesis gene expression via redox and light-modulated interaction with the repressor PpsR [25]. The structure of AppA is shown in Fig. 1.5; the labelled green molecule is FAD which binds to AppA as the chromophore. AppA has two domains: the amino (N) terminal light sensing domain and the carboxy(C) terminal PpsR

repressor binding domain. The N-terminal portion of AppA is a BLUF domain that binds flavin which enables the protein to absorb blue light and ultimately alter the conformation of the cysteine rich C-terminal domain to release PpsR [24].

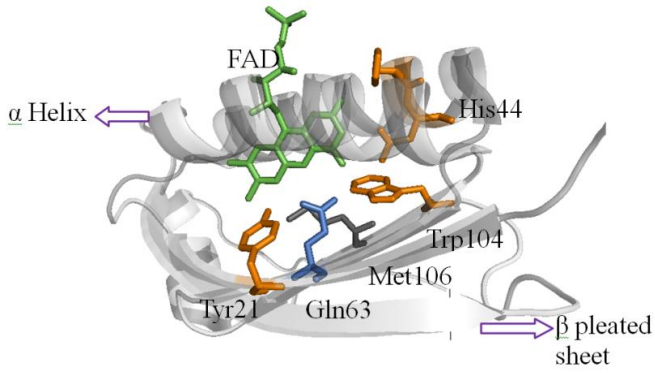

Fig. 1.5. Structure of AppA

The mechanism of AppA can be explained as follows: in normal cases, AppA binds to PpsR, thereby preventing it from binding to the DNA. Consequently transcription of the photosynthesis genes occurs. However, once it is blue-light illuminated (or under high oxygen), this disrupts the AppA structure interaction, releasing PpsR and thus restoring its repressor activity, so that the gene transcription would be terminated, as shown in Fig.1.6. The FAD, as the chromophore bound in the 'N' terminal BLUF domain of AppA, will be discussed in the next section.

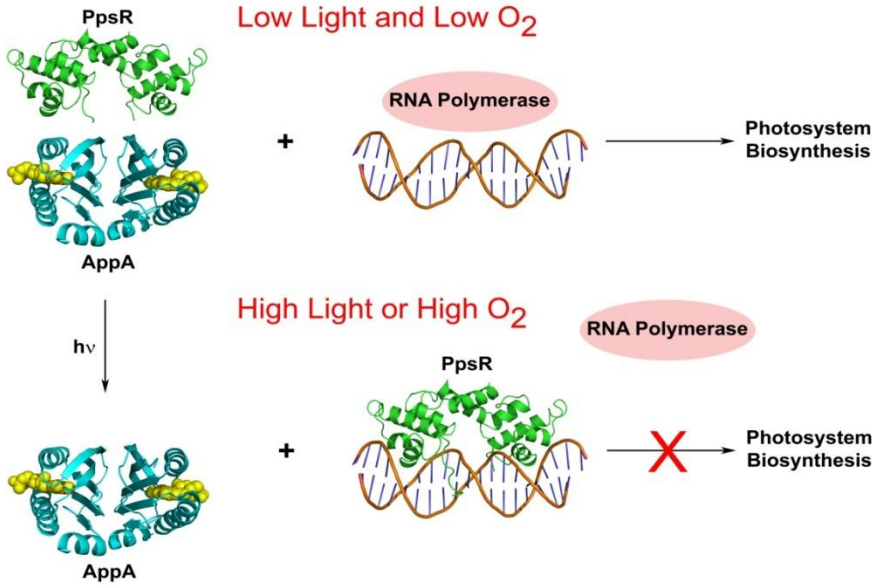

Fig. 1.6. Schamatic Representation of AppA Mechanism

1.4 Flavin Chromophore: FAD and FMN

FAD, as the chromophore in BLUF domain proteins (like AppA), is a member of a group of organic compounds based on pteridine, which is formed by the tricyclic heter-nuclear isoalloxazine ring. The biochemical source of FAD is the vitamin riboflavin. The flavin moiety is often found in nature attached with an adenosine diphosphate to form FAD, however under other circumstance, it is found as flavin mononucleotide (FMN). The formula of FAD and FMN are shown in Fig. 1.7.

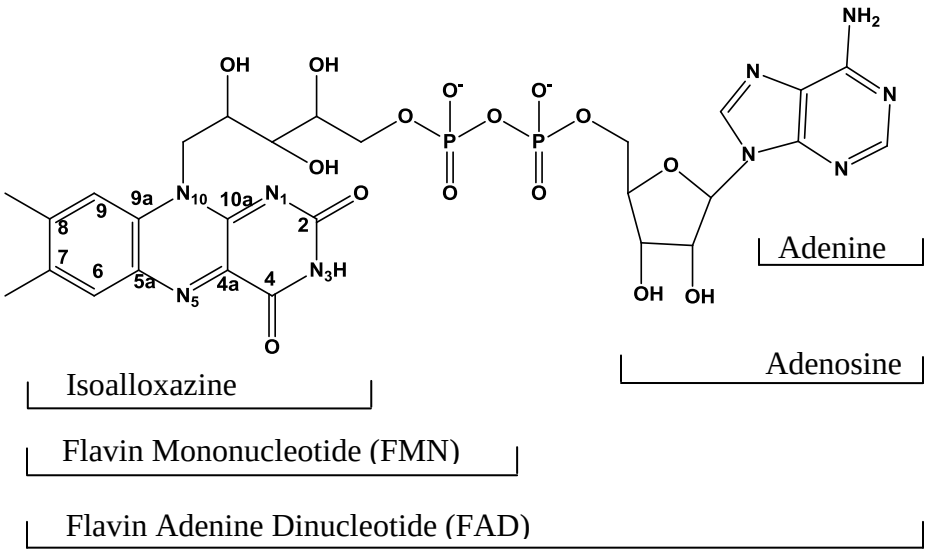

Fig. 1.7. Structural Formulae of FAD and FMN

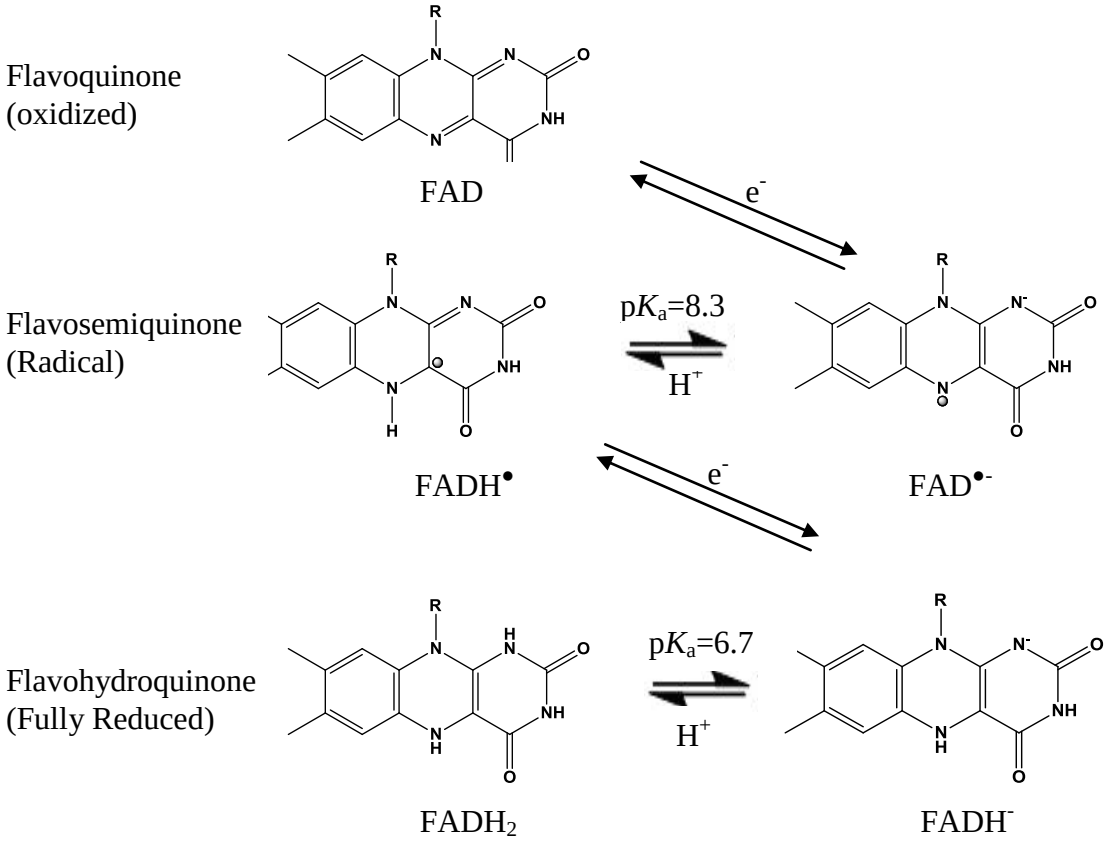

Fig. 1.8. Different Redox States of FAD under Physiological Conditions [26]

FAD gains its importance in biochemistry because it is able to undergo oxidation-reduction reactions, and can generally accept either one electron in a two-step process or two electrons in one-step [25]. Reduction is achieved by adding hydrogen atoms to specific nitrogen atoms on the isoalloxzine ring system. So in this case, FAD can have several states: oxidized form, one-electron reduced radical semiquinone, and two-electron fully reduced hydroquinone. Semiquinone and hydroquinone have pK_a values of 8.3 and 6.7, respectively, [26, 27] (Fig. 1.8) so they can both be present in their neutral or anionic forms under physiological conditions. This redox chemistry is a key feature for understanding the mechanism of flavoprotein photosensing. Our aim is to characterise these redox states by transient spectroscopy with the long term aim of identifying transient oxidation states. We will achieve this through electronic and vibrational spectroscopy.

1.5 UV and fluorescence spectrometer

Electronic absorption spectroscopy typically involves using light in the UV-Vis region. In this region, electronic transitions are excited in aromatic and unsaturated molecules [30]. The absorption reflects transitions from the ground state to electronically excited states, while fluorescence spectroscopy measures the converse transition (nonradiative relaxation and phosphorescence, will be discussed later) [27]. The basic apparatus for absorption and fluorescence are shown below in Fig. 1.9. For absorption the light transmitted by the sample as a function of wavelength is measured. To obtain spectra a reference cell is used and the data plotted as optical density using the Beer-Lambert law (below). For the fluorimeter, the Xe-lamp light source was transformed to near monochromatic light by the monochromator and then used to excite the sample from ground state to excited state. The excited molecule may emit photons which will be detected as the fluorescence and measured as a function of wavelength.

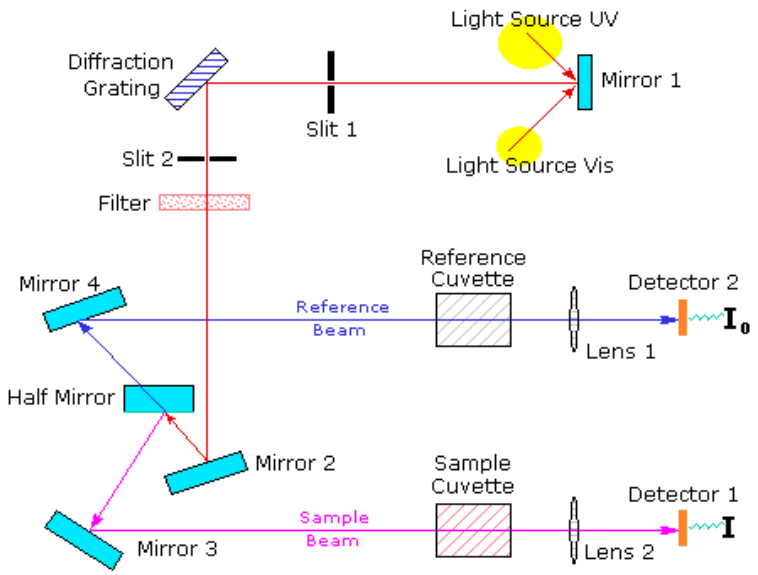

Fig. 1.9a) Scheme of UV spectroscopy Set-up with Sample and Reference Beam

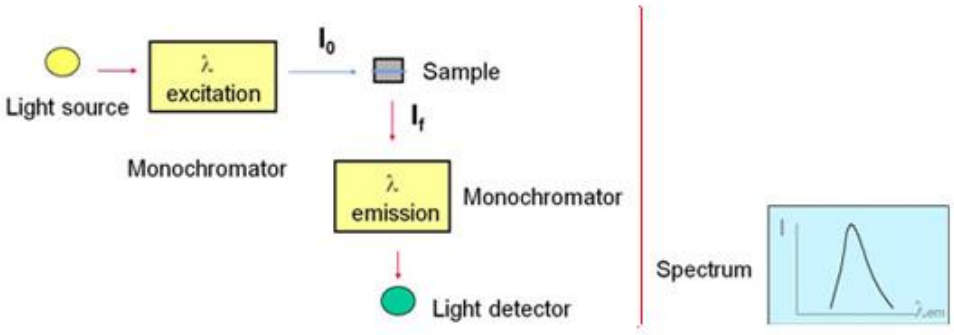

b) Fluorometer Set-up with 90^o geometry

1.5.1 Beer-Lambert Law

The Beer-Lambert law relates the absorbance of a solution to the concentration of the sample and the path length of the cell, where absorbance is obtained from the measured transmitted intensities I and I_0. Therefore, it is possible to find the concentration of a sample solution by UV spectroscopy under a fixed path length provided we know the extinction coefficient of the molecule at given wavelength.

The Beer-Lambert law is expressed as:

$$A = -\log T = -\log(I / I_0) = lc\varepsilon \text{ [28]} \qquad 1.1$$

Where A is the absorbance, T is the transmittance, I_0 is the intensity of the incident light at a given wavelength, I is the transmitted intensity, l the path length through the sample (in cm), and c the concentration of the absorbing species. The constant ε is the extinction coefficient for each species and is in general wavelength dependent [28]. Given a solvent, at a particular temperature and pressure, this constant ε is a basic molecular constant; the higher the extinction coefficient of a molecule at a given wavelength, the more the light at this wavelength can be absorbed by the sample.

1.6 Photophysical process

Various photophysical processes in addition to absorption and fluorescence might be important. Some of these can be shown on a Jablonski diagram below:

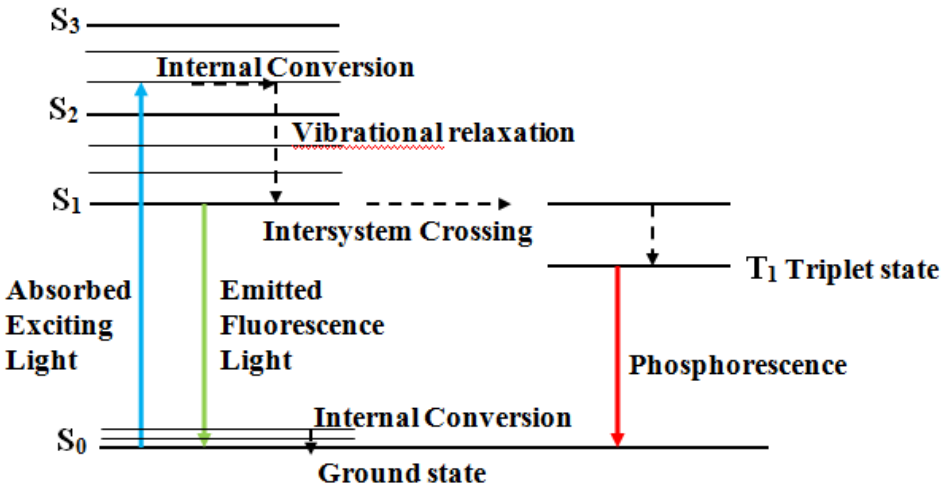

Fig. 1.10 A typical Jablonski Diagram [29]

Absorption may be to higher vibrational level of S_1 or S_2. Molecules in condensed phases will relax to the lowest vibrational level of S_1 as fluorescence very quickly, through internal conversion and vibrational energy redistribution and relaxation processes which normally happens within 10^{-12} s or less [29].

Emission to vibrational ground states results in a mirror image of the absorption spectrum for large molecules such as benzene or isoalloxazine ring which have a large amount of electrons (small molecules do not have this property). This surprising similarity can be explained as electronic excitation does not change the nuclear geometry greatly in these large pi electron systems. Accordingly, the spacing of the vibrational energy levels of the excited states is similar to that of the ground state, so the absorption and the emission spectra show similar vibrational structure. This general mirror symmetry is not observed for molecules which undergo large structure change in the excited state.

Molecules in the S_1 state can also undergo a spin conversion to the triplet state T_1, called intersystem crossing. Emission from T_1 is termed phosphorescence, and is shifted to longer wavelengths (lower energy) relative to the fluorescence. Transition from T_1 to the singlet ground state is forbidden, and as a result the rate constants for triplet emission are several orders of magnitude smaller than those for fluorescence. Molecules containing heavy atoms such as bromine and iodine are frequently phosphorescent. The heavy atoms are not only conducive to intersystem crossing, but also contribute to enhancement of phosphorescence quantum yields [29].

1.6.1 Stoke shift

The Jablonski diagram (Fig. 1.10) shows that the energy of the emission is usually less than that of absorption. This was firstly observed by Stokes [30] who pointed out that it is quite common that fluorescence occurs at lower energies or longer wavelengths than absorption. One explicit reason for the Stokes shift is the rapid decay of population to the lowest vibrational levels of S1. Solvation phenomena which further stabilise excited states (especially in polar solvents) also contribute to the Stokes shift.

1.7 Fluorescence lifetime and quantum yield

The fluorescence lifetime and quantum yield are very important characteristics of a fluorophore. Quantum yield is the number of emitted photons relative to the number of absorbed photons while lifetime describes the mean time a fluorophore stays in the excited state.

The meanings of quantum yield and lifetime are best represented by a simplified Jablonski diagram (Fig. 1.11). In this diagram, two processes of decay from the excited state are illustrated. Specifically, the emission rate of the fluorophore (k_f) and the nonradiative decay rate (k_{nr}) are very important to determine the quantum yield and lifetime.

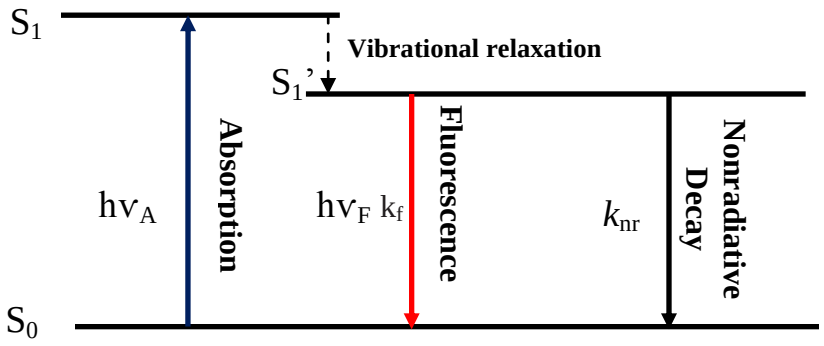

Fig. 1.11. Simplified Jablonski Diagram to Illustrate Meaning of Quantum Yields and Lifetimes [29]

The fluorescence quantum can be represented by the rates of these processes, hence the quantum yield, is given by:

$$\phi_f = \frac{k_f}{k_f + k_{nr}} \qquad 1.2$$

As we see from the equation, the quantum yield approaches unity if the radiationless decay rate is much less than the rate of radiative decay (fluorescence), that is $k_{nr} << k_f$. We note that the energy yield of fluorescence is always less than unity because of Stokes losses. The fluorescence lifetime is similarly determined from these rates as:

$$\tau = \frac{1}{k_f + k_{nr}} \qquad 1.3$$

References

[1] Bard, A. J. (1982) *Journal of Physical Chemistry 86*, 172-177.

[2] Vincent, A. S. (2011) PhD Thesis in *Photochemical Sciences,* Flavins and Their Analogues as Natural and Artificial Catalysts, 1-2, Bowling Green State University, Bowling Green.

[3] Hagfeldt, A. and Gratzel, M. (1995) *Chemistry Review 95*, 49-68

[4] Metzler, D. E. (2003) *Biochemistry,* Volume 2: The Chemical Reactions of Living Cells, Academic Press, 2nd ed.

[5] Eisenberg, A. (2008) *Assignment of Vibrational Modes to the Bands of the Raman Spectra of the Oxidized Flavin and the Flavin Radical,* ProQuest.

[6] Briggs, W.R. and Huala, E. (1999) *Annual Review of Cell and Developmental Biology 15*, 33-62.

[7] Gomelsky M, K.G. (2002) *Trends in Biochemical Sciences 27(10)*, 497-500.

[8] Van der Horst, M. A. and Hellingwerf, K. J. (2004) *Accounts of Chemistry Research 37*,13-20.

[9] Armitage, J. P. and Hellingwerf, K. J. (2003) *Photosynthesis Research 76*, 145–155.

[10] Hoff, W.D. (2009) *Photobiology: Photomovement of Bacteria and Archaea*.

[11] Weber, S. and Schleicher, E. (2012) *Radicals in Flavoproteins , Topics in Current Chemistry 321*, 41-66.

[12] Christie, J.M. (2008) *Photobiology* :*Blue Light Sensing in Plants, all you need is a little LOV*.

[13] Huala, E., Oeller, P.W., Liscum, E., Han, In-Seob., Larsen, E. and Briggs, W. R. (1997) *Science 278(5346)*, 2120-2123.

[14] Gressel, J. (1979) *Photochemistry and Photobiology 30 (3)*, 749–754.

[15] Fukushima, Y., Okajima, K., Shibata, Y., Ikeuchi, M. and Itoh, S. (2005) *Biochemistry 44(13)*, 5149-58.

[16] Gauden.M, Yeremenko, S., Laan, W., van Stokkum, I.H.M., Ihalainen, J.A., van Grondelle, R., Hellingwerf, K.J. and Kennis, J.T.M. (2005) *Biochemistry 44*, 3653-3662

[17] Yoshikawa S, S.T., Watanabe M and Iseki M. (2005) *Photochem Photobiol Sciensce 4(9)*,727-731.

[18] Iseki, M., Matsunaga, S., Murakami, A., Ohno, K., Shiga, K., Yoshida, K., Sugai, M., Takahashi, T., Hori, T. and Watanabe, M. (2002) *Nature 415(6875)*,1047-1051.

[19] Hasegawa, K., Masuda, S. and Ono, T. (2004) *Biochemistry 43*(47), 14979-14986.

[20] Masuda, S., Hasegawa, K., Ishii, A. and Ono, TA. (2004) *Biochemistry 43(18)*, 5304-5313.

[21] Huala, E., Oeller, P., Liscum, E., Han, In-Seob and Larsen, E. (1997) *Science Blog- Blue Light And The LOV Domain: Scientists Uncover Regulatory Domain With Wide Convergence*.

[22] Wiegand, C. and Klemm, D. (2006) *Chemistry and Material Science 13*, 485 – 492.

[23] Shimada, H. , lba, K. and Takamiya, K. (1992) *Plant Cell Physiol 33*, 471-475.

[24] Bauer C., Elsen S., Swem L. R., Swem D. L., Masuda S. (2003) *Philosophical Transactions of the Royal Society B: Biological Sciences 358*, 147–154.

[25] Mu¨ller, F. editor, *Chemistry and Biochemistry of Flavoenzymes*. CRC Press: Boca Raton, FL: (1990-1991), Vols. I-III.

[26] Kao, YT., Saxena, C., He, TF. , Guo, L., Wang, L. , Sancar, A. and Zhong, D. (2008) *Journal of the American Chemical Society 130(39)*, 13132-13139.

[27] Rendell, D. (1987) *Fluorescence and Phosphorescence (Analytical Chemistry by Open Learning)*, Crown.

[28] Ingle, Jr. J. D. and Crouch, S. R. (1988) *Spectrochemical Analysis*, 1st ed, Prentice Hall.

[29] Lakowicz, J.R. (2006) *Principles of fluorescence* , 3rd ed, Springer.

[30] Elumalai, P., Atkins, P. de Paula and Atkins, J. (2002) *Physical Chemistry*,Oxford University Press.

Chapter 2 Sample Preparation and Experiments

2.1 Synthesis of Model flavin samples

The oxidized FAD and FMN were purchased from Sigma-Aldrich and used without further purification. The fully reduced flavohydroquinones: $FADH^-$ and $FADH_2$ were prepared by chemical reduction with sodium dithionite under anaerobic conditions. The radical flavosemiquinones, $FADH^\bullet$ and $FAD^{\bullet -}$, were prepared in the flavoprotein Glucose Oxidase (GOx) either by chemical reduction with sodium dithionite titration or photoreduction with ethylenediaminetetraacetic acid (EDTA) also under the anaerobic conditions. The methyl FAD (or FMN) neutral radical samples were obtained by anaerobic chemical reduction with sodium cyanoborohydrate, sodium dithionite and deuterated formaldehyde using the procedure described by Eisenberg and *et al* [1], details will be shown in the relevant paragraph. Preparation of these samples has been reported before [1-5] but the specific procedures used in this project will be presented for completeness.

2.1.1 Synthesis of fully reduced flavohydroquinones: FADH- and FADH2

(1) 12.5mM phosphate buffers were prepared at pH 5 and 8.5 respectively, by balancing the molar ratio of KH_2PO_4/K_2HPO_4 buffer solutions (Sigma-Aldrich).

(2) FAD was dissolved in the buffer solution with the concentration of 700μM in a 2ml glass flask, and then 2ml dithionite with concentration of 4mM was prepared in the same buffer solution in another flask.

(3) The samples were put into a glove bag which was emptied and refilled with nitrogen gas several times to make the conditions anaerobic.

(4) The two solutions were degassed by bubbling dry nitrogen inside the bag for 30 mins and were then mixed together (50:50) in a cell with 10 mm pathlength (sealable cap, Starna), so that both the concentration of FAD and dithionite were reduced to half. The sample cell lid was tightened inside the bag to make sure the anaerobic atmosphere was

maintained. Teflon thin film was stuck to the inside screw of the cell cap to make a better seal.

(5) The sample cell was taken out from the bag and kept in the dark for several minutes to give sufficient time to complete the reduction reaction. The final product depended on the pH of the buffer; the chemical structures are shown in Fig. 2.1 below.

(6) The absorption and steady state emission were recorded to confirm the formation of the reduced flavin.

(7) The dithionite has weak florescence, so the dithionite buffer solution with the same concentration was used as reference for these measurements, and its emission was subtracted to yield the final flavin fluorescent results. The raw data and the subtracted spectra are shown in Fig. 2.2 and 2.3 with a comparison of literature spectra.

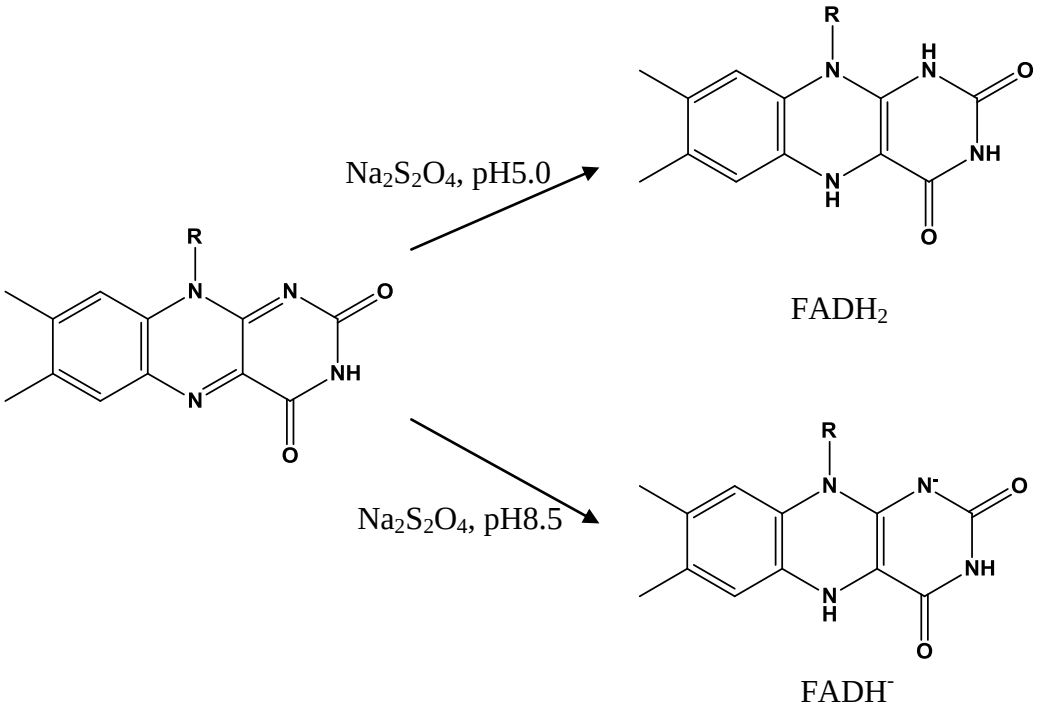

Fig. 2.1 Scheme of fully reduced $FADH^-$ & $FADH_2$ preparation from FAD_{ox}

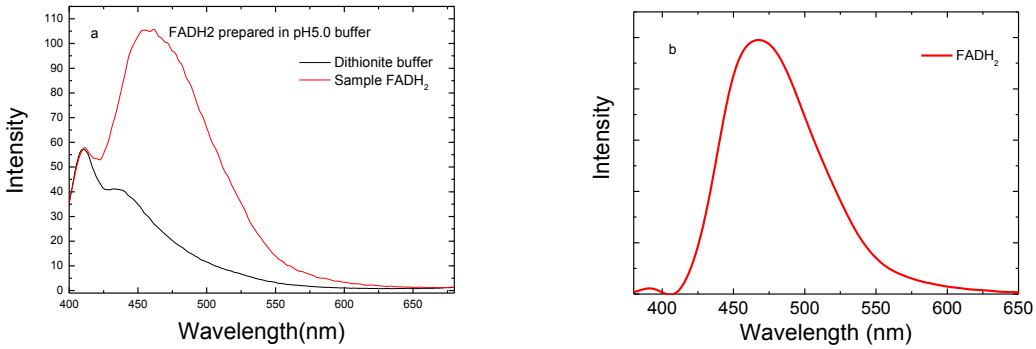

Fig. 2.2 Fluorescence data of $FADH_2$ before (a) and after (b) buffer solution spectra subtracted

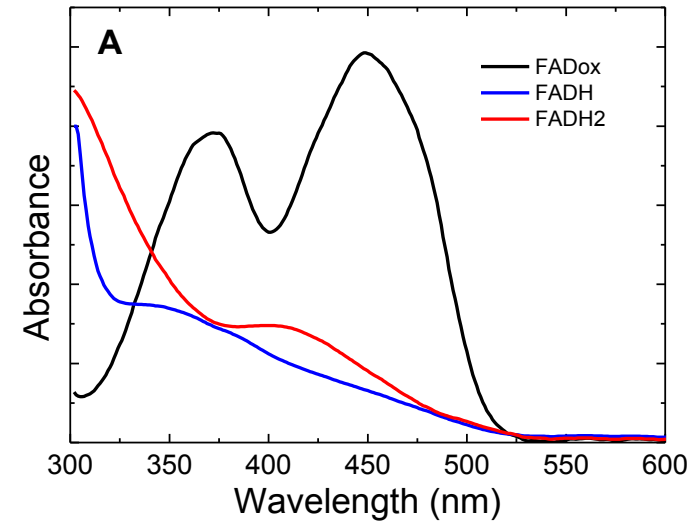

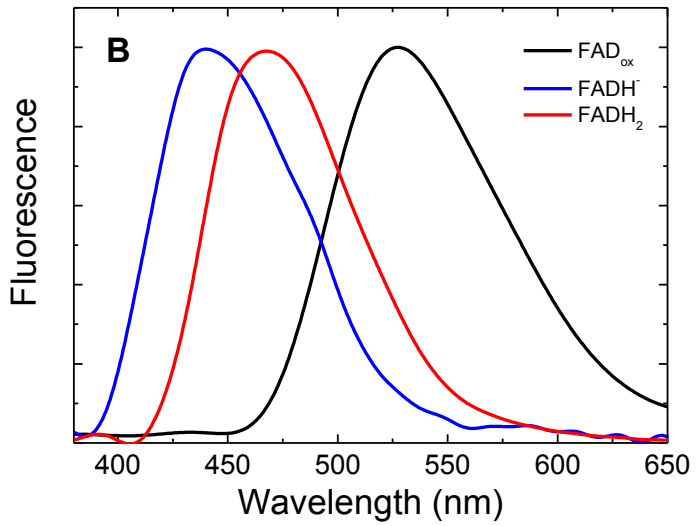

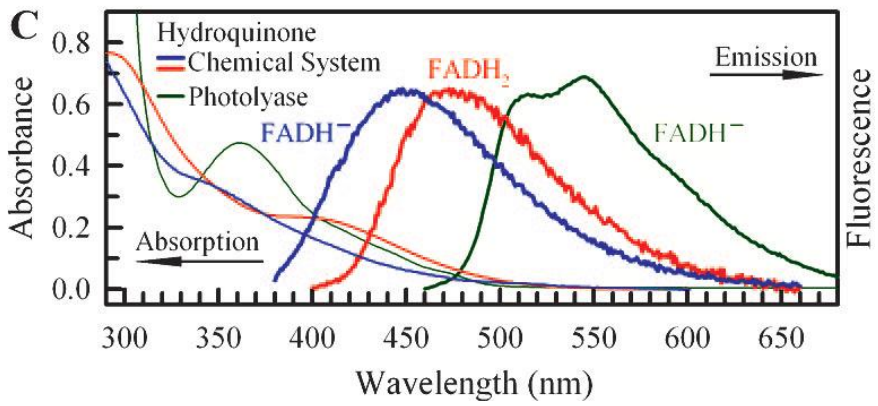

Fig. 2.3 UV-Vis absorbance (A) and fluorescence emission spectra (B) of FAD_{ox}, $FADH_2$ and $FADH^-$ compared with literature spectra (C) (spectra taken from [2]).

Fig. 2.3 shows the absorption (A) and emission spectra (B) for $FADH^-$ and $FADH_2$ compared to those for FAD_{OX}. FAD_{OX} exhibits two broad absorption bands, peaked at 450 nm and 375 nm. The emission band of oxidized flavin is around 530 nm when excited at 400 nm. Upon 360 nm-excitation, we observed fluorescence emission peaking at 455 nm for anionic hydroquinone ($FADH^-$) and at 480 for neutral hydroquinone ($FADH_2$). The emission spectra of the fully reduced anionic and neutral flavins ($FADH^-$ and $FADH_2$) are consistent with those previously reported by Kao *et al* (Fig. 2.3C) [2]:

2.1.2 Synthesis of flavosemiquinones in Protein GOx and Flavodoxin: $FADH^{\bullet}$ and $FAD^{\bullet -}$

According to the literature, the radical state of flavin can only be stabilized in a protein or a micelle rather than in free solution [4], because the protein residues can stabilize the free radical in the molecule better than the solution environment. Glucose Oxidaze (GOx) was chosen as a flavoprotein to make stable radical state of the flavin. GOx is an oxido-reductase that catalyses the oxidation of glucose to hydrogen peroxide and D-glucono-δ-lactone. It has a molecular weight of 160 kDa ($160\times10^3 gmol^{-1}$), the structure of GOx is illustrated in Fig. 2.4: FAD as the chromophore is bound to it surrounded by different protein residues. Flavodoxin was a second flavoprotein involved in this project, which includes a FMN molecule, the molecular weight of flavodoxin is rather small and is about 1/10 or the GOx, which makes it more suitable for transient IR studies than GOx, as described below

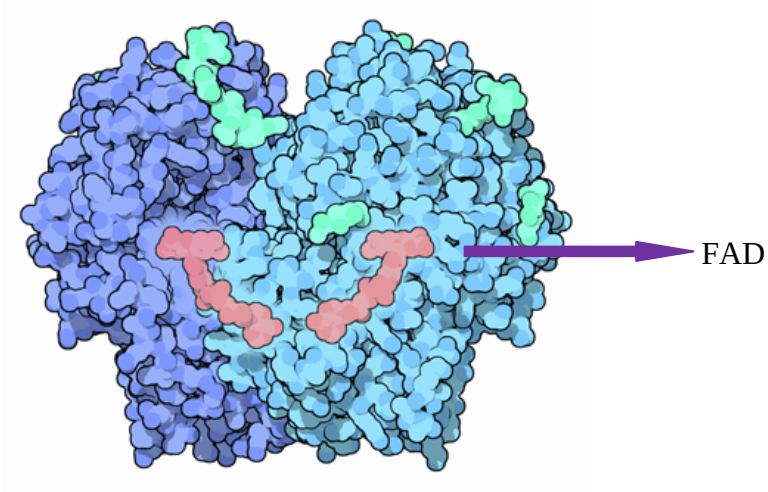

Fig.2.4 Crystal structure of glucose oxidase

The flavin radical states $FADH^{\bullet}$&$FAD^{\bullet-}$ can be made either chemically or photochemically.

2.1.2.1 Chemical reduction

Glucose Oxidase (GOx) solution was made with a concentration of 1 mM, in phosphate buffer (K_2HPO_4 and KH_2PO_4) at pH 6 for $FADH^{\bullet}$ and pH 9.5 for $FAD^{\bullet-}$. The preparation procedure is based on the description of Pan *et al* [4]:

(1) The 500μM GOx sample was made and put in the sonicator for 30mins (to remove dissolved air) before it was moved into the oxygen free bag, where only the surface of the sample solution was degassed by a flow of nitrogen. This was due to the high viscosity of concentrated GOx solution and the resultant formation of bubbles if nitrogen flowed through the sample.

(2) The degassed dithionite solution was titrated into the GOx sample to make $FADH^{\bullet}$ and $FAD^{\bullet-}$ separately, checking the absorbance after each drop until the sign of formation of each state appears and reaches its maximum. The absorbance at 570 nm increases as $FADH^{\bullet}$ is formed while absorbance of shoulder band appears at 400 nm for $FAD^{\bullet-}$, as illustrated in Fig. 2.5 and Fig. 2.6.

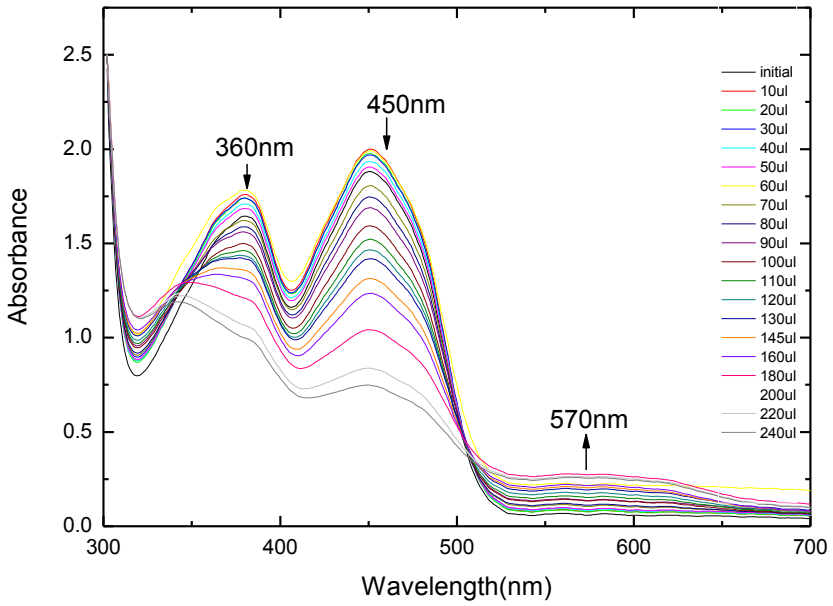

Fig. 2.5 UV spectra of FAD and $FADH^{\bullet}$ during the dithionite titration

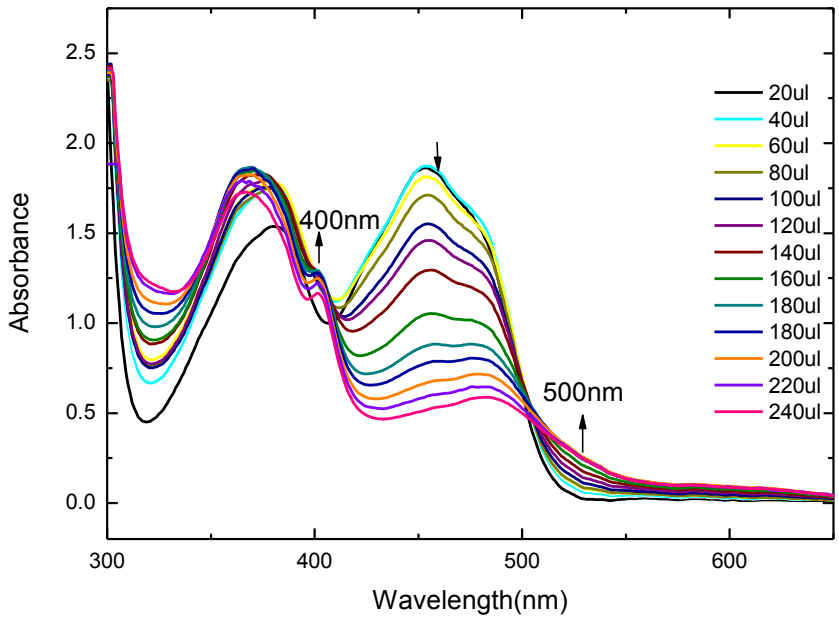

Fig. 2.6 UV spectra of FAD/$FAD^{\bullet -}$ state during dithionite titration

According to the spectra shown in Fig. 2.5 and 2.6, FAD reduction in GOx occurs as shown by the decrease in FAD peak values at 360 and 450 nm and the appearance of a broad peak at 570 nm assigned to the $FADH^{\bullet}$ (ε_{570} ~4400 M^{-1} cm^{-1} [4]). The increase of the small shoulder band at 400 nm is the sign of the formation of $FAD^{\bullet -}$ state. The titrations were stopped when the absorbance spectrum reached to the maximum of the radical states of the flavin.

2.1.2.2 Photochemical reduction

$FADH^{\bullet}$ was prepared from GOx in pH 6.0 phosphate buffer with a flavin concentration of 500 μM following Pan's method [4] by anaerobic photo-reduction. In the presence of 10 mM EDTA, the sample was extensively degassed on its surface in a 1cm path length cell by nitrogen gas flow. Subsequently, at $0^{o}C$ it was illuminated with a UV lamp (365 nm). Oxidized FAD in GOx was reduced to the neutral radical form ($FADH^{\bullet}$) by EDTA under UV light illumination in a few minutes. Care had to be taken because further treatment with blue light leads to the formation of fully-reduced $FADH^{-}$ (Fig. 2.7).

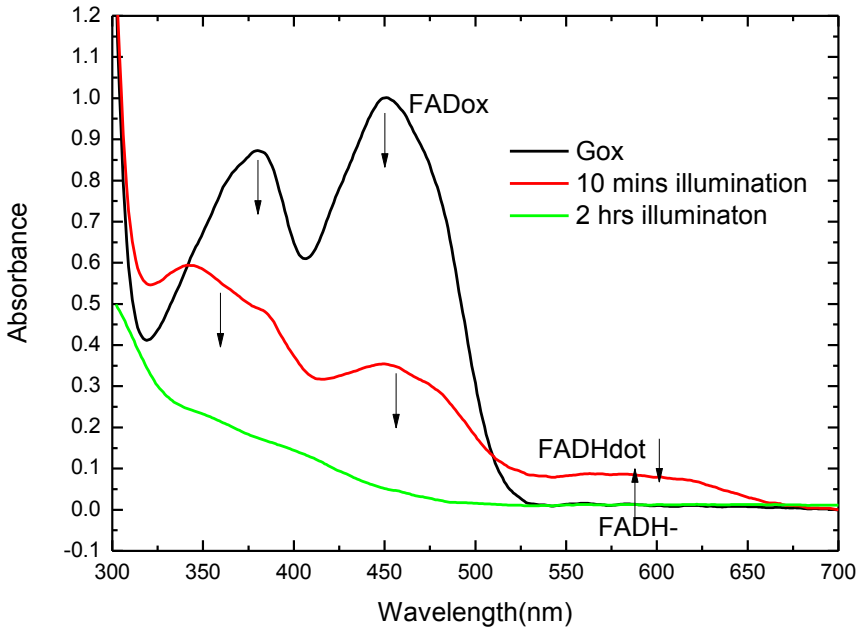

Fig. 2.7 UV spectra of photoreduction process of FAD in GOx

2.1.3 Synthesis of flavosemiquinones in solution: methylated FAD and FMN radicals

For studies of the flavin radical in solution, the N-5 methyl flavin had to be synthesized, which was achieved through the method of Eisenberg *et al* [1]. The idea was to use a flavin where the N-5 atom was a secondary amine, which is true for the fully reduced flavin. Therefore the oxidized flavin would first have to be turned into its fully reduced form. Once this was done, the N-5 position of the flavin is the most available site for nucleophilic attack by a formaldehyde molecule. After attack by a nucleophilic hydrogen, provided by $NaCNBH_3$, the N-5 atom had its methyl group attached. This product was the N-5 methyl fully reduced flavin, which has a UV-vis spectrum the same as $FADH_2$ (Fig. 2.3). This compound was rather stable as long as oxygen was excluded from its solution. Then by adding distilled water, the fully reduced N-5 methyl flavin was oxidized to its radical state, the whole chemical process is illustrated in Fig. 2.8.

The experimental details were as follows. Sodium cyanoborohydride (Sigma-Aldrich) was dissolved in 1 ml 2.2 M formaldehyde D_2O solution. Separately, 10 mg FAD (or 5 mg FMN) and 5.6 mg sodium dithionite were dissolved in 2 ml 0.5 M D_2O phosphate buffer at pD 5.0. Both solutions were degassed by bubbling nitrogen gas for 30 mins. The sodium dithionite reduced the FAD to $FADH_2$ (or FMN to $FMNH_2$) and the $FADH_2$ ($FMNH_2$) solution was transferred with a gas tight syringe into the sodium cyanoborohydride/formaldehyde solution in a 4 ml glass vial sealed with a rubber septum. The solution was stirred for 1 hour resulting in the formation of the 5-methylated fully reduced states. The radical state was prepared by removing 50 µl of this stock solution and placing it in a 1 ml eppendorf then adding 500 µl distilled water or D_2O; after shaking the radical state was formed. Complete formation of the radical form and its concentration were determined by UV-Vis spectroscopy (spectra are shown in Fig. 2.9).

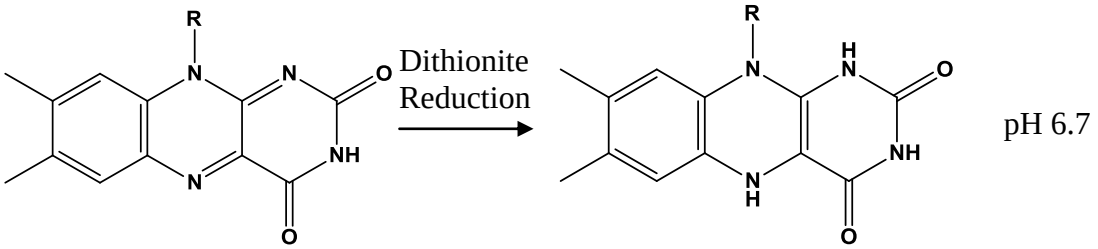

Oxidized flavin Fully reduced flavin

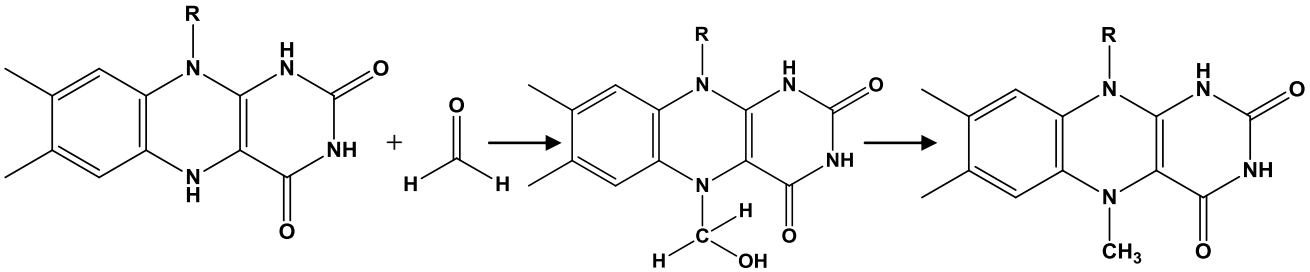

Fully reduced flavin Hemiaminal N-5 methyl flavin, fully reduced

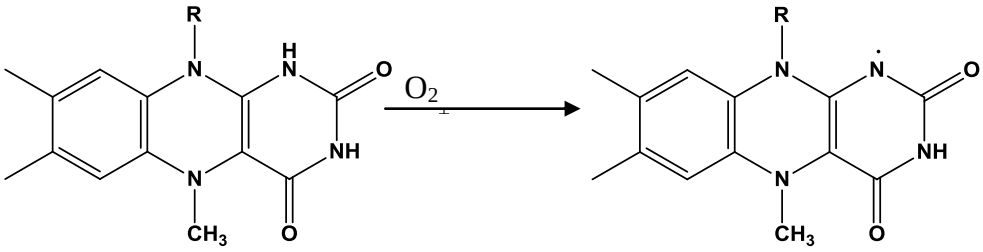

N-5 methyl flavin fully reduced N-5 methyl flavin radical

Fig. 2.8 Synthesis of the N-5 methyl flavin radical from oxidized flavin

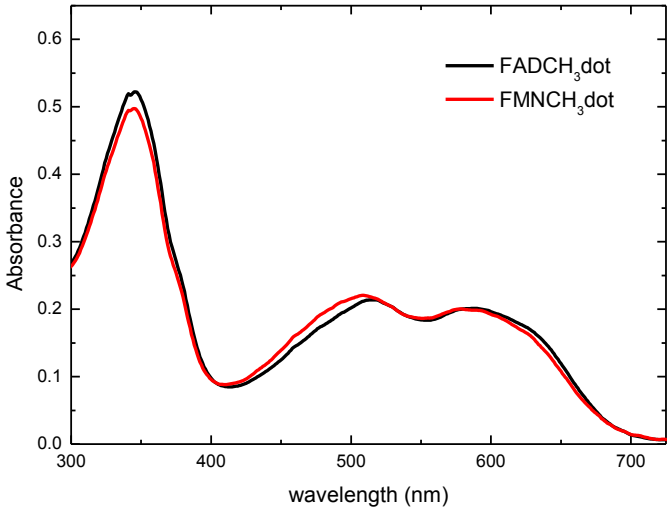

Fig. 2.9 Electronic Absorption spectra of $FADCH_3$/$FMNCH_3$ neutral radicals in solution

2.2 Measurements

2.2.1. UV & Fluorescence meausurements

The general principles of electronic spectroscopy were mentioned in Chapter 1. The UV-visible absorption spectra were recorded on a Hitachi U-3000 and a Perkin Elmer Lambda XLS UV-spectrophotometer. The operation settings used were: slits 1μm and scan speed 500 nm/min.

The Fluorescence studies were carried out on a Fluoromax 2 fluorimenter with a Xenon arc lamp as excitation source and a photomultiplier for detection. The instrument was set up as follows:

Parameter	Value
Excitation slit	5μm
Emission slit	5μm
Intergration time	1second

Table 2.1. Fluorescence measurement set-up

The excitation wavelength was 400 nm for FADox and 360 nm for fully reduced flavins $FADH_2$ and $FADH^-$ and 520 nm for all radical samples either made in GOx protein or solution (Methylated radicals). The emission spectra were collected starting from a wavelength 20 nm longer than excitation wavelength to 850 nm.

2.2.2. Temperature dependent fluorescence measurements

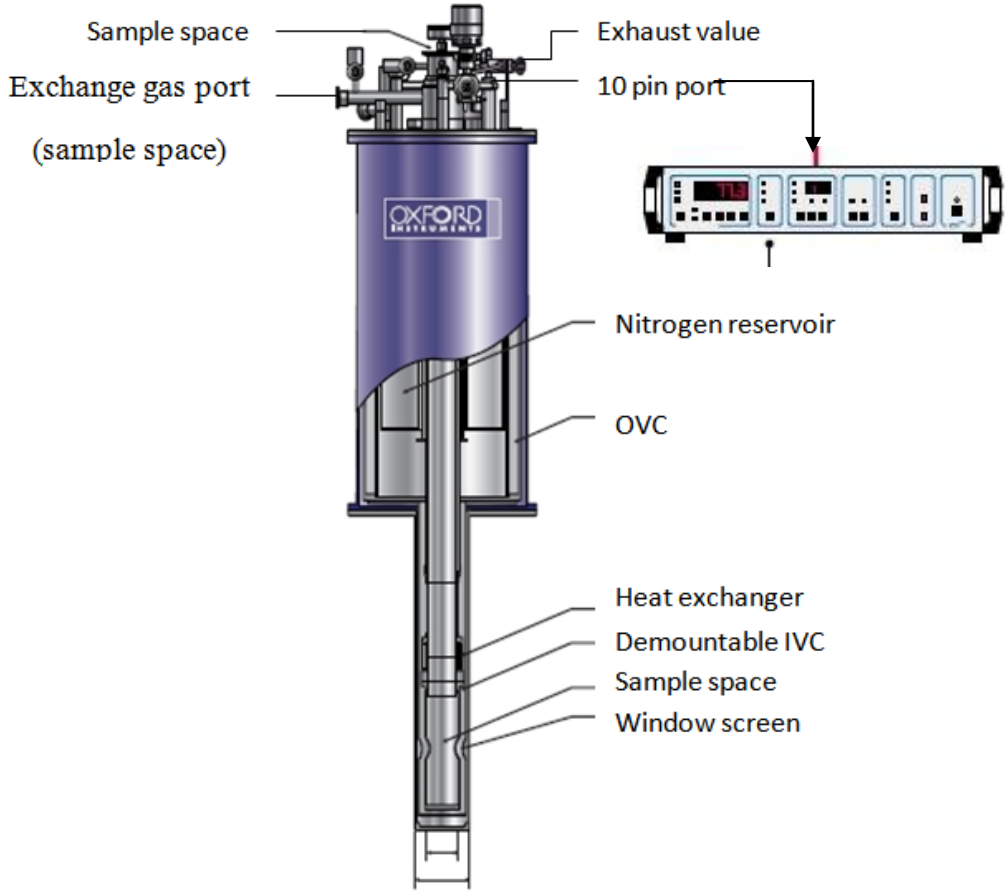

Fig. 2.10 Fluorescence measurement through cryostat and temperature controller

The low temperature fluorescence measurements were made using a top loading liquid nitrogen cryostat (Oxford Instruments DN1704). The diagram of the instrument is shown in Fig. 2.10. The temperature of sample can be varied continuously and accurately between 77K and 300K, when operated with a temperature controller (Oxford Instruments ITC502). The system consists of a liquid nitrogen reservoir surrounding the central sample space. An ‘exhaust value’ on top of the cryostat controls the flow of

liquid. An outer vacuum chamber (OVC) functions as isolating the reservoir and sample space from the ambient temperature. The vacuum in OVC was achieved by pumping with a combination of a mechanical and oil diffusion pumps. After pumping the OVC, the sample space must then be filled with dry nitrogen gas and also a balloon filled with dry nitrogen gas was attached to the sample space exchange gas port, to maintain atmospheric pressure of the sample space at all temperatures. To cool down the cryostat the liquid nitrogen reservoir is filled and the required temperature could be set and measured by the controller, which balances heating with evaporative cooling.

For low temperature experiments the oxidized FAD and FMN, fully reduced states as well as radical states samples were dissolved in Ethylene glycol/Water (volume ratio: 1:1) to make solutions at the concentrations of 5 μM. The mixture of ethylene glycol and water forms a transparent glass during the cooling process down to 77 K. Temperature dependent measurements are not possible in aqueous solutions as the glass typically cracks and is not optically transparent. The samples were contained in a fused silica tube (5mm inner diameter), which was attached to the bottom of a long glass tube by a graded seal to fit into the sample space of the cryostat. Fluorescence measurements were made at right angles with the cryostat in the Fluoromax 2 fluorimenter. The UV spectra were taken before the low temperature fluorescence measurements to check the concentration of the sample for the fluorescence measurement, which requires absorbance at excitation wavelength to be around 0.2 (About 37% excitation light absorbed and 63% transmitted). The low temperature measurement was operated by the combination of the cryostat and the temperature controller, which allowed a series of fluorescence spectra of samples at temperatures, ranging from 295K to 77K (liquid nitrogen temperature). For each spectrum about 30mins was allowed to equilibrate the temperature in sample space to the temperature value set in the controller.

2.2.3. Steady state FTIR measurements

Samples were dissolved in deuterium oxide (D_2O) which does not absorb strongly in the Infra-red range on which we focused on (1400-2000 cm^{-1}) and placed in the Harrick IR cell (Fig. 2.11). The cell has calcium fluoride (CaF_2) window with 25 mm diameters and

the thickness of the sample spacer can be varied from 1000 μm to only several μm (6 μm). For the majority of measurements, a spacer with 50 μm thickness was used to avoid any absorbance effect due to the solvents. For air sensitive samples the Harrick cell was prepared and filled in the glove bag.

Fig. 2.11 Harrick Demountable Liquid IR Cells

The FTIR spectra were recorded on a Perkin Elmer 1600 spectrometer. For the FTIR measurements used in this project, the settings are listed in the table below:

Setting	Value
Scan Range	2000-1400 cm^{-1}
Scan Number	16 times for average which can give a good signal to noise ratio
Resolution	2 cm^{-1}
Signal measured	Absorbance

Table 2.2. FTIR measurement set-up

2.2.4. Time resolved Infra-Red (TRIR) measurements

Time resolved infra-red (TRIR) measurements were carried out at the Central Laser Facility, Rutherford Appleton Laboratory (RAL), Didcot, Oxford. Their laser system set-up used for the TRIR measurement is shown in Fig. 2.12 below: with 10 kHz repetition rate and ~ 100 fs time resolution [6]. For this source the excitation spot size was ~ 100 μm radius and the pulse energy was kept below 400 nJ. The sample was placed in a 50 μm pathlength cell and the sample holder was rastered in the beam path to avoid photo

bleaching. The IR probe was used to measure transient difference spectra (pump on – pump off) at time delays between 1 ps and 2 ns. The infrared transmission was measured in the ~1400-1800 cm^{-1} region by two carefully matched 128 pixel detectors, yielding a resolution of 3 cm^{-1} per pixel. Spectra were calibrated relative to the IR transmission of pure cis stilbene standard sample placed at the sample position.

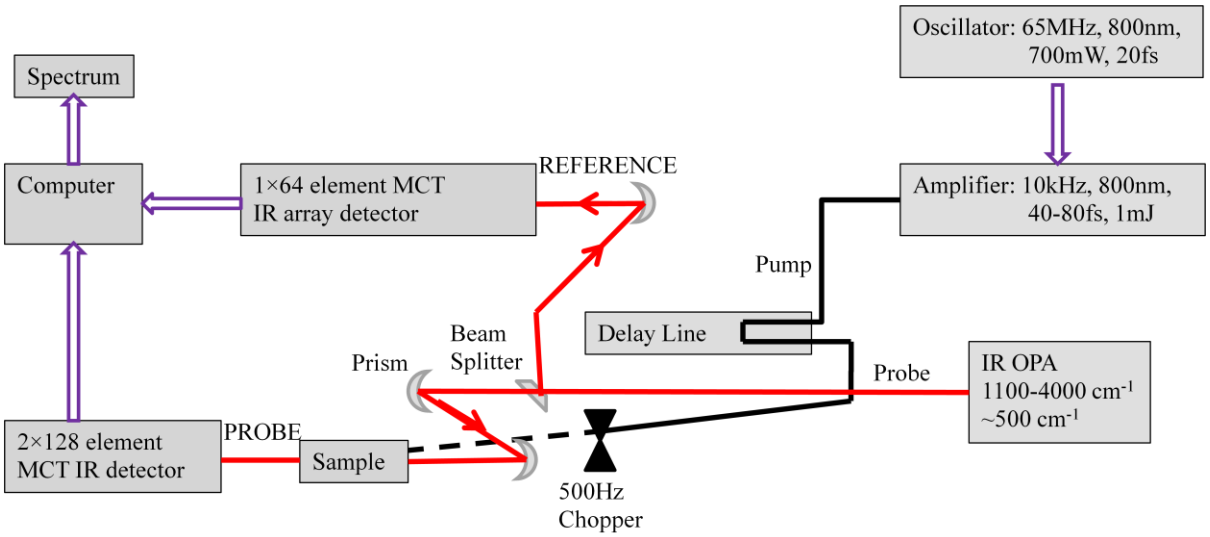

Fig. 2.12 Time Resolved Infra-Red Experimental set-up in RAL

The equations used to calculate the difference absorption (ΔA) spectra from these raw data are listed below [7]:

$$\Delta T_N = \frac{\left[\left(\frac{I_{probe}}{I_{ref}}\right)_{pumpon} - \left(\frac{I_{probe}}{I_{ref}}\right)_{pumpoff}\right] + \Delta T_{N-1}(N-1)}{N} \qquad 2.1$$

$$\Delta A_N = -\log\left(1 + \left(\frac{I_{ref}}{I_{probe}}\right)_{pumpoff} \Delta T_N\right) \qquad 2.2$$

Where ΔT is the transmittance difference, I_{ref} and I_{probe} are the final averages of spectra on the reference and probe side measured for both pump-on and pump-off, respectively (controlled by the chopper), and N is the total number of acquisitions.

For most measurements, the time delays were set at intervals from 1 ps up to 2000 ps to give absorption difference spectra at time delays to investigate the kinetics of ultrafast and slower decay components. The data will be shown in the following chapters.

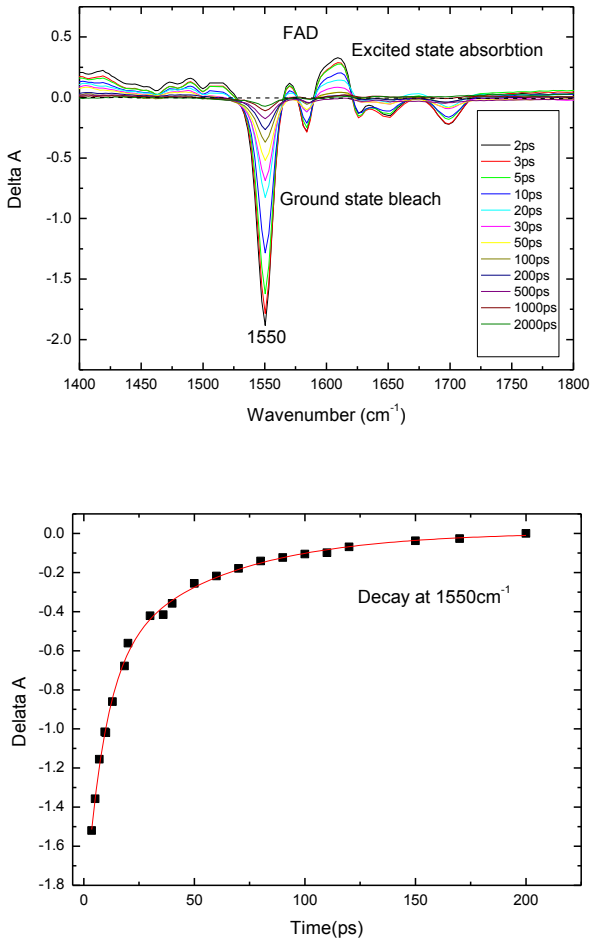

Fig. 2.13. a) TRIR spectra of FAD_{ox} at various time delays b) Decay curve at 1550 cm^{-1} band

An example of TRIR spectra of FAD_{ox} along with the decay fitting at 1550 cm^{-1} are shown in Fig. 2.13. These illustrate different contributions to the spectra, from various processes:

(1) Ground-state bleach: the pump pulse promotes a fraction of the absorbing molecules to an excited state, so the number of molecules in the ground state would be decreased which causes the reduction of the ground-state absorbance. Consequently, a negative

signal in the ΔA spectrum is observed within the wavenumber region of ground state absorption [8] (Shown as the negative bands in the spectra in Fig. 2.13 a). For directly excited ground state species this negative signal appears during the laser pulse.
(2) Excited-state absorption: After excitation with the pump pulse, the molecules which have been promoted to the excited state absorb the light, so a positive signal in the ΔA spectrum is observed in the wavelength region of excited-state absorption (Shown as the positive bands in the spectra in Fig. 2.13 a).
(3) Product absorption: during the excitation process of the sample a photoreaction may occur and result in some new products which would appears as a positive signal in the ΔA spectrum [8]. The rate of appearance would indicate the kinetics of the reaction.

A variety of samples were prepared for TRIR studies. Oxidized samples, (FAD, FMN, and GOx) and some isotope labelled flavin samples (provided by our collaborator Professor Peter Tonge, Stony Brook University, New York, US) were brought to RAL and kept in the freezer (-20^{o}C). The fully reduced flavin and protein radical samples were freshly prepared (See section 2.1.1 and 2.1.2) and measured straight away due to their oxygen sensitivity. The Harrick cell was filled in the N_2 glove bag. The methylated radical samples were made in our lab UEA as the stock solution (see section 2.1.3) and brought to RAL followed by conversion to the radical sample.

Solution samples were prepared with 50 μm spacer while those made in protein were prepared with thinner spacer (25, 12 or 6 um) to reduce the effect of protein absorption (mainly the amide I band) in the final spectra. This was less of a problem for flavodoxin, than for GOx, as it is a smaller protein.

2.2.5. UV transient absorbance measurements

The UV transient absorbance (TA) measurements were carried out on instruments built in our lab at UEA. Measurements were performed using a Clark-MXR 1000 regenerative amplifier providing ~350 nJ pulses centred at 800 nm at a repetition rate of 1 kHz. The output of the amplifier was split into two (10 %/90 %). The pulse with the smaller energy was used for white light continuum generation in a CaF_2 crystal to be used as the probe beam. The CaF_2 crystal was continuously translated in the beam to increase stability [6].

The higher energy pulse was frequency doubled to 400 nm and attenuated to ~200-400 nJ before being used as a pump beam. The pump beam was chopped at 500 Hz. Polarization of the probe was set to magic angle (54.7^{o}) compared to excitation (As shown in Fig. 2.14). In order to avoid photo degradation, the sample was moved with the help of a Lissajous scanner [6] and flowed by a peristaltic pump. Absorbance change was measured with an Andor CCD and collected by home written Labview data acquisition software. The fully reduced and oxidized flavin samples were made in a quartz curvette with 1mm path length and excited at 400 nm. The radical samples were excited at 520 nm which was generated using the 90% output of the amplifier to pump an optical parametric oscillator. The data were collected in the range over which the continuum was stable, from 420 nm to 620 nm. For radical samples which were excited at 520 nm, the final output spectra were split into two parts: 420 nm to 510 nm and 530 nm to 620 nm, to avoid scattered excitation light. One example of spectra from TA measurements of FAD oxidised state is shown in Fig. 2.15. The negative band at 450 nm represents the ground state bleach then the positive broad band at 500 nm implies the excited absorption.

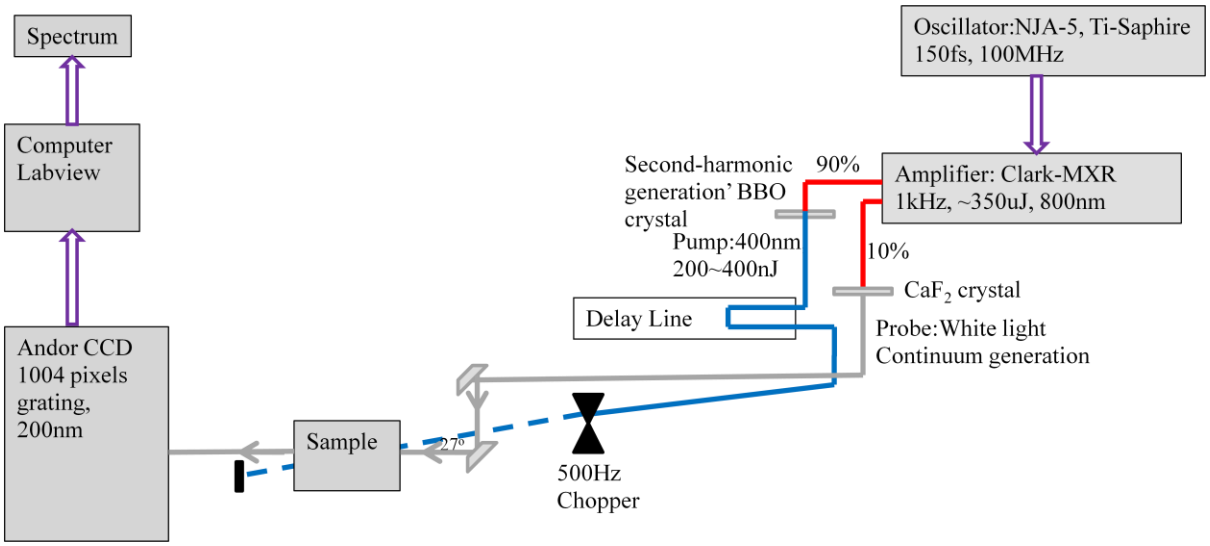

Fig. 2.14 Transient Absorption Experimental set-up

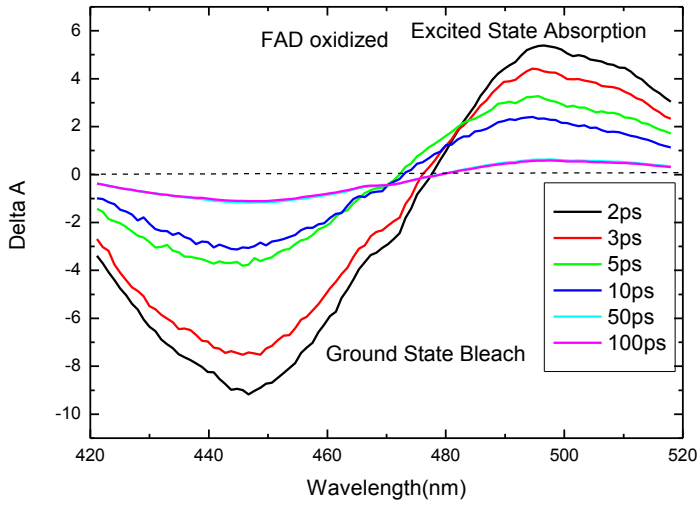

Fig. 2.15 Transient Absorption spectra of FAD_{OX} excited at 400 nm

2.2.6 Gaussian DFT

Gaussian is a software package which is widely used in theoretical chemistry [12]. It is an electronic structure package which ouputs a variety of information about the molecule, such as the energies and structure, vibrational frequencies, IR and Raman spectra, atomic charges and so on [12]. In this project, Gaussian was used to help us estimate TRIR spectra and assign the vibrational modes of the bands seen in TRIR spectra (mainly for the ground state bleaches). Density functional theory (DFT), the main calculation method for all the samples involved in this project, is a quantum mechanical theory used to investigate the electronic structure of mainly the ground state of molecules.

Because we aim to use the Gaussian simulated spectra to identify our measured IR and TRIR spectra we calculated both non-deuterated and deuterated examples, where exchangeable H atoms were swapped for D, as they would be in the TRIR experiment. For non-deuterated cases, we could run both optimization and frequency calculation in one go, but for deuterated cases, optimization was run first and then frequency calculations were made with the isotope changed at the required positions

The Gauss View input for calculating oxidized ‘FAD’ is shown in Fig. 2.16. In fact to simplify the calculation we use the lumiflavin, which lacks the phosphate and adenosine

groups of FAD. The sample molecule was optimized (Set in Job Type option) first with the ‘Method’ set as ‘Ground State, DFT, Default Spin, B3LYP, Basis Set: 6-311G, +,d,p, Charge: 0, Spin: Singlet’. Then the optimized sample molecule was calculated (Cal Freq) with the command typed as ‘freq=readisotopes’ in the ‘Additional Keywords’ bar and also the ‘H’ at N3 position was changed to ‘D’.

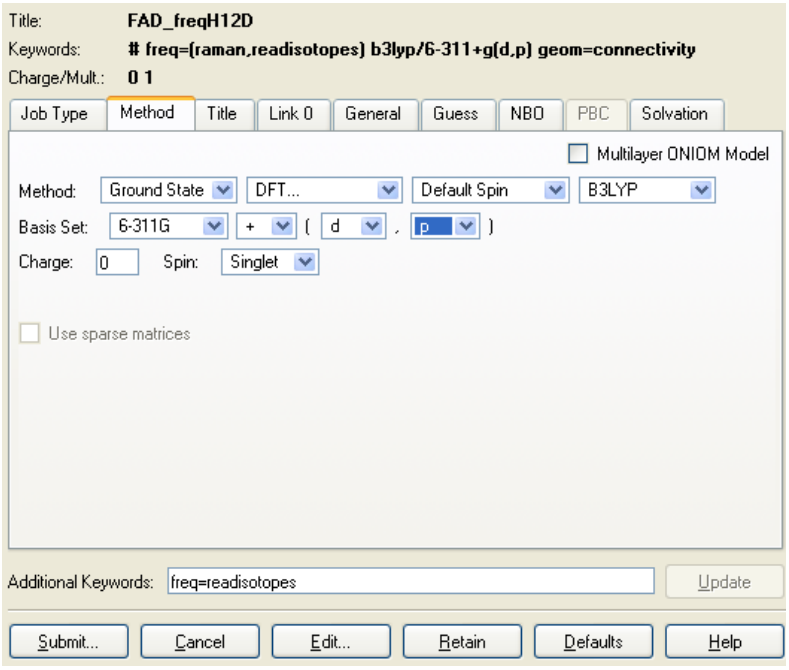

Fig. 2.16 An example of Gaussion DFT settings of a FAD caulculation

The oxidized FAD, two fully reduced states ($FADH_2$ and $FADH^-$), radical states ($FADH^\bullet$ and $FAD^{\bullet-}$) as well as the methylated radical state ($FADCH_3^\bullet$) were calculated with Gaussian using essentially the same method settings shown in Fig. 2.13. Just The 'Charge' was selected as '0' for oxidized and neutral radical state of flavin ($FADCH_3^\bullet$, $FADH^\bullet$ & $FADH_2$). The 'Multiplicity' which is '2S+1' (Spin is 0) equals to 'Singlet' for the oxidised and fully reduced forms; 'Charge' '-1' was selected for anionic flavin samples ($FADH^-$ & $FAD^{\bullet-}$) and the 'Multiplicity' was changed to 'Doublet' (spin is 1/2) for the radicals.

For some cases, specific water solvent molecules were introduced to the calculation. For example we put two D_2O molecules close to the two carbonyl bonds (as shown in Fig. 2.17 a) to calculate the effect of hydrogen bonding on the spectra. The other settings and calculations are the same as described above. One example of the Gaussian simulated spectra of FAD oxidised state are shown in Fig. 2.17 b. As we introduce the solvent molecules to the C_2 and C_4 carbonyls of FAD, a down shift of the relative bands were observed due to the hydrogen bond formed with the solvents.

(a)

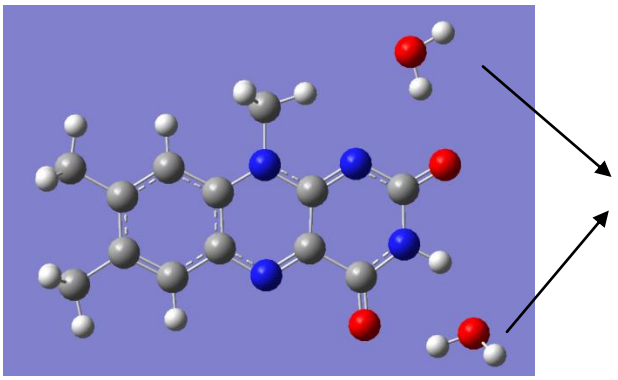

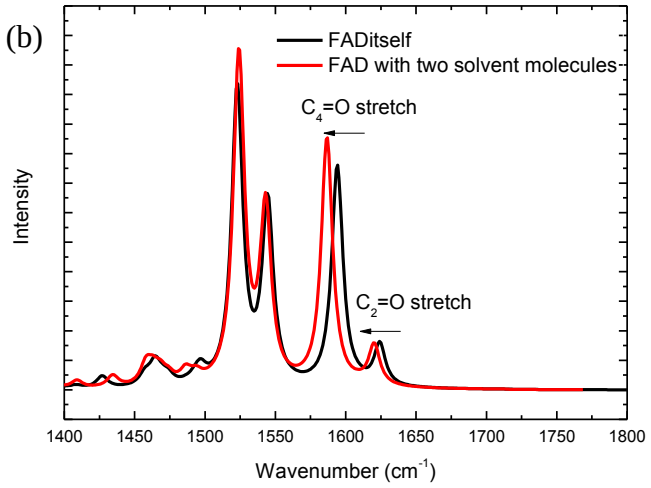

Fig. 2.17 Gaussian input molecule of FADox with two D_2O molecules added (a) and the gaussian calculated spectra with the solvent introduced shifts (b)

The comparison of polarisation resolved TRIR measurements and Gaussian calculated vibrational transition moments were used to further check assignments. The angle θ_{expt} between vibrational and electronic transition moments can be measured in TRIR. These are obtained from the ratio of the change in absorbance with the excitation polarization aligned parallel ($\parallel$) and perpendicular ($\perp$) to the probe polarization, such that the degree of polarisation $D = (\Delta A_{\parallel})/(\Delta A_{\perp})$. The angle between the electronic transition moment of the chromophore and the transition dipole moment of a vibrational mode: θ can be determined using the equation 2.3:

$$\cos\theta = \left(\frac{2D-1}{D+2}\right)^{1/2} \qquad 2.3$$

In which D can take values between 0.5 ($\theta = 90^o$) and 3 ($\theta = 0^o$). One example of the polarisation resolved TRIR measurements of $FADH^-$ is shown in Fig. 2.18 below: the spectrum measured at magic angle 57.4^o is in between the two spectra measured at polarisation condition 0^o (parallel) and 90^o (perpendicular) respectively, as it should be.

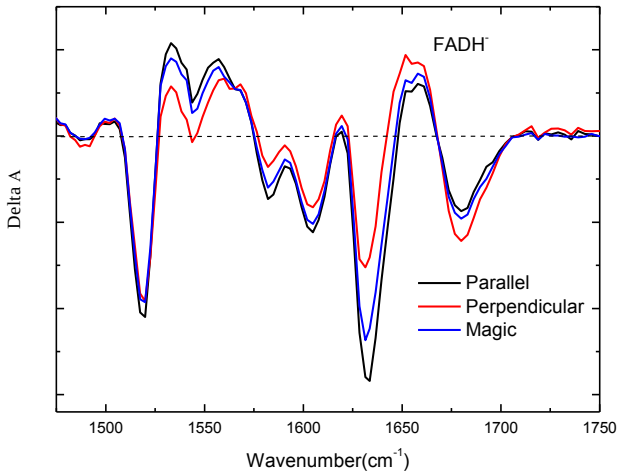

Fig. 2.18 Polarisation resolved TRIR measurements of fully reduced flavin $FADH^-$ at 3ps

These data can be compared with DFT calculated vibrations, knowing that the oxidized FAD molecule has its electronic transition moment along a line connecting the C_4 and C_9 atoms (Fig. 2.19) [9, 10].

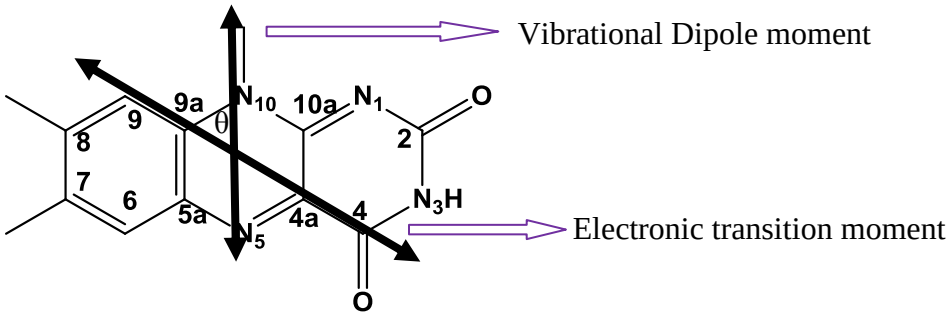

Fig. 2.19 Schematic of calculated θ angle of FAD oxidized molecule

In contrast both $FADH_2$ and $FADH^-$ have their electronic transition moment oriented approximately along a line connecting N_{10} and N_5 atoms (Shown in Fig. 2.20) [11], and the transition dipole moment for any given vibrational band can be obtained from the calculation, the angle between them is the θ_{cald}. One example of the comparison of θ_{cald} and θ_{expt} for sample $FADH^-$ is summarized in table 2.3.

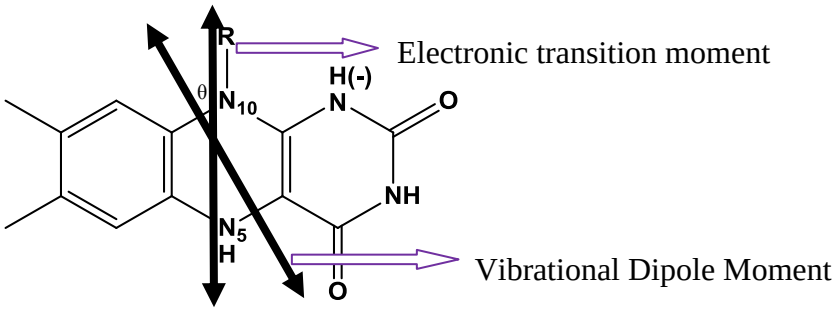

Fig .2.20 Schematic of calculated θ angle of $FADH_2$ or $FADH^-$ molecule

Experimental (cm^{-1})	D	θ_{expt} (^{o})	θ_{cald} Gas/Solvents
1517	1.06817	52	54/60
1578	2.01618	29	20/26
1601	1.29987	45	50/36
1633	2.01549	29	30/20
1679	0.6524	70	70/78

Table 2.3. Comparison of θ_{expt} and θ_{cald} for $FADH^-$ at 3ps

References:

[1] Eisenberg, A. S. and Schelvis, J. P. M. (2008) *Journal of Physical Chemistry A 112,* 6179-6189.

[2] Kao, YT., Saxena, C., He, TF. , Guo, L., Wang, L. , Sancar, A. and Zhong, D. (2008) *Journal of the American Chemical Society 130(39)*, 13132-13139.

[3] Massey, V. (2000) *Biochemical Society Transactions 28(4),* 283-296.

[4] Pan, J.B.M., Aubert, C., Eker, A. P. M., Brettel, K. and Vos, M. H. (2004) *Journal of Physical Chemistry B 108(28)*, 10160-10167.

[5] Massey, V.P and Palmer, G. (1966) *Biochemistry 5(10)*, 3181-3189.

[6] Lukacs, A., Zhao R. K., Haigney, A., Brust, R., Greetham, G. M., Towrie, M., Tonge, P. J. and Meech, S. R. (2012) *Journal of Physical Chemistry B 116*, 5810−5818

[7] Rendell, D. (1987) *Fluorescence and Phosphorescence (Analytical Chemistry by Open Learning)*, Crown.

[8] Berera, R., Van Grondelle, R. and Kennis, J.T. (2009) *Photosynthesis Research 101*, 105-118.

[9] Kondo, M., Ronayne, K. L., Stelling,A.L., Tonge, P. J. and Meech, S. R. (2006) *Journal of Physical Chemistry B 110(41)*, 20107-20110.

[10] Johansson, L.B.A., Davidsson, A., Lindblom, G. and Razi-Naqvi, K. (1979) *Biochemistry 18*, 4249.

[11] Siddiqui, M.S.U, Kodali, G. and Stanley,R.J. (2008) *Journal of Physical Chemistry B 112*, 119-126.

[12] Frisch, M. J.; Trucks, G. W.; Schlegel, H. B.; Scuseria, G. E.; Robb, M. A.; Cheeseman, J. R.; Scalmani, G.; Barone, V.; Mennucci, B.; Petersson, G. A.; Nakatsuji, H.; Caricato, M.; Li, X.; Hratchian, H. P.; Izmaylov, A. F.; Bloino, J.; Zheng, G.; Sonnenberg, J. L.; Hada, M.; Ehara, M.; Toyota, K.; Fukuda, R.; Hasegawa, J.; Ishida, M.; Nakajima, T.; Honda, Y.; Kitao, O.; Nakai, H.; Vreven, T.; Montgomery, Jr., J. A.; Peralta, J. E.; Ogliaro, F.; Bearpark, M.; Heyd, J. J.; Brothers, E.; Kudin, K. N.; Staroverov, V. N.; Kobayashi, R.; Normand, J.; Raghavachari, K.; Rendell, A.; Burant, J. C.; Iyengar, S. S.; Tomasi, J.; Cossi, M.; Rega, N.; Millam, J. M.; Klene, M.; Knox, J. E.; Cross, J. B.; Bakken, V.; Adamo, C.; Jaramillo, J.; Gomperts, R.; Stratmann, R. E.; Yazyev, O.; Austin, A. J.; Cammi, R.; Pomelli, C.; Ochterski, J. W.; Martin, R. L.; Morokuma, K.; Zakrzewski, V. G.; Voth, G. A.; Salvador, P.; Dannenberg, J. J.; Dapprich, S.; Daniels, A. D.; Farkas, Ö.; Foresman, J. B.; Ortiz, J. V.; Cioslowski, J.; Fox, D. J. Gaussian, Inc., Wallingford CT, 2009.

Chapter 3 Ultrafast transient mid IR to visible spectroscopy of fully reduced flavins

3.1 Introduction

As described in Chapter 1 it was established recently that a number of flavoproteins are involved in a range of blue light regulated processes, including phototropism, through Light-Oxygen-Voltage (LOV) domain proteins [1,2], DNA repair (through photolyase) [3,4], and gene expression involving blue light using FAD, BLUF domain proteins [5,6]. The role of these flavoproteins in light activated processes involves blue light absorption by the isoalloxazine ring of FAD or FMN. However, the mechanism of this blue light action is still not fully known, and is currently under study by transient spectroscopy. In this chapter I will measure the TRIR and UV-Vis transient spectroscopy of the flavin chromophore in its different redox states as an aid to the interpretation of the data measured in proteins.

Previous research has been done on the electronic spectroscopy of FMN and FAD in their oxidized, fully reduced and semi-quinone states, in aqueous solution and in proteins by a number of groups [8-12]. In these studies the transient behavior was observed through ultrafast electronic spectroscopy. However, there was no studies on transient vibrational spectroscopy of these states have been reported. Such studies are important for two reasons: 1) vibrational spectroscopy yields a more definite assignment of an intermediate than the rather broad featureless spectra of reduced or oxidized flavins in solution; 2) if individual modes can be assigned, the spectral shifts observed between aqueous solution and protein, and between different mutants of the same protein, will yield information on factors such as the H-bonding state and conformation of the flavin in its binding site. From our previous research [13], transient measurements have been reported for oxidized FAD and the photoactive protein AppA, which revealed significant differences between the dark adapted and signaling forms of the protein. The search for potential intermediates will require spectroscopy of reduced forms of FAD.

The chemical structures of FAD in its two fully reduced states are shown in Fig. 3.1. There is equilibrium between these two states with a dissociation constant pK_a of 6.7. In

this chapter, we present a systematic study of excited-state dynamics of the flavin molecule: FAD and these two fully reduced hydroquinones: neutral $FADH_2$ and anionic $FADH^-$, using mid-IR transient absorption spectroscopy. Ground and excited state frequencies of the characteristic carbonyl modes are observed and assigned with the aid of DFT calculations. Excited state decay and ground state recovery dynamics of the two states are reported.

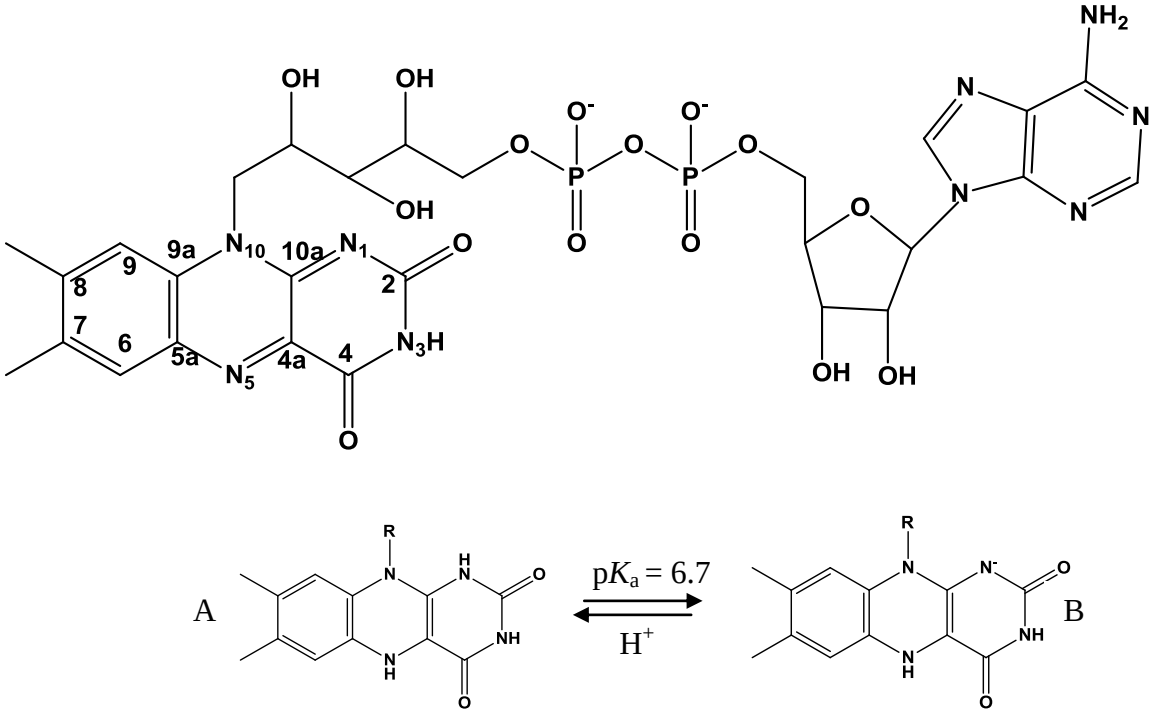

Fig. 3.1. Chemical structures of FAD and two flavohydroquinones (Fully reduced forms) $FADH_2$ (A) and $FADH^-$ (B) (Only the isoalloxazine ring is shown for clarity).

3.2 Materials and Experimental Methodology

3.2.1 Sample preparation and Steady State Measurements

FAD was purchased from Sigma-Aldrich and used without further purification. Anionic hydroquinone ($FADH^-$) and a neutral hydroquinone ($FADH_2$) forms were generated according to the methods described in Section 2.1.1. Complete reduction was confirmed by absorption spectra (Fig. 2.3, Chapter 2). Fluorescence spectra were measured using the FluoroSENS Fluorimeter the samples were excited at 360 nm for reduced states and 400 nm for the oxidized state. The emission spectra for the fully reduced forms are very

weak and were recovered only after the solvent Raman were subtracted (Fig. 2.3, Chapter 2). The FTIR spectra were recorded with the reduced samples being first prepared and loaded into the *Harrick* Demountable Liquid IR Cell inside the anaerobic bag. The oxidized sample was made normally in the lab when exposed to the air. The settings for the FTIR measurements are introduced in Section 2.2.3.

3.2.2Transient Optical Absorption Spectroscopy

Ultrafast transient optical absorption measurements were performed using the home built ultrafast transient absorption system driven by Lab view data acquisition software. The laser set-up is introduced and illustrated in Section 2.2.5.

3.2.3 TRIR measurements

Time resolved infrared measurements were carried out in the Central Laser Facility (STFC) Rutherford Appleton Lab (Oxford) using a system described in Section 2.2.4. Again the sample preparation for the TRIR measurements was also described there.

3.2.4 DFT Calculations

Calculations were performed as described in section 2.2.6 using Gaussian 03, using B3LYP and the 6-31G basis set. The basis set was chosen for consistency with our calculations on the oxidised FAD. It gave very good agreement with the measured carbonyl frequencies, and was also very successful at reproducing the observed effects of H/D isotope exchange.

3.3 Results and Discussion

The results are described in two parts: first the steady state and transient UV-Vis spectroscopy and then the infra-red data.

3.3.1 Optical Spectroscopy

Fig. 3.2 shows the absorption and emission spectra for $FADH^-$ and $FADH_2$, compared with those for FAD_{OX}. These data were also shown in Chapter 2 to illustrate sample preparation and characterisation. The spectroscopy will be described here. The oxidised form exhibits two broad absorption bands, peaks at 450 nm and 375 nm. The emission peak of oxidized flavin is around 530 nm when excited at 400 nm, and the emission is strong. The fluorescence quantum yield of FAD has been reported as 0.03 and for FMN as 0.26 [14, 15]; the origin of the difference is the intermolecular quenching between flavin isoalloxazine and the adenine moiety in the case of FAD [14]. The emission spectra of fully reduced anionic and neutral flavins ($FADH^-$ and $FADH_2$) are consistent with those previously reported by Kao *et al* [9]: Upon 360 nm-excitation, we observed fluorescence emission peaking at 455 nm for anionic hydroquinone ($FADH^-$) and at 480 nm for neutral hydroquinone ($FADH_2$). Kao *et al* also observed the excitation wavelength dependent fluorescence emission for these two fully reduced states, but it was not observed in our measurements.

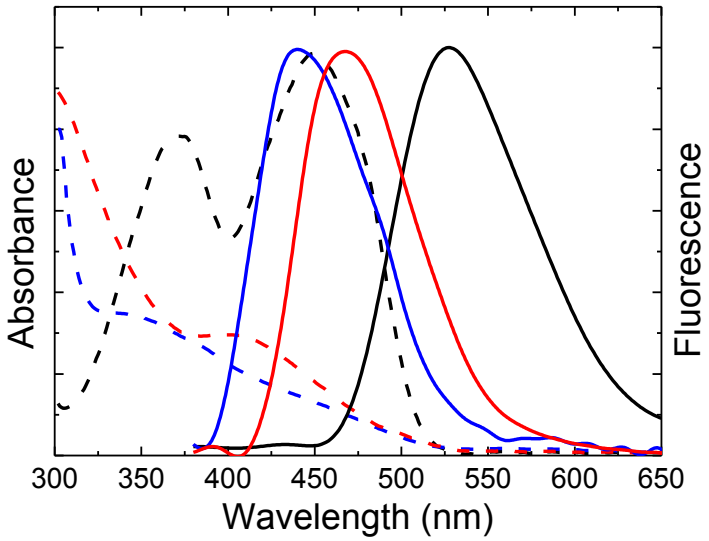

Fig. 3.2. Electronic absorption (dash lines) and emission (solid lines) spectra for FAD_{OX} (Black) and its reduced forms $FADH^-$ (blue) and $FADH_2$ (red), Emission spectra were recorded following excitation at 400 nm (FAD_{OX}) or 360 nm (reduced forms).

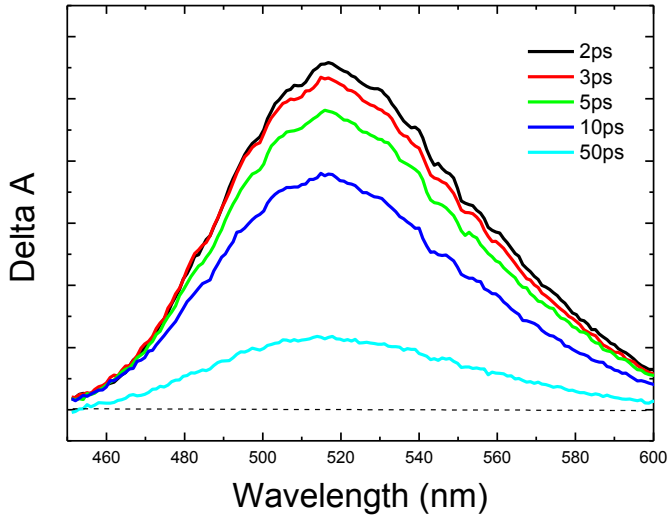

Fig. 3.3. Transient absorption spectra of $FADH^-$, the excitation wavelength was 400 nm.

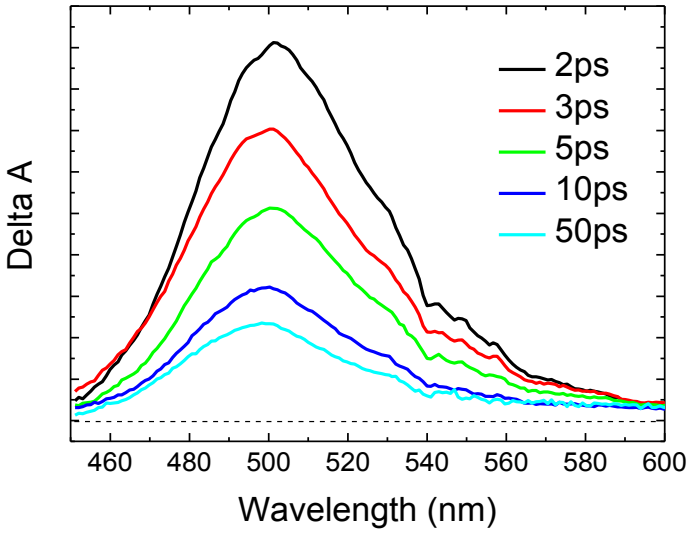

Fig. 3.4. Transient absorption spectra of $FADH_2$, the excitation wavelength was 400 nm.

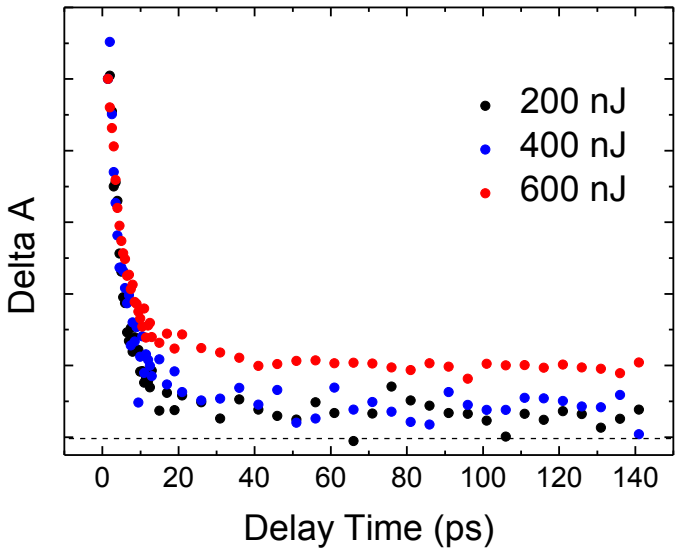

Fig. 3.5 Intensity dependent relaxation of the transient absorption signal at 500 nm of $FADH_2$ as a function of energy/pulse (Black, 200 nJ, Blue 400 nJ, Red 600 nJ).

Fig. 3.3 and 3.4 display the time resolved transient absorption spectra of $FADH^-$ and $FADH_2$ respectively. Both the spectra are dominated by a broad excited state absorption band (positive delta absorbance) which decays with time without any spectral shift. Fig. 3.5 presents the power dependence of this band for the $FADH_2$ sample. As can be seen, with pulse energies in excess of 500 nJ a long lived (> 5 ns) transient absorption was observed. When the energy per pulse was reduced this transient band disappeared. From these data we conclude the long lived state to be a transient which is induced by multi-photon absorption. Brazard *et al* [8] found similar results for the sample of $FADH^-$. They assigned the transient absorption to a combination of the neutral radical product and solvated electron. It is likely that a similar long lived transient is observed here for $FADH_2$ which is related to the reduced flavin cation and solvated electron, but no further investigation of the multi-photon induced transient was made. We conclude that multi-photon ionisation/electron ejection of the reduced forms probably occurs and the excitation energy was kept at 200 nJ per pulse for all subsequent measurements to avoid this. It is also worth noting that there might be other long lived states underlying the multiphoton induced product. For example Kao *et al* [9] reported long lived decay

components in the emission of $FADH_2$. However, our data provide evidence to suggest these will be at most minor components. Both excited state absorption and ground state recovery (see TRIR data below) are effectively complete in <100 ps for both $FADH_2$ and $FADH^-$, suggesting a very low population for any long lived transient.

The excited state decay kinetics for both $FADH^-$ and $FADH_2$ were analysed by fitting of the broad transient band at wavelengths between 470 nm and 560 nm. There was no wavelength dependence detected for either of the reduced forms, which is consistent with the decay of a single state. However, the decay of the excited state population departs from single exponential kinetics and a multiple-exponential fit for both the reduced forms was needed. This departure was slight for $FADH_2$ in which a fast excited state decay dominates (4±1 ps with a weight of >0.9 and 20 - 30 ps with a weight <0.1) but more marked for the case of $FADH^-$ where the decay times are 4 ps (weight ~0.3) and 20 - 30 ps (~0.7) respectively (Fig. 3.6, Table 3.1); the kinetics observed here for $FADH^-$ in H_2O are in good agreement with the report of Brazard *et al*, who found 5.5 ps and 32 ps components [8]. Since no wavelength dependence in the decay was observed on the picosecond time scale, the decay of $FADH^-$ must reflect a genuinely non single exponential evolution of the excited state population. One plausible assignment for this is the presence of two (or more) forms of the ground state of $FADH^-$, with different excited state lifetimes. This is unexpected, but may suggest different H-bonding environments.

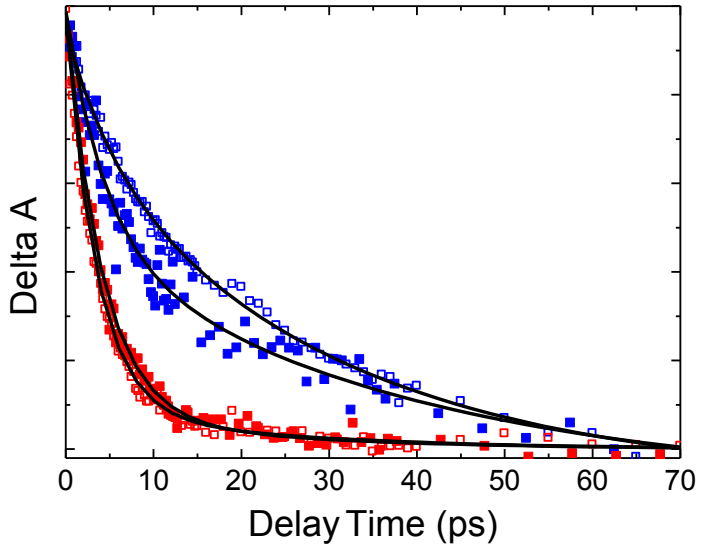

Fig. 3.6 Deuterium isotope effect on the transient absorption of $FADH/D_2$ (red) and $FADH/D^-$ (blue) at 500 nm (Open symbols H, Filled D) with the fitting lines in black.

	Solvent	A_1	τ_1/ps	A_2	τ_2/ps	τ_{single}/ps
$FADH^-$	H_2O	0.24	5.3±0.7	0.76	29±1.4	24±3.2
$FADD^-$	D_2O	0.30	3.7±0.6	0.70	20±2.1	15±2.1
$FADH_2$	H_2O	0.92	3.5±0.1	0.08	32±2.3	5.8±0.2
		1.00	3.9±0.5			
$FADD_2$	D_2O	0.91	4.1±0.2	0.09	23±3.4	5.6±0.3
		1.00	4.6±0.4			

Table 3.1 Transient optical absorption decay kinetics fit to a sum of two exponential terms (the corresponding single exponential fits for $FADH_2$ is also shown)

Even more unexpectedly we can see from Fig 3.6 and Table 3.1 that there is a previously un-reported solvent isotope effect on the excited state decay of $FADH^-$: When H_2O is exchanged for D_2O there is a significant *decrease* in the mean lifetime; this can be thought of as an anomalous or an inverse kinetic isotope effect. In normal cases of the kinetic isotope effect, the reaction will go slower when H_2O exchanged for D_2O) [16, 17]. This decrease is reflected as decreasing both short and long relaxation times (Table I), so

all ground states seem equally effected. Also the absorption spectrum is unchanged when the solvent is changed from H_2O to D_2O, suggesting that it is the same ground state (or distribution of ground states) which exists in both H_2O and D_2O solutions. Consequently, these observations indicate an effect of isotope exchange on the radiationless relaxation rate of $FADH^-$. The decay of $FADH_2$ is unaffected by H/D exchange.

The mechanism of radiationless decay that was proposed to explain the weakly emissive nature of reduced flavins was rapid internal conversion. It is known that the fully reduced flavin has a bent ground state structure as shown in DFT calculation (Fig. 3.7). It was suggested that it should therefore have the 'butterfly' motion in which the ring 1 and ring 3 wag about the axle of ring 2.

Fig.3.7. Bent structure of reduced flavin of $FADH^-$ and $FADH_2$

It was proposed that excited state decay occurs via a conical intersection reached as a result of motion along this 'butterfly' inversion coordinate of the bent isoalloxazine ring [9]. This mechanism has been supported by the observation that the excited state decay time becomes longer when the solvent viscosity is increased; we will return to this topic when we discuss the temperature dependent data in Chapter 5, where the fluorescence in the glass phase is found to be complex, but still weak, inconsistent with the butterfly mode. Further, it is not really apparent that such a low frequency mode involving motion of all the atoms in the chromophore would be sensitive to H/D exchange. Consequently we propose that the radiationless decay rather involves a significant contribution from either an H-bonding mode or XH bond in the radiationless relaxation coordinate.

It is also interesting to note that we observe the "inverse" nature of the isotope effect – the deuterated form has the faster excited state decay times. In detail, the normal isotope effect, which is the slow reaction for the deuterated form, arises when there is a weakening of an XH bond in the reactive state. The opposite effect happens when there is a strengthening of a bond – called an anomalous deuterium isotope effect [16, 17]. Therefore an increase in the strength of a solvent-solute H-bond on electronic excitation can be considered as a reasonable assignment of the effect observed. It may be significant that the effect is only found for $FADH^-$, which has an unprotonated N atom, which is capable of forming H-bonds to the surrounding solvent molecules (Fig. 3.1). Moreover, this phenomenon has implications for photoactivity in flavoproteins, where the flavin has a rather specific H-bonding environment. Thus it is plausible to expect that the excited state decay of $FADH^-$ may be sensitive to the H-bonding environment in the protein.

3.3.2 Infra-red Spectroscopy

Fig. 3.8 illustrates the experimental steady state IR spectra of FAD_{OX} and its two fully reduced forms. The primary interest in the IR spectra is in the carbonyl frequency range, which is strong in the IR (at least for FAD_{OX}) and the frequency is a good indication of the strength of H-bonding interaction with the flavin environment [18]. It is notable that at least the highest frequency carbonyl modes are shifted down to lower frequency for the reduced flavins (see also Table 3.2).

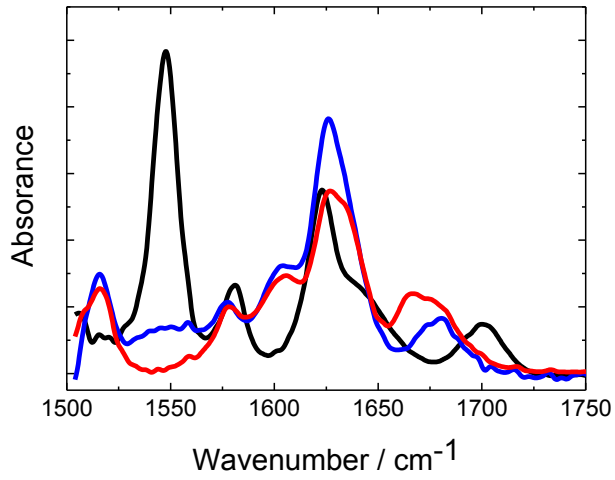

Fig. 3.8 Steady state Infra-Red spectra: FAD_{OX} (black); $FADH^-$ (blue); $FADH_2$ (red).

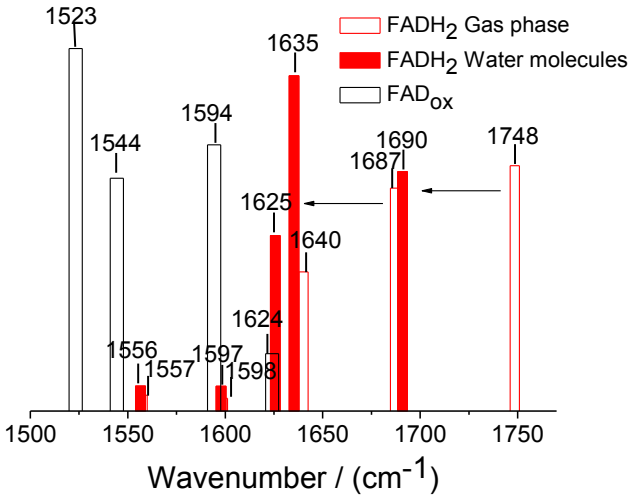

Fig. 3.9 Frequency and amplitude of DFT calculated IR spectra for $FADH_2$; empty boxes gas phase, solid solvated by two water molecules at the carbonyls.

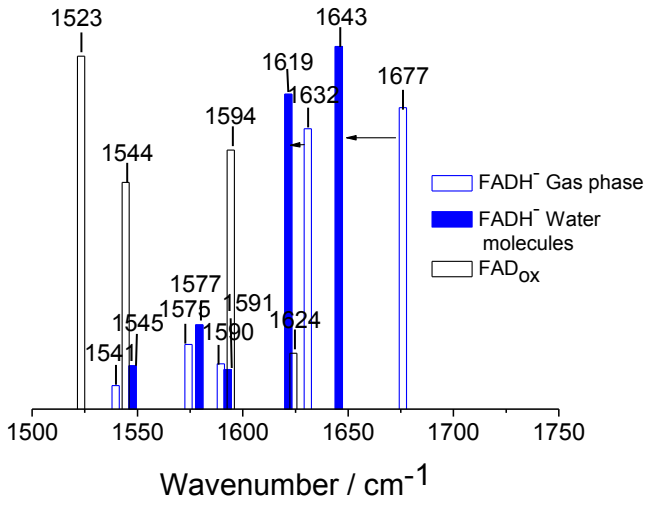

Fig. 3.10 Frequency and amplitude of DFT calculated IR spectra for $FADH^-$; empty boxes gas phase, solid solvated by two water molecules at the carbonyls.

In Fig. 3.9 and 3.10, the IR spectra calculated by DFT are shown for the reduced forms of the flavins. Calculations were made for the isolated molecule in the gas phase and also with two H-bonded solvent water molecules introduced, placed close to the carbonyl oxygen atoms (Fig. 2.17, Chapter 2). The results are presented in Table 3.2 along with the assignments (based on the DFT calculations). According to these calculations the highest and next highest frequencies in the IR spectra are assigned to carbonyl stretches correspond to the C_2=O and the C_4=O bonds (Fig.1.7 Chapter 1). In each case the carbonyl stretch also involves the N_3H wagging motion. The third relatively intense mode near 1600 cm^{-1} is assigned by DFT to the stretch of the C_{4a}=C_{10a} double bond. Exchange of H for D on the N atoms leads to a slight change in the nature of the carbonyl mode from largely isolated on their respective C=O stretches to a coupled symmetric or anti-symmetric motion of both carbonyl bonds. The addition of solvent water molecules at the carbonyl groups leads to a significant downshift of the calculated carbonyl frequencies, bringing them into closer accordance with experiment.

Experimental/ cm^{-1} ($FADH_2$)	Assignment	DFT/cm^{-1} $(H_2O)_2$ solvated/Gas phase	Experimental/ cm^{-1} ($FADH^-$)	Assignment	DFT/cm^{-1} $(H_2O)_2$ solvated/Gas phase
1517	Iso ring 1st	1556/1557	1517	Iso ring 1st	1545/1541
1578	Iso ring 2nd	1597/1598	1578	Iso ring 2nd	1577/1575
1601	C_{4a}=C_{10a} stretch	1625/1640	1601	C_{4a}=C_{10a} stretch	1591/1590
1636	C4=O stretch with N_3H wag	1635/1687	1633	C4=O** stretch with N_3H wag	1619/1632
1676	C2=O with N_1H+N_3H wag	1690/1748	1679	C2=O* with N_3H wag	1643/1677

*On deuteration this mode includes anti-symmetric stretch of the C_4=O mode. **On deuteration this mode includes symmetric stretch of the C_2=O mode.

Table 3.2. Comparison of measured and calculated vibrational frequencies and assignments.

In order to check the veracity and consistency of the calculations, we compared the calculated θ angle and experimentally determined value for the two fully reduced flavins (see Section 2.2.6). The agreement between theory and calculation is good and also can give more confidence in the calculation; the data are tabulated in table 3.3 and 3.4.

Experimental (cm^{-1})	*D*	θ_{expt} (^{o})	θ_{cald} Gas/Solvents	Assignment	DFT (cm^{-1}) Gas/Solvents
1517	1.1583	49	/50	Iso ring 1st (C_{10a}=N_1&C_{4a}=N_5 in FAD_{ox})	1556/1557
1578	3.23041	23	25/26	Iso ring 2nd	1597/1598
1601	1.43019	42	70/50	C_{4a}=C_{10a} (New double bond)	1625/1640
1636	1.74059	35	30/26	C_2=O, C_4=O anti-sym	1635/1687
1676	0.7732	63	60/65	C_2=O, C_4=O sym	1690/1748

Table 3.3.Comparson of θ_{expt} and θ_{cald} for $FADH_2$ at 3ps

Experimental (cm^{-1})	*D*	θ_{expt} (^{o})	θ_{cald} Gas/Solvents	Assignment	DFT (cm^{-1}) Gas/Solvents
1517	1.06817	52	/60	Iso ring 1st (C_{10a}=N_1&C_{4a}=N_5 in FAD_{ox})	1545/1541
1578	2.01618	29	20/26	Iso ring 2nd	1577/1575
1601	1.29987	45	50/36	C_{4a}=C_{10a} (New double bond)	1591/1590
1633	2.01549	29	30/20	C_2=O, C_4=O anti-sym	1619/1632
1679	0.6524	70	70/78	C_2=O, C_4=O sym	1643/1677

Table 3.4. Comparison of θ_{expt} and θ_{cald} for $FADH^-$ at 3ps

3.3.3 Time resolved infra-red spectroscopy

Fig. 3.11 presents the transient IR absorbance difference spectra recorded 3 ps after excitation for both fully reduced flavins. Negative values of ΔA which appear instantaneously upon excitation correspond to vibrations of the bleached ground state, while positive bands reflect those of the excited state. By combining the steady state spectra (Fig. 3.7) and transient difference spectra (Fig. 3.11), we can recover the IR spectrum of the first excited singlet state.

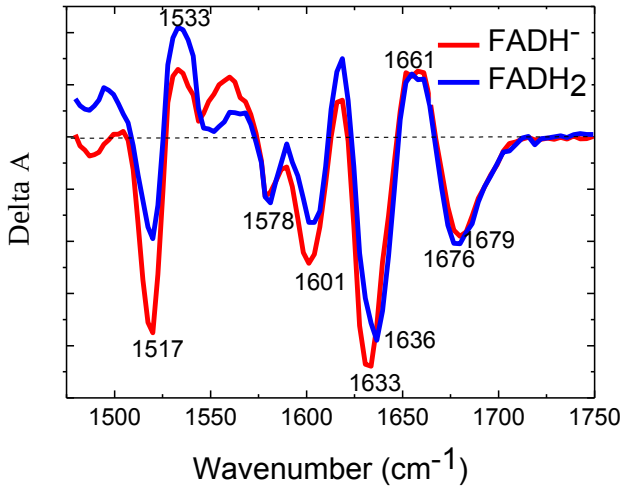

Fig. 3.11. Transient IR difference spectra recorded 3 ps after excitation for $FADH^-$ and $FADH_2$

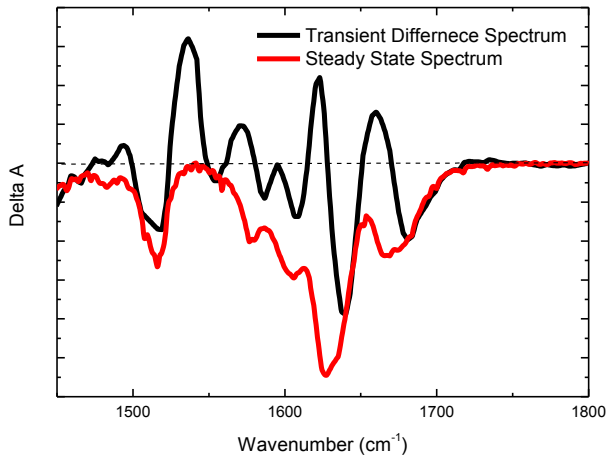

Fig. 3.12 Example of $FADH_2$ subtractions to acquire the excited state spectrum

We firstly normalize the ground state spectrum to the transient difference spectrum on the highest frequency edge (assumed to represent pure ground state bleach of the carbonyl, as shown in Fig. 3.12) and then subtract the two spectra from one to another. This is not quite straightforward for FAD_{OX} and its reduced forms as the adenine moiety contributes to the ground state absorption spectrum but not to the difference spectrum (because it is

not bleached by electronic excitation, as it is not part of the chromophore). By separately recording the IR spectra of adenosine and subtracting its contribution from the spectra, it is then possible to recreate the IR spectrum of FAD reduced forms in the S_1 excited singlet state (Fig 3.13). The C_2=O and C_4=O carbonyl modes both shift down in frequency on excitation, by 15 - 20 cm^{-1} compared with the ground state. Smaller shifts are seen for other modes (mainly ring modes) and a new band appears in the excited state spectrum at around 1530 cm^{-1}, which has no obvious relative in the ground state. Further assignment of these modes requires the study of additional isotopes. Unfortunately TDDFT calculations of excited states are not able to produce accurate calculated vibrational spectra to further test these assignments.

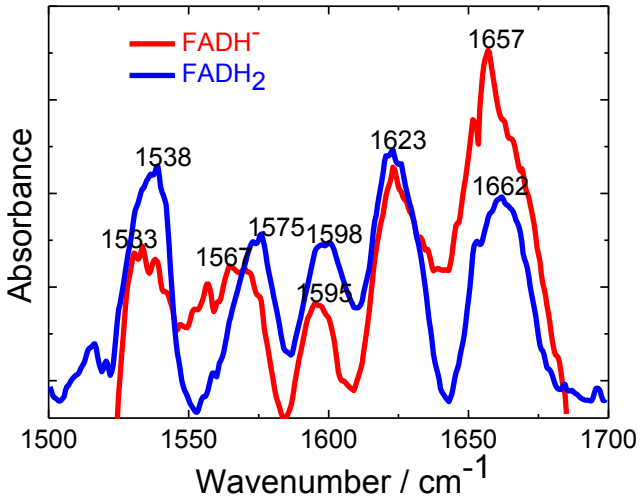

Fig. 3.13. Excited state IR spectra obtained from difference of difference spectra and steady state spectra (corrected for adenosine absorption – introduced in text).

According to the time evolution of the difference spectra shown in both Fig. 3.14 and 3.15, only a monotonic decrease in the strength of either bleach or absorption with time was observed, and there was no shape change. This is consistent with the presence of only two states (excited and ground). The kinetic data are shown in Fig 3.16 which were recorded at wavenumbers corresponding to ground state recovery (bleach at 1635 cm^{-1}) and excited state decay (transient absorption at 1660 cm^{-1}). Both bleach and absorption

reach their maximum value within the pump pulse, indicating that the transient is the excited electronic state of the reduced form, formed directly from the ground state.

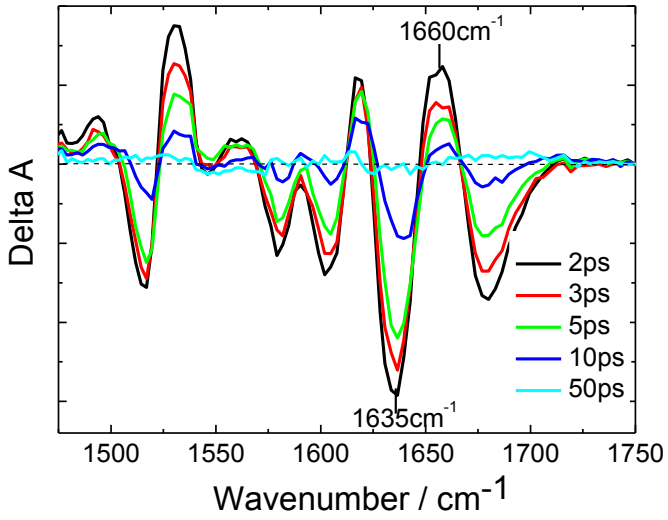

Fig. 3.14 Temporal developments of the IR difference spectra for $FADH_2$ in D_2O.

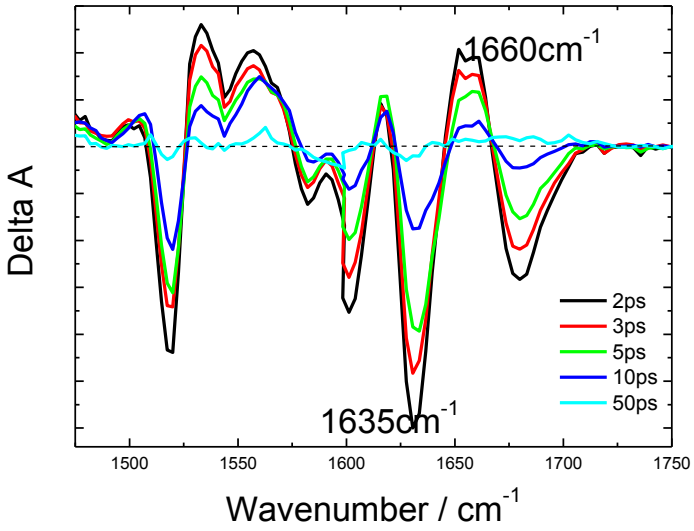

Fig. 3.15 Temporal developments of the IR difference spectra for $FADH^-$ in D_2O.

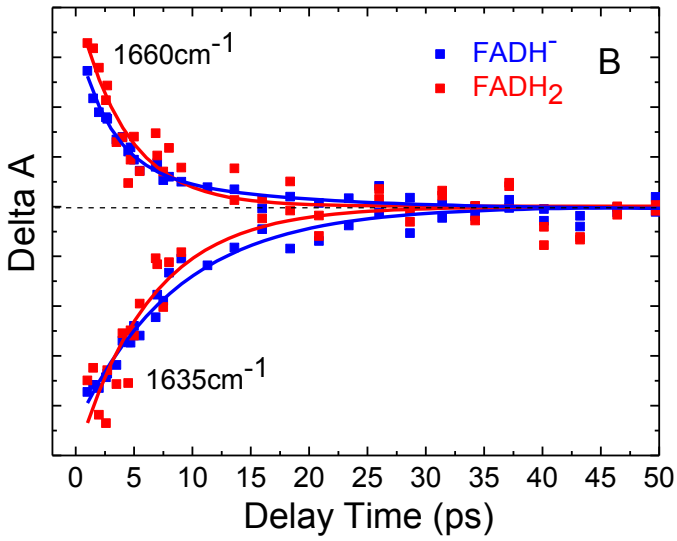

Fig. 3.16 Transient kinetics for $FADH^-$ (blue points) and $FADH_2$ (red points) in D_2O shown at the 1660 cm^{-1} transient absorption and the 1635 cm^{-1} bleach. Fits (solid lines) were made to a single exponential for $FADH_2$ and a sum of two exponentials for $FADH^-$, with the long component fixed at 30 ps.

The decay kinetics of the transient absorption in the vibrational spectrum reflects those observed in the optical measurements (Fig. 3.6). While $FADH_2$ decays in a single exponential relaxation with a 4 ps time constant, $FADH^-$ decays in a bi-exponential process and it can accurately fit with the decay kinetics measured in the transient optical spectra. Fitting data are presented in Table 3.5, the IR data had insufficient signal to noise to accurately extract the amplitude and time constant of the long lived state, so the slower decay constant (though not its amplitude) was fixed at 30 ps. The ground state recovery is complete in <100 ps, which supports $S_1 \rightarrow S_0$ internal conversion as the mechanism of ultrafast radiationless decay [19]. However, the recovery of the ground state is approximately a factor of two slower than the decay of the excited state. This indicates the formation of a short lived transient intermediate during the ground state recovery because a dark state arises from the structural rearrangement in the excited state. However, there is no spectrally distinct intermediate state observed in either transient optical or IR measurements. Alternatively the delayed ground state recovery may arise

from the initial formation of a hot ground state following $S_1 \rightarrow S_0$ internal conversion, which relaxes to the thermalised ground state on the picosecond timescale [20]. The tens of picoseconds timescale is typical for vibrational cooling of large molecules in solution.

TRIR (D_2O) Measurement	Excited Absorbance			
	A_1	τ_1/ps	A_2	τ_2/ps
$FADH_2$	1	4±0.61		
$FADH^-$	0.7	4±0.63	0.3	30

Table 3.5. Lifetimes and pre-exponential factors of time resolved Infra-Red data for $FADH^-$ and $FADH_2$

3.4 Conclusion

This chapter reports the transient IR and electronic spectra of two fully reduced forms of FAD. Measurements of the ground state recovery show that the mechanism of radiationless decay is internal conversion. There is a short lived transient intermediate in the ground state recovery cycle, which is plausibly assigned to a vibrationally hot form of the ground state. The protonated form $FADH_2$ has a faster excited state decay than $FADH^-$ which exhibits an unexpected inverse deuterium isotope effect. This is assigned to an H-bonded mode involved in determining the radiationless relaxation rate. Vibrational modes of the two carbonyl groups were observed and assigned using the DFT calculations. Experimental data also revealed the corresponding frequencies in the excited electronic state. These data can be used to provide the basic data needed to assign transient photon induced electron and proton transfer reactions in proteins which involve the fully reduced flavins.

References

[1] Briggs, W.R. and Huala, E. (1999) *Annual Review of Cell and Developmental Biology 15*, 33-62.

[2] Huala, E., Oeller, P.W., Liscum, E., Han, In-Seob., Larsen, E. and Briggs, W. R. (1997) *Science 278(5346)*, 2120-2123.

[3] Brautigam, C.A., Smith, B.S., Ma, Z., Palnitkar, M., Tomchick, D.R., Machius, M., and Deisenhofer, J. (2004) Proceeding of National Academic Science *(USA) 101*, 12142-12147

[4] Gressel, J. (1979) *Photochemistry and Photobiology 30 (3)*, 749–754.

[5] Fukushima, Y., Okajima, K., Shibata, Y., Ikeuchi, M. and Itoh, S. (2005) *Biochemistry 44(13)*, 5149-58.

[6] Yoshikawa S, S.T., Watanabe M and Iseki M. (2005) *Photochemical and Photobiological Sciensces 4(9)*,727-731.

[7] Gauden.M, Yeremenko, S., Laan, W., van Stokkum, I.H.M., Ihalainen, J.A., van Grondelle, R., Hellingwerf, K.J. and Kennis, J.T.M. (2005) *Biochemistry 44*, 3653-3662.

[8] Brazard, J., Usman, A., Lacombat, F. Ley, C., Martin, M. M. and Plaza, P. (2011) *Journal of Physical Chemistry A 115 (15)*, 3251-3262.

[9] Kao, YT., Saxena, C., He, TF., Guo, L., Wang, L., Sancar, A. and Zhong, D. (2008) *Journal of the American Chemical Society 130(39)*, 13132-13139.

[10] Stanley, R. J. and MacFarlane, A. W. (2000) *Journal of Physical Chemistry A 104*, 6899-6906.

[11] Enescu, M., Lindqvist, L. and Soep, B. (1998) *Photochemistry and Photobiology 68*, 150-156.

[12] Li, G. F. and Glusac, K. D. (2008) *Journal of Physical Chemistry A 112*, 4573-4583.

[13] Stelling, A. L., Ronayne, K. L., Nappa, J., Tonge, P. J. and Meech, S. R. (2007) *Journal of the American Chemical Society 129*, 15556-15564.

[14] Valeur, B. and Brochon, J.C (2001) *New Trends in Fluorescence Spectroscopy: Applications to Chemical and Life Sciences*, Springer, 462-463.

[15] Feenstra, K. A. (2002) PhD thesis: *Long Term Dynamics of Proteins and Peptides*, University of Groningen, Netherland.

[16] Hennig, C., Oswald, R. B. and Schmatz, S. (2006) *Journal of Physical Chemistry A 110*, 3071-3079.

[17] Cleland, W. W. (2003) *Journal of Biological Chemistry 278 (52)*, 51975–51984.

[18] Valle, L., Morán Vieyra, F. E. and Borsarelli, C.D. (2012) *Photochemical & Photobiological Sciences 11*,1051-61.

[19] Zhao, R. K., Lukacs, A., Haigney, A., Brust, R., Greetham, G.M., Towrie, M., Tonge, P.J and Meech, S.R. (2011) *Physical Chemistry Chemical Physics 13*, 17642–17648.

[20] Lukacs, A., Haigney, A., Brust, R., Zhao, R. K., Clark, I., Towrie, M., Greetham, G. M., Meech, S. R. and Tonge, P. J. (2011) *Journal of the American Chemistry Society 133*, 16893-900.

Chapter 4 Ultrafast transient mid IR to visible spectroscopy study of excited state structure and dynamics of the neutral and anionic flavin radicals

4.1 Introduction

Redox properties of flavin molecules enable flavoproteins to have wide diversity in their functions. In photoactive flavoproteins, the blue light absorbing flavin plays an important role in light activation processes. Among the different redox states, the neutral and anionic flavin radicals (Shown in Fig. 4.1), which are the main topic of this chapter, have been suggested to be essential in forming the signalling state of photoactive flavoproteins such as BLUF domain proteins, as described in Figs. 1.1 and 1.2 Chapter 1. Particularly in some ultrafast studies BLUF domain protein was analysed revealing a kinetically complex photocycle with a number of steps occurring on the picosecond time scale [1, 2]. It was suggested that this was connected with an electron transfer reaction on excitation: the initial oxidized flavin cofactor is reduced by a nearby tyrosine protein residue to form the anionic radical state, which then transformed to the neutral protonated state through a proton transfer reaction before finally forming the signaling state. However, our first transient visible and mid IR spectroscopy measurements did not identify any intermediate radical states between dark and light activated signaling state [3, 4].

In this chapter, I will present ultrafast transient absorption measurements in both visible and mid-infrared regions performed on neutral and anionic flavin radicals, both in solution and bound to proteins. These data are compared with the results of Gaussian density functional theory calculations. With these observations we are able to identify specific spectroscopic signatures of potential flavin redox intermediates in various flavoproteins, and to record their formation and decay kinetics. These data were then applied to the analysis of the quenching of oxidized FAD in glucose oxidase (GOx), which has been previously assigned to an electron transfer on the picosecond timescale [3,5]. In this way I aim to characterise the transient spectroscopy of flavin radical states to allow a more accurate interpretation of the BLUF domain transients.

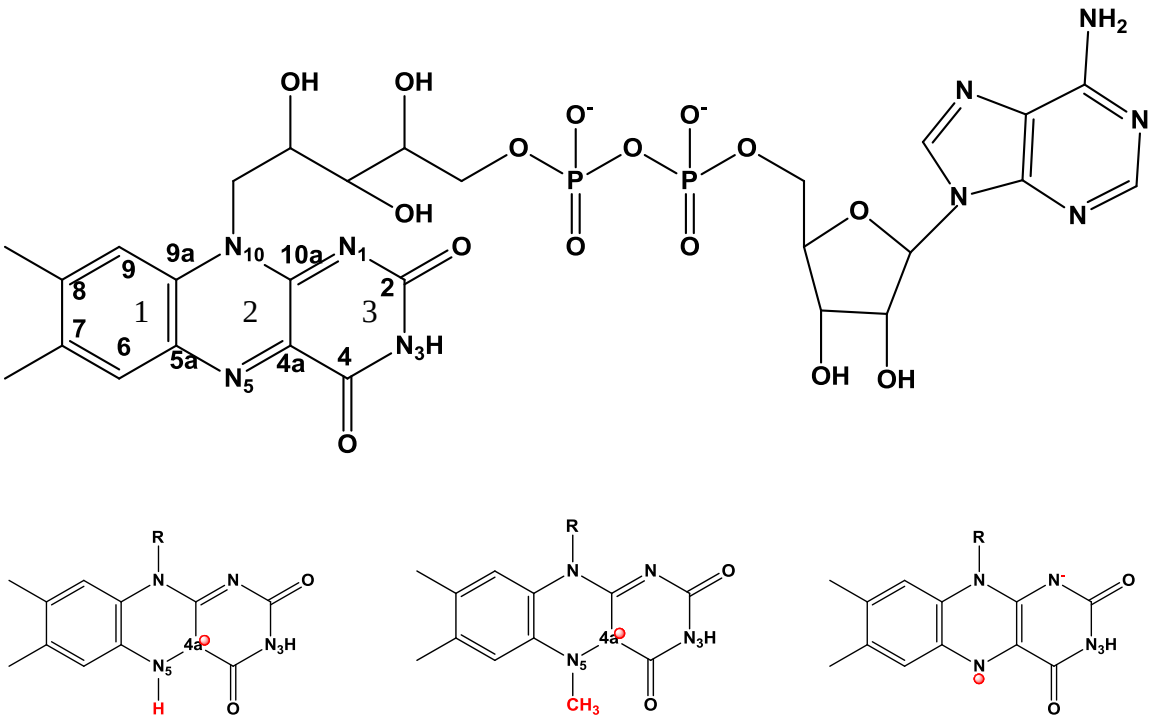

(A) (B) (C)

Fig. 4.1 Chemical structures of FAD and flavoquinones: neutral flavosemiquinone (radical) $FADH^{\bullet}$ (A), synthetic (methylated) $FAD(CH_3)^{\bullet}$ or $FMN(CH_3)^{\bullet}$ radicals (B) and anionic flavosemiquinone (radical) $FAD^{\bullet -}$ (C)

4.2 Materials and Experimental Methodology

4.2.1 Synthesis of neutral N_5-methyl flavin radicals

The 5-methyl FAD radical (5-$CH_3FAD^{\bullet}$) and 5-methyl FMN radical (5-$CH_3FMN^{\bullet}$) were made according to the preparation methods introduced in Section 2.1.3. Complete formation of the radical form and its concentration were determined by UV-Vis spectroscopy. This stable radical allows us to characterise the spectroscopy in buffer solutions.

4.2.2 Synthesis of $FADH^{\bullet}$ in GOX and Flavodoxin

Glucose oxidase (GOx) from *Aspergillus niger* was purchased from Sigma and used without further purification. Flavodoxin from *Desulfovibrio gigas* given by our collaborators was originally stored for a 50 mM MOPS buffer, pH 7.0. Before the time resolved IR (TRIR) measurement the buffer was exchanged in 50 mM phosphate buffer pD 7.0, and the final concentration of the sample was ~150 mM. The semiquinone radical forms of both GOx and flavodoxin were prepared according to the method described in Section 2.1.2.

4.2.3 Time Resolved Infra- Red (TRIR) and Transient absorption measurements

Time resolved infrared measurements were carried out as described in Sections 2.2.4 and 2.2.5.

4.2.5 Density Functional Theory Calculations

Density functional theory (DFT) calculations were performed to assign the measured ground state IR spectra of flavin radical samples. The DFT calculations were performed using the Gaussian 03 software package, B3LYP function and 6-31G (++ d,p) basis set. The 'Multiplicity' which is '2S+1' (Spin is ½ for radicals) equals to 'doublet'was selected for all radical samples, The 'Charge' was selected as '0' for neutral radical state ($FADCH_3^{\bullet}$ and $FADH^{\bullet}$); and '-1' for anionic radical state ($FAD^{\bullet -}$).

H-bonding effects of the solvent were investigated by adding specific water molecules H-bonded to the C_2=O and C_4=O carbonyl oxygen atoms, as was done for the fully reduced forms (Chapter 3). To simulate the experimental data (recorded in D_2O) we exchanged the H atom at the N_3 position for D (As shown in Fig. 4.1). The calculated frequencies were multiplied by 0.96 (recommended scaling factor for the B3LYP/6-31G calculations [6]) in all cases.

4.3 Results and Discussion

According to our previous literature research most flavin radical measurements have been carried out when they are prepared in protein environments, because of the instability of the radical state in solution [7]. However, Eisenberg *et al* [8] managed to measure the vibrational resonance Raman spectra of flavin neutral radicals in solution by stabilizing the radical state through attaching a methyl group to the N_5 atom (Fig. 4.1B). Following this method we successfully performed measurements on 5-CH_3FAD$^\bullet$ and 5-CH_3FMN$^\bullet$ neutral radicals in aqueous solutions using TRIR and visible transient absorption spectroscopy. Further, we made measurements of neutral radicals photochemically generated in GOx and flavodoxin (FADH$^\bullet$ and FMNH$^\bullet$ respectively). By comparing those results, the effect of a protein environment on radical states can be obtained which will be discussed further in the following paragraphs. Electronic absorption spectra of methylated neutral flavin radicals in solution and FADH$^\bullet$/ FMNH$^\bullet$ in GOX / flavodoxin are shown in Fig. 4.2. The FADH$^\bullet$ spectrum in GOx shows two sharp absorption bands peaked at 350 nm and 450 nm with a broad band at 570 nm, which is very different from the other three, which have similar spectra: a sharp band at 350 nm and two partially overlapped board bands at 500 nm and 600 nm. The red shifted features are characteristic of the radical state. The additional features in GOx appear to reflect the existence of a population of unconverted FAD, which remains in the oxidized state.

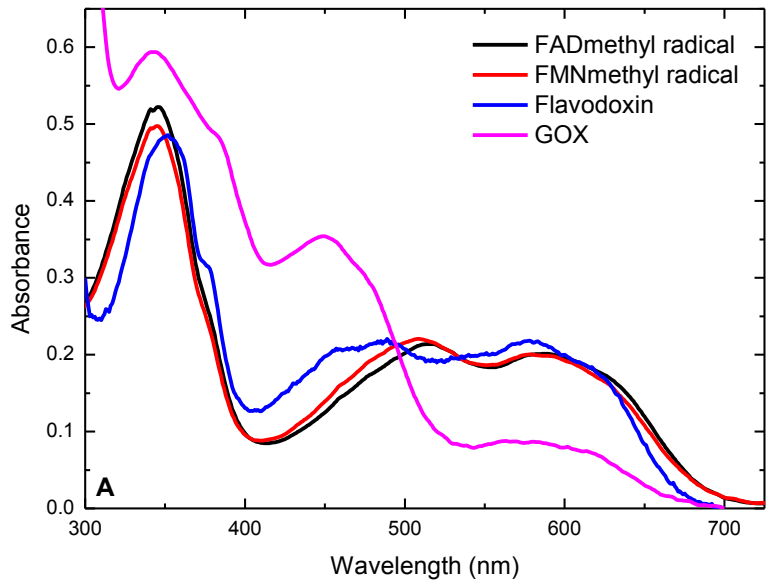

Fig. 4.2 Absorption spectra of $FADH^{\bullet}$/$FMNH^{\bullet}$ in solution, in flavodoxin and glucose oxidase

4.3.1 Transient Vibrational Spectroscopy of Flavin Radicals

As shown in Fig. 4.3, the TRIR spectra of 5-$CH_3FAD^{\bullet}$ and 5-$CH_3FMN^{\bullet}$ are very similar; they both show strong bleaches at 1514 cm^{-1}, 1528 cm^{-1}, 1595 cm^{-1} and 1628 cm^{-1}. However, the bleach appeared in 5-$CH_3FMN^{\bullet}$ at 1664 cm^{-1} was upshifted to ~ 1675 cm^{-1}, and became broader with lower intensity in 5-$CH_3FAD^{\bullet}$. The modes at higher frequencies appear broader for 5-$CH_3FAD^{\bullet}$ than 5-$CH_3FMN^{\bullet}$, and the modes at 1528 cm^{-1} and 1514 cm^{-1} look the same for both the radical cases. The differences between 5-$CH_3FAD^{\bullet}$ and 5-$CH_3FMN^{\bullet}$ suggest some changes due to the interaction between the adenine moiety and the isoalloxazine radical, where FAD oxidized is quenched by an electron transfer reaction between adenine and the flavin ring [9].

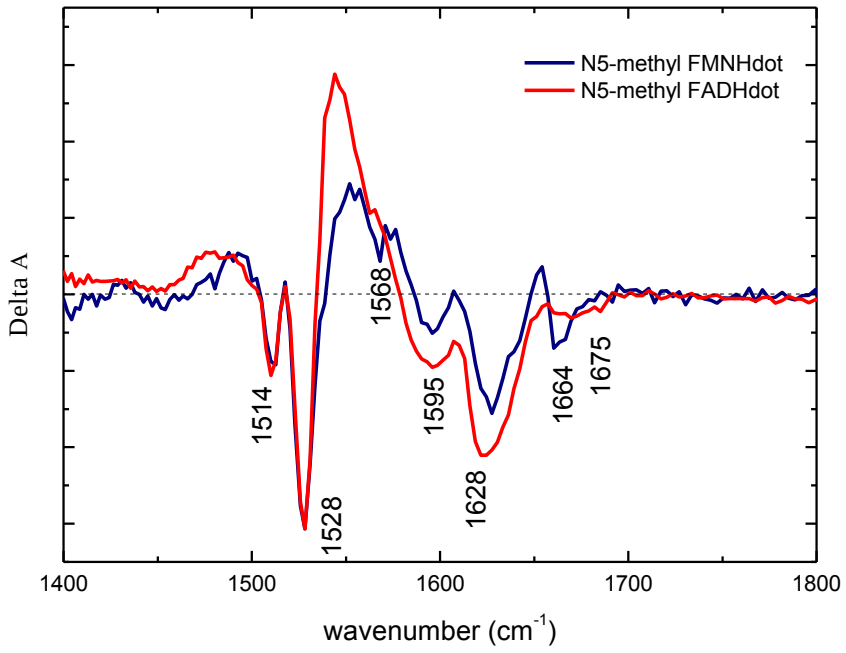

Fig. 4.3 TRIR spectra of N5-methyl FADH$^{\bullet}$ /FMNH$^{\bullet}$ observed at 1 ps delay.

The TRIR measurements on flavodoxin when FMN was in its FMNH$^{\bullet}$ state were performed and the spectra (at 1ps after excitation) are shown in Fig. 4.4 with the spectrum of 5-CH_3FMN$^{\bullet}$ shown for comparison. The spectra of flavodoxin stabilised FMNH$^{\bullet}$ are in good agreement with 5-CH_3FMN$^{\bullet}$: there is a similar ground state bleach at ~1528 cm^{-1}, and excited state absorption at ~ 1552 cm^{-1}. However, the ground state bleach observed at ~1628 cm^{-1} in 5-CH_3FMN$^{\bullet}$ is slightly down shifted for the case of protein, to around 1626 cm^{-1}. The data we observed here, specifically the ground state bleach band at 1628 cm^{-1}, are very useful information in characterising the existence (or not) of the neutral radical state in the BLUF domain photocycle.

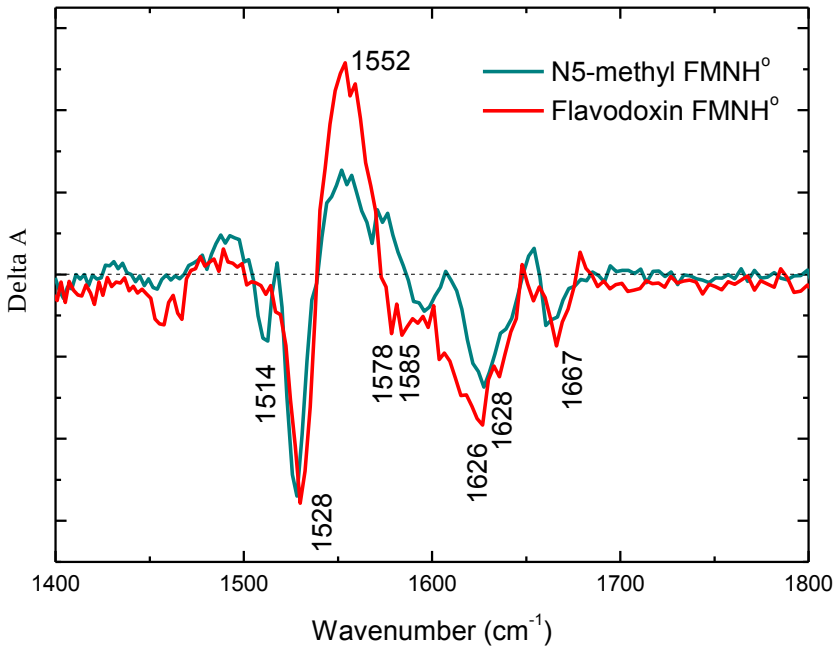

Fig. 4.4 Comparison of TRIR spectra of N5-methyl FMNH$^{\bullet}$ in solution and FMNH$^{\bullet}$ in flavodoxin

DFT calculations were performed on both unmethylated and 5-methylated flavin to compare with the experimentally measured neutral radical states: FMNH$^{\bullet}$ and 5-CH_3FMN$^{\bullet}$, and also to identify and assign the different vibrational modes. To investigate the H-bonding interactions, relevant water molecules were introduced into the calculation, placed close to C_2=O and C_4=O to form any possible hydrogen bonds (Fig. 2.17(a) Chapter 2). The calculated spectra are illustrated in Fig. 4.5, in which the frequency values are generally in very good agreement with the observed experimental values (summarized in Table 4.1). The highest calculated frequencies, 1651 cm^{-1} in the case of the methylated radical, are associated with the highest experimental frequency ~ 1666 cm^{-1} in both 5-CH_3FMN$^{\bullet}$ and flavodoxin-FMNH$^{\bullet}$ (Fig. 4.4). This mode is assigned as a displacement of O=C_2-N_3-C_4=O group, but mainly as C_2=O localised stretch. Calculation data shows this transition is unaffected by methylation, which is consistent with experimental observations (Fig. 4.4). The second highest calculated frequency at

1592 cm^{-1} in the methylated case or 1602 cm^{-1} in the non-methylated case is associated with the experimentally observed bleach at 1628 cm^{-1} and assigned as a mainly C_4=O localised stretch also as involving a O=C_2-N_3-C_4=O groups stretching.

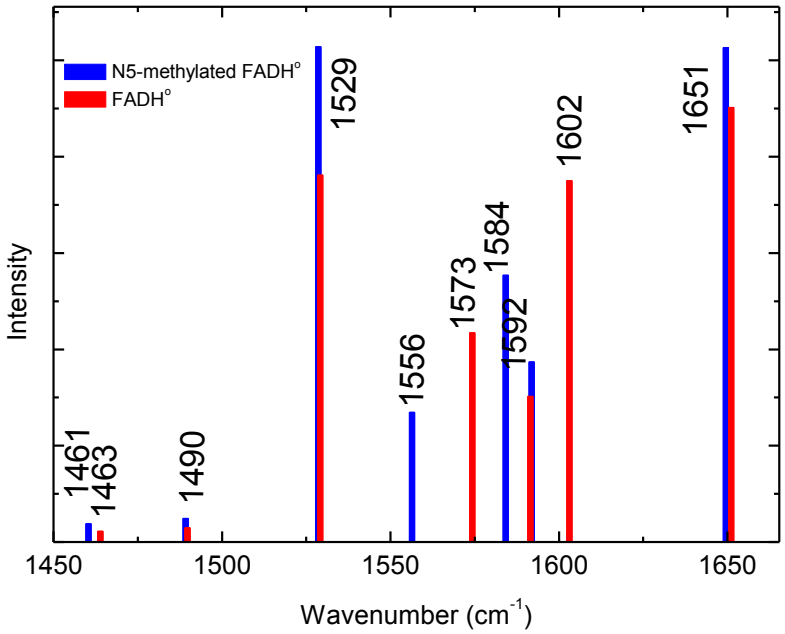

Fig. 4.5 DFT calculations on methylated and non-methylated flavin neutral radical

Measured/cm^{-1}	1666	1628	1595	1568	1528	1514
DFT/cm^{-1}	1651	1592	1584	1556	1529	1490
Assignment	C_2=O loc.	C_4=O loc.	C=O/Ring I	$C_{10a}N_1$/ $C_{4a}N_5$	Ring	Ring

Table 4.1 Mode assignments for the Methylated radical

The experimentally observed ~ 1595 cm^{-1} bleach in the methylated radical and the poorly resolved 1585 cm^{-1} bleach observed in the flavodoxin neutral radical are associated with the calculated 1584 cm^{-1} and 1592 cm^{-1} (non-methylated case) transitions respectively; these modes involve the C_4=O carbonyl stretch and an asymmetric stretch of ring 1. The calculated 1556 cm^{-1} transition in the methylated radical and 1573 cm^{-1} in the non-methylated are associated with the experimental bleach observed at 1568 cm^{-1} in 5-CH_3FMN$^{\bullet}$ and at 1578 cm^{-1} in flavodoxin-FMNH$^{\bullet}$; those both involve the $C_{10a}N_1$, $C_{4a}N_5$ stretching modes. The strong calculated transition at ~ 1529 cm^{-1} matches the experimentally observed value at 1528 cm^{-1} is assigned as C-C stretches of the ring 1 and $C_{4a}N_5$, $C_{10a}N_1$ stretches. The only obvious counterpart of the 1514 cm^{-1} mode observed in the experimental spectra for the methylated compounds matches the mode calculated at 1490 cm^{-1} which involves vibrations of the same atoms as the 1529 cm^{-1} mode. This mode is absent in the spectrum of FMNH$^{\bullet}$ in flavodoxin, but present in the calculated data, though weaker than FADH$^{\bullet}$ (Fig. 4.5). The DFT calculations show that this mode involves the N_5H wag in FMNH$^{\bullet}$, and is very sensitive to H-bonding, which can reduce the intensity. Addition of specific water molecules H-bonded to C_2=O and C_4=O reduced the intensity by 2. Thus we suggest that the disappearance of the 1490 cm^{-1} bleach in flavodoxin reflects the specific H-bond environment of FMNH$^{\bullet}$. The intense transient absorption around 1552 cm^{-1} arises from the excited state so cannot be assigned by our ground state DFT calculations, but is likely to be associated with the carbonyl modes.

We also performed UV-Visible transient absorption measurements on the N_5-methyl FADH$^{\bullet}$ and FADH$^{\bullet}$ in GOX samples, for which the spectra are illustrated and compared in Fig. 4.6. From these transient spectra, it is apparent that there is an excited state absorption peak at 460 nm of GOx-FADH$^{\bullet}$ while it is much less intense for the methylated radical (the maxima could not be determined exactly because of our data collection range limitation). The bleach spectra in the region of 500-600 nm have the features (two broad bands) observed in the linear absorption spectra (Fig. 4.2), in which the two transitions are clearly resolved in the ground state bleach. However, beyond that crude assignment the broad diffuse nature of the ground and excited state spectra makes

them less useful in characterizing the flavin radical state than the more characteristic vibrational spectra.

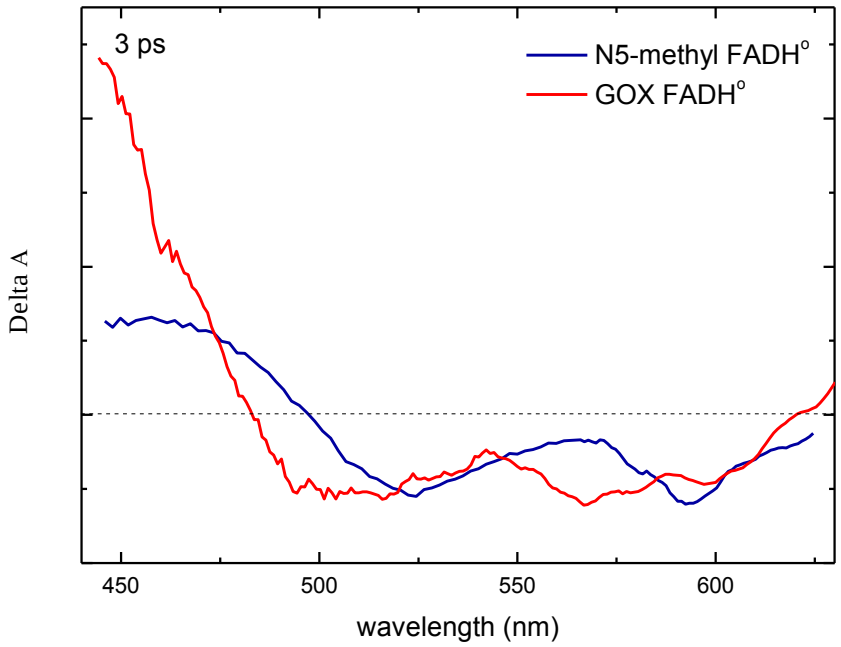

Fig. 4.6 UV-Visible transient absorption spectra of N5-methyl $FADH^{\bullet}$ and GO_X-$FADH^{\bullet}$

4.3.2 Kinetics of the Excited Neutral Flavin Radical

According to the visible transient absorption measurements, the kinetics of 5-$CH_3FAD^{\bullet}$ and 5-$CH_3FMN^{\bullet}$ radicals in D_2O are essentially the same, with a ground state recovery time of 13±0.5 ps (Fig. 4.7). A similar value was observed for the decay of the excited state absorption for the same two radicals measured by transient infrared at 1552 cm^{-1} (Fig. 4.8). Interestingly, the adenine moiety does not play a role in the excited state decay of the radical state, unlike the case of FAD itself. So the agreement of excited state decay and ground state recovery proves that the radiationless decay mechanism in the radical states is internal conversion from S_1 to S_0.

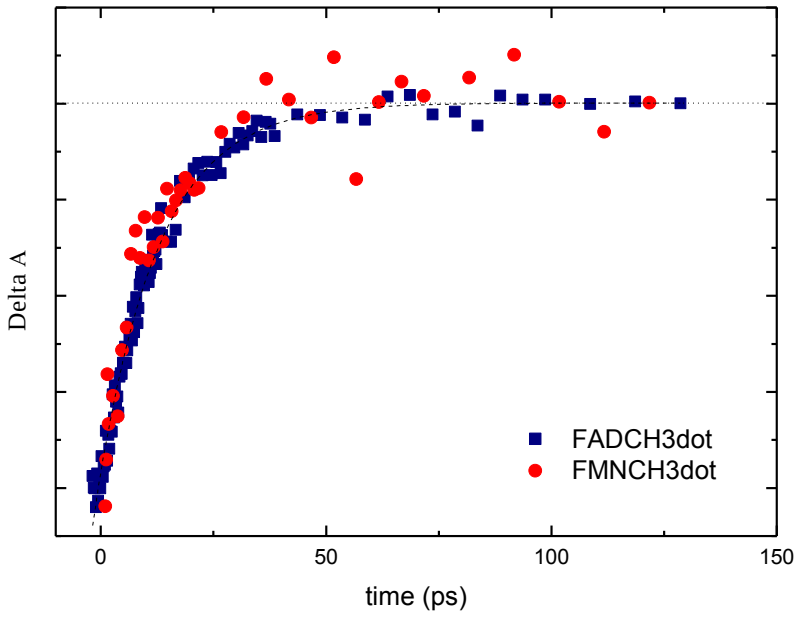

Fig. 4.7 Ground state recovery of N5-methyl FADH$^{\bullet}$/ FMNH$^{\bullet}$ measured by UV-Visible transient absorption

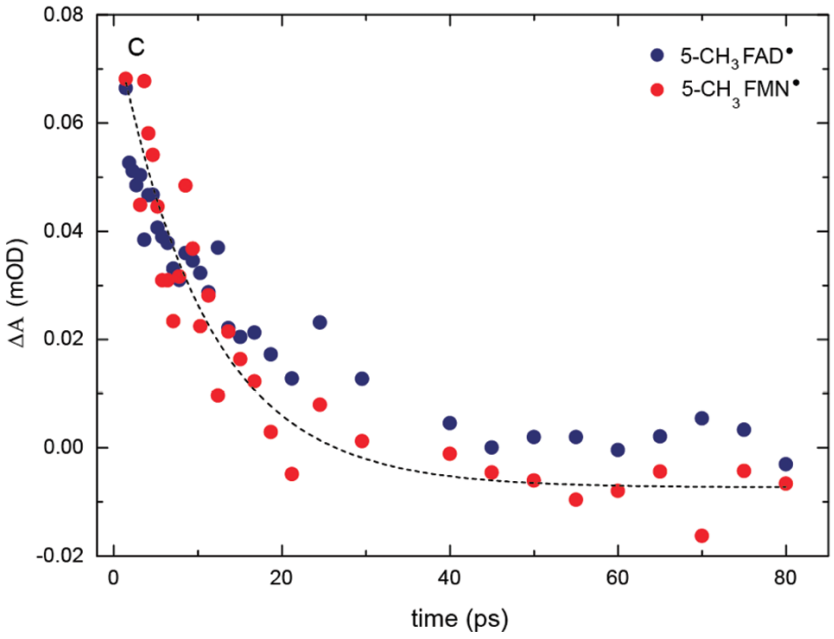

Fig. 4.8 Excited state decay of N5-methyl FADH$^{\bullet}$/ FMNH$^{\bullet}$ measured by TRIR

In contrast to $FADH^{\bullet}$ and $FMNH^{\bullet}$ there are significant differences in the excited state kinetics among flavin radicals prepared in flavodoxin, GOx and in solution. Fig. 4.9 and 4.10 shows the excited state kinetics of methylated radicals in solution compared with both the neutral radical states and the oxidized states of flavin bound to flavodoxin (FMN) and GOx (FAD) respectively, the lifetimes are summarized in table 4.2. Interestingly, it was found that in flavodoxin the decay time for both oxidized and radical states is faster than the radical in solution, while in GOX the oxidized FAD decay time is faster, but for the radical state it is slower, than for the radical in solution. Evidently the protein binding site has a major effect on the decay kinetics which will be further discussed.

	Oxidized	Radical in protein	Methylated radial in solution
Flavodoxin	‹500fs	1.7±0.3 ps	13±0.5 ps
GOx	3±0.3 ps	67±6 ps	13±0.5 ps

Table 4.2 Lifetime of Flavodoxin and GOx in oxidized and radical states

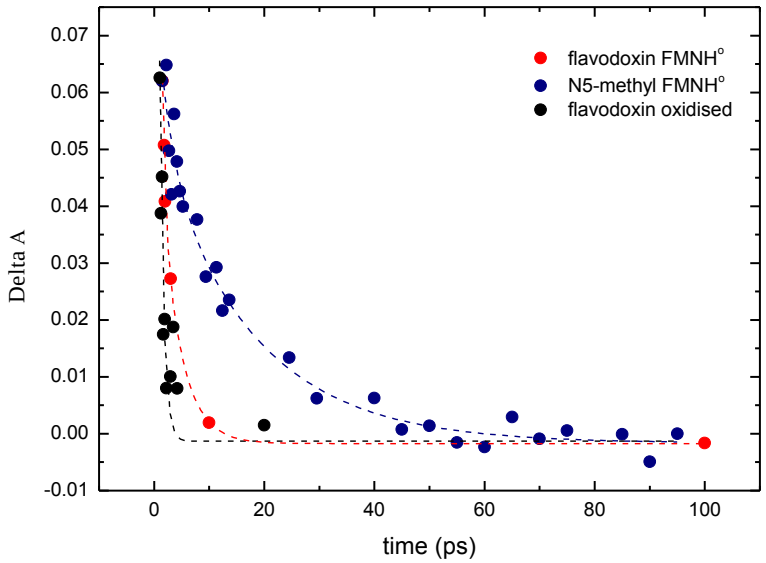

Fig. 4.9 Excited state decay of flavodoxin with FMN oxidized, $FMNH^{\bullet}$, and methylated $FMNH^{\bullet}$ fitted with dotted lines in black, red and blue respectively.

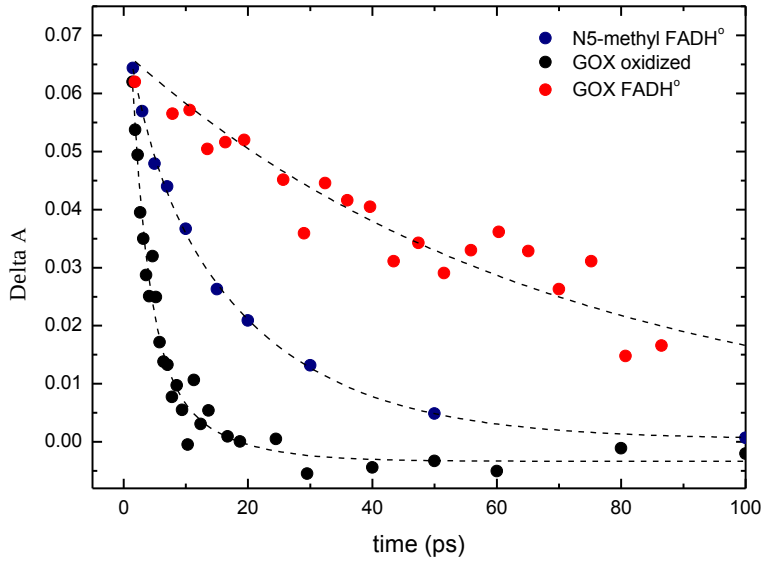

Fig. 4.10 Excited state decay of glucose oxidase with FAD oxidized, $FADH^{\bullet}$ and methylated $FADH^{\bullet}$ fitted with dotted lines in black, red and blue respectively.

The TRIR measurements at 1561 cm^{-1} on oxidized flavodoxin revealed an ultrafast sub 500 fs excited state decay time (Fig. 4.9 black line). Because of the limitation of signal to noise achieved in our TRIR measurements and also the low concentration of the sample, the present data can be regarded as being in good agreement with the fluorescence data measured by Mataga and co-workers using time resolved fluorescence up-conversion [10], in which they found that the decay was dominated by an ultrafast component of 158 fs. This decay was assigned to quenching by electron transfer from surrounding protein residuals, like tryptophan and/or tyrosine residues to FMN, as shown in Fig. 4.11 [11].

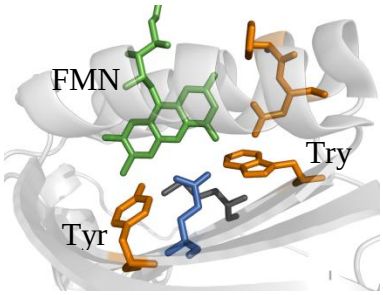

Fig. 4.11 Crystal structure of flavodoxin

The excited state decay of flavodoxin-FMNH$^{\bullet}$ was also measured before by Vos and co-workers using visible transient absorption spectroscopy [7], in which they found the excited state decay time as 2.3±0.3 ps at 700 nm. Our TRIR measurement is in good agreement with their data: the decay observed at 1552 cm^{-1} was fit with a single exponential, and found to have a decay constant of 1.7±0.3 ps. For both the oxidized and semiquinone states, the quenching was induced by the electron transfer, with the different rate probably reflecting the different redox potentials of oxidized and semi-quinone states.

The decay time of excited state FADH$^{\bullet}$ in GOx measured by TRIR at 1550 cm^{-1} is observed as 67±6 ps which is consistent with the value 59±5 ps measured by Vos and co-workers using visible transient absorption [7]. This is much slower than both 5-CH_3FAD$^{\bullet}$ and 5-CH_3FMN$^{\bullet}$ in solution (Fig. 4.10). Because there is no electron donor available in the solution system, the electron transfer induced quenching mechanism cannot be applied as an explanation for the short lifetime. In this case, the slow decay time in FADH$^{\bullet}$ GOx must correspond to suppression of radiationless decay by the protein. In section 3.3.3 the radiationless decay by internal conversion in the fully reduced flavins was thought, on the basis of deuterium sensitivity, to be promoted by motion along a coordinate, which is sensitive to the H-bonding environment. Then the longer decay in GOx oxidised could be ascribed to the restriction of this motion due to the rigid (H-bonded) protein environment.

Fig. 4.12 shows the TRIR data for GOx: flavin cofactor in its $FADH^{\bullet}$ and $FAD^{\bullet-}$ states compared to in the oxidized state. For the oxidized FAD, the excited state decay measured at the 1611 cm^{-1} transient IR was fit with a single exponential function as a 3±0.3 ps component, while the ground state recovery observed at 1553 cm^{-1} can be fit with two exponentials: 3.2±0.2 ps and 26±3 ps (Fig. 4.13). The quenching mechanism can be assigned to electron transfer from surrounded protein residuals like tryptophan or tyrosine to the excited FAD.

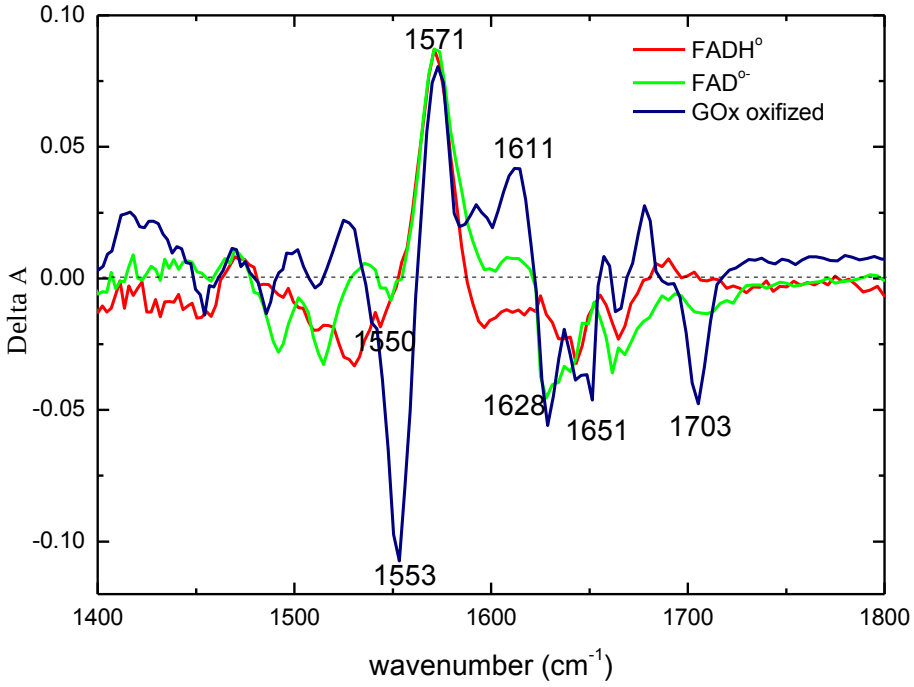

Fig. 4.12 TRIR for GO_X: flavin cofactor in oxidized FAD, $FADH^{\bullet}$ and $FAD^{\bullet-}$ states

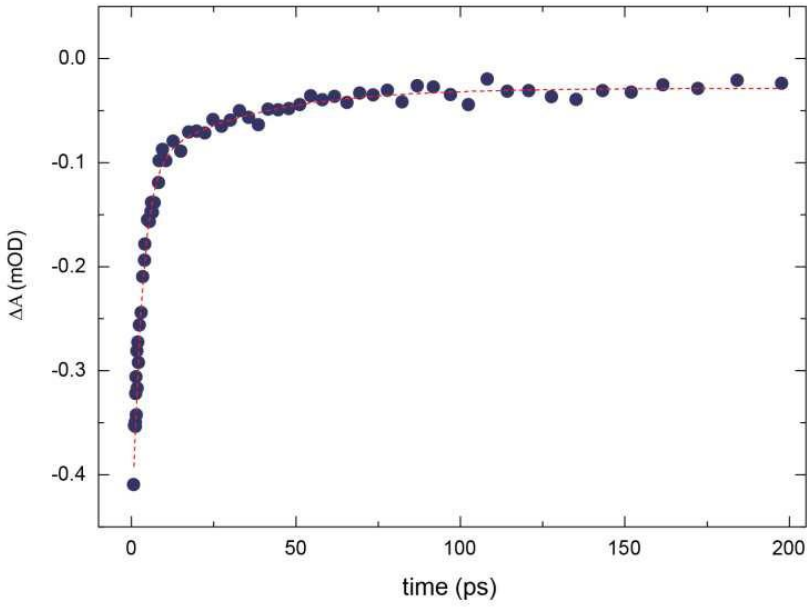

Fig. 4.13 Ground state recovery of oxidized GO_X measured at 1553 cm^{-1} fitted with a biexponential function (dotted line), the recovery times being 3.2±0.2 ps and 26±3 ps.

The spectrum of the oxidized GOx (Shown in Fig. 4.12) at early time delays after excitation is very similar to the spectrum of oxidized FAD (Fig. 2.13a, Chapter 2). The major ground state bleaches at 1553 cm^{-1}, 1651 cm^{-1} and 1703 cm^{-1} have been assigned through DFT calculation to mainly $C_{10a}N_1$, C_2=O and C_4=O localized stretch of the isoalloxazine ring respectively. This is as expected, as FAD is in its oxidized form.

The spectra of GOx with the flavin cofactor in its anionic radical and neutral radical states recorded 1.5 ps after excitation are also shown in Fig. 4.12. The $FADH^{\bullet}$ spectrum is very similar to the spectrum of the methylated radical (Fig. 4.3) although the strong excited state absorption is shifted up to ~ 1571 cm^{-1}. The absence of the remarkable 1628 cm^{-1} peak and the appearance of a peak at ~ 1640 cm^{-1} are possibly artefacts of the measurement arising from the very strong infrared absorption of the GOx backbone in this region which makes the calculation of ΔA noisy. It also can be seen from the TRIR data that there are only small differences between $FAD^{\bullet-}$ and $FADH^{\bullet}$ spectra in GOX. The $FAD^{\bullet-}$ has a more obvious ~ 1514 cm^{-1} peak and an additional peak at 1491 cm^{-1}.

Since both the radicals have the same chromophore, it is likely that these additional features are associated with a protein mode shifted on the excitation.

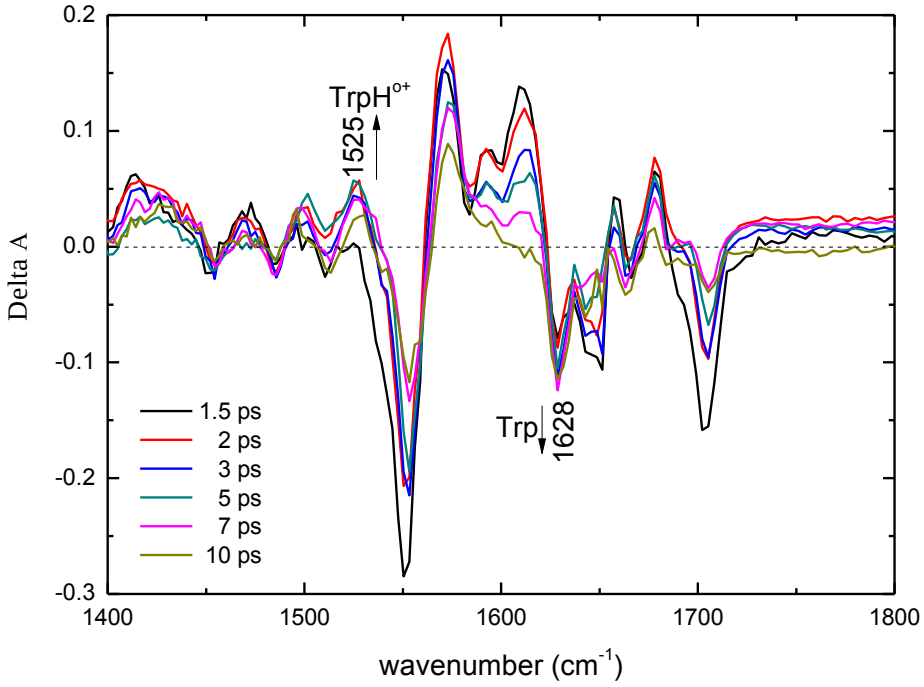

Fig. 4.14 TRIR spectra of oxidized GOx at different delay times

Fig. 4.14 demonstrates the time dependent TRIR spectra for oxidized FAD in GOX. Again, they are very close to the spectra of oxidized FAD at early times, with the strong bleach recovering within the tens of picoseconds timescale. The faster kinetics (3 ps) are evidenced between 1550 and 1650 cm^{-1}: the decay of the band near 1610 cm^{-1} on a fast timescale indicates a reactive species; similarly the bleach at 1628 cm^{-1} becomes stronger when the other bleach modes recover, which is also consistent with a reaction which caused ground state population depletion. From these data it is clear that there is an excited state reaction in GOx.

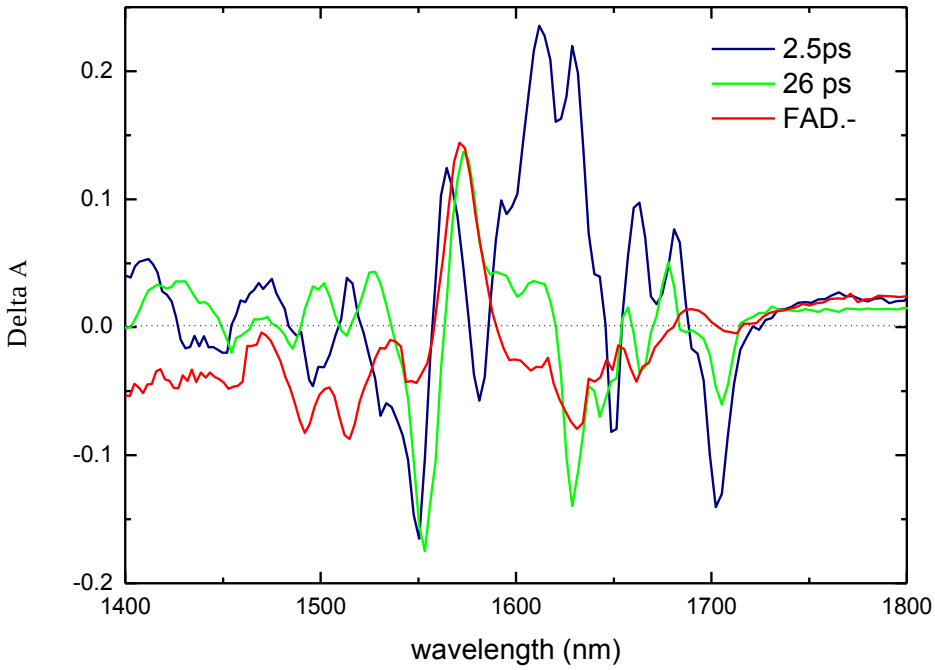

Fig.4.15 Decay associated spectra of oxidized glucose oxidase given by global fit

We performed a global analysis on the oxidized GOx data to analyse the TRIR data further. The global fit was best when two exponentials were applied in the analysis with the decay times of 2.5 and 26 ps. The decay associated spectrum (Fig. 4.15) assigned to the 2.5 ps component has an intense transient peak at ~ 1628 cm^{-1}. The 2.5 ps kinetics are close to the main component of the quenching reported in time resolved fluorescence which was assigned to an electron transfer reaction [12]. The fast decay of the 1628 cm^{-1} mode may be due to a vibration of a protein residue, like tryptophan, which disappears during the reaction. This would be consistent with an electron transfer reaction. The 26 ps DAS component can be described as a mixture of the GO_X oxidized and GO_X-$FAD^{\bullet-}$ state. As seen in Fig. 4.12 the 1550 cm^{-1} peak belongs to the oxidized state but it is not as big as observed in '26 ps' spectrum; the transient at 1611 cm^{-1} and bleach at 1703 cm^{-1} are stronger than in $FAD^{\bullet-}$, which are both in agreement with the assumption that the $FAD^{\bullet-}$ state is formed during the excitation process.

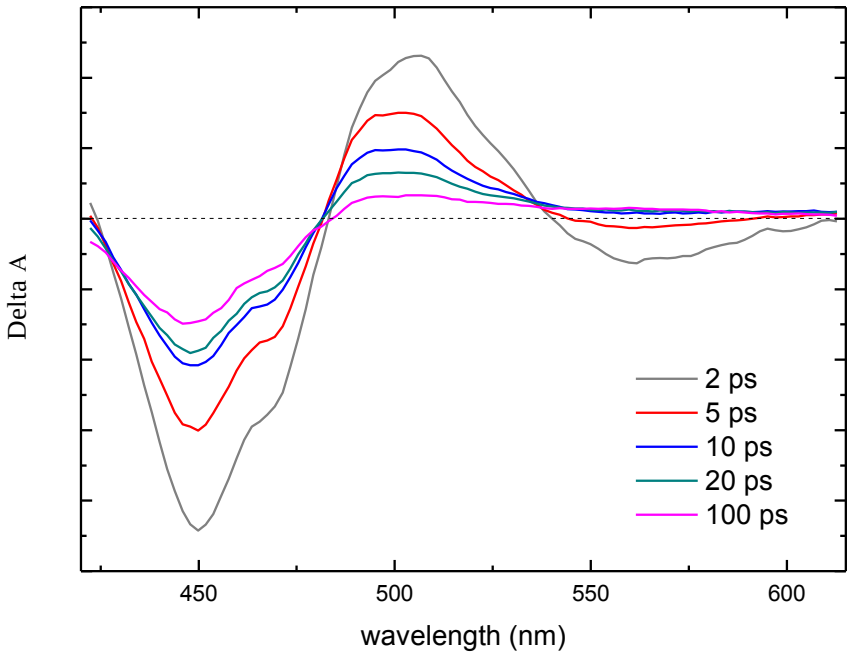

Fig. 4.16 Transient absorption spectra of oxidized GOx at different time delays

The UV-Visible transient absorption data measured for oxidized GO_X are shown in Fig. 4.16, which further supports the assignment of the two components observed in the TRIR data (2.5 and 26 ps, Fig. 4.14 and 4.15) with providing the two very similar time components with the global analysis (Fig. 4.17). The fast (3 ps) component can be assigned as usual oxidized FAD spectrum; while the slow (24 ps) component is less readily assigned, but it can be very approximately modelled as ($FAD^{\bullet -}$ + $TrpH^{\bullet +}$) – (FAD_{ox} – Trp) which is in good agreement with the TRIR data and a reaction involving formation of a Trp radical cation (rather than simply the Trp radical).

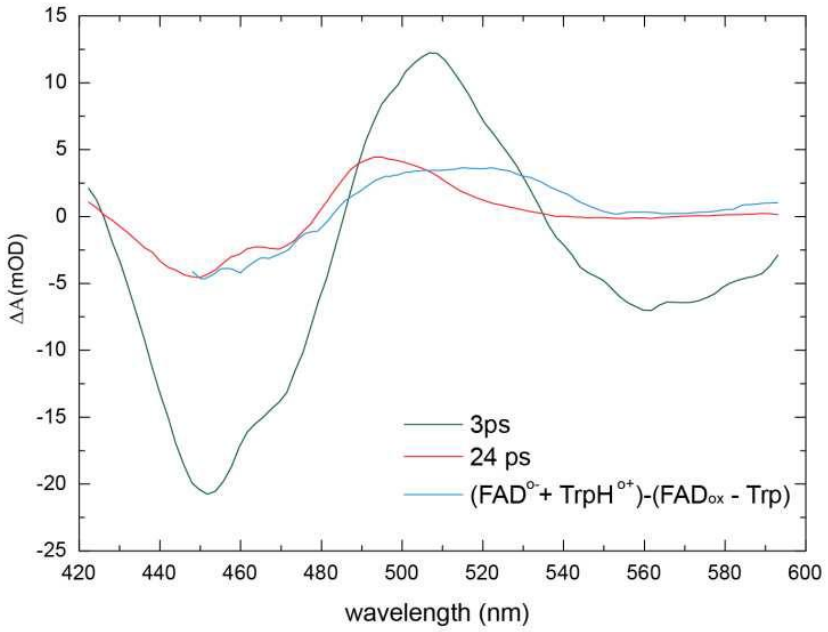

Fig. 4.17 spectra obtained by global analysis associated to the 3 ps (black line) and 24 ps (red line) time constants. Blue line shows the difference spectra of (FADo-+ TrpHo+)-(FADox – Trp).

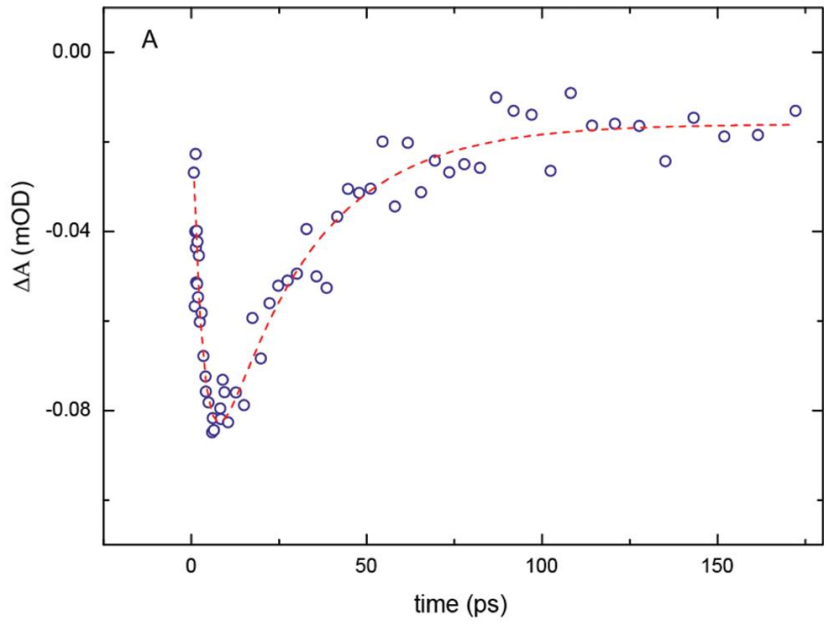

Fig. 4.18 Kinetics of oxidized glucose oxidase observed at 1628 cm^{-1}

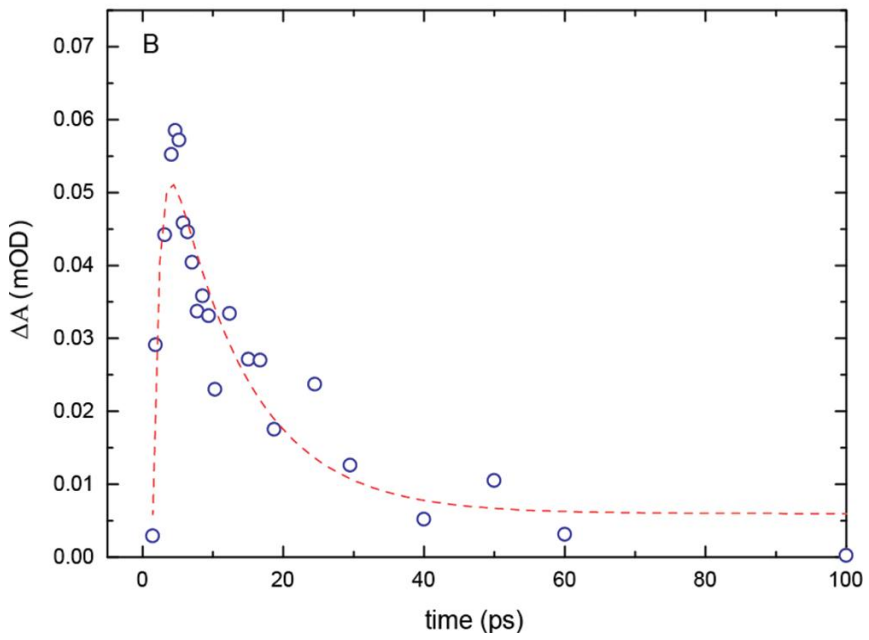

Fig. 4.19 Kinetics of oxidized glucose oxidase observed at 1525 cm^{-1}

Analysis on the TRIR kinetics at individual peaks adds some support to this assignment. Based on the experimental data measured on the GOx-Oxidized at 1628 cm^{-1} (Fig. 4.14), a fast bleach within 3±0.5 ps and a slow recovery in 26±3 ps (As shown in Fig. 4.18) are observed from the fitting. A possible explanation for this behaviour is that the fast decay is due to protonation of the Trp radical (though tyrosine is an alternative possibility) residue which functioned as a electron donor to FAD. The disappearance of the absorption of an aromatic residue (Trp/Tyr) results in the increasingly negative value in the difference spectra. A transient species was observed at 1525 cm^{-1} which has been assigned to an $FAD^{\bullet-}$ + $TrpH^{\bullet+}$ peak (see Fig. 4.14) [13]. Analysing the kinetics measured at 1525 cm^{-1} (Fig 4.19) reveals that a new state is formed within ~ 1.5 ps. This is then the product of the reaction. According to the UVRR measurements of Johnson *et al* [13], this band may be assigned to the formation of $TrpH^{\bullet+}$ based on their spectrum in aqueous solution. Thus the data are consistent with electron transfer quench in < 3 ps and reverse electron transfer to restore the ground state in tens of picoseconds. This is consistent with earlier measurements of Zhong and Zewail, but the vibrational data and confidence to the assignment also serves to better characterise radical intermediate states in proteins.

4.4 Conclusion

The photophysical properties of methylated FAD and FMN radicals were characterised by ultrafast transient visible and infrared spectroscopy. The ground state bleach transitions were assigned with the aid of DFT calculations. The excited state decay of these methylated flavin radicals was analyzed as ~13 ps, and the decay mechanism is internal conversion. The transient infrared spectra of flavodoxin and GOx were also measured when the flavin FAD was in its radical state, from which we found that the decay kinetics are a sensitive function of protein binding site, which could be refer to electron transfer induced quenching or environmental dependent suppression of radiationless decay by the protein, depending on the protein environment. In addition, the mechanism of FAD quenching in GO_X was confirmed as electron transfer to a tryptophan. These data will be useful in characterisation the BLUF domain photocycle.

References

[1] Gauden.M, Yeremenko, S., Laan, W., van Stokkum, I.H.M., Ihalainen, J.A., van Grondelle, R., Hellingwerf, K.J. and Kennis, J.T.M. (2005) *Biochemistry 44(13)*, 3653-3662.

[2] Fukushima, Y., Okajima, K., Shibata, Y., Ikeuchi, M. and Itoh, S. (2005) *Biochemistry 44(13)*, 5149-5158.

[3] Haigney, A., Lukacs, A., Zhao, R. K., Stelling, A. L., Brust, R., Kim, R. R., Kondo, M., Clark, I., Towrie, M., Greetham, G. M., Illarionov, B., Bacher, A., Romisch-Margl, W., Fischer, M., Meech, S. R. and Tonge, P. J. (2011) *Biochemistry 50*, 1321-1328.

[4] Stelling, A. L., Ronayne, K. L., Nappa, J., Tonge, P. J. and Meech, S. R. (2007) *Journal of the American Chemical Society 129*, 15556.

[5] Lukacs, A., Haigney, A., Brust, R., Zhao, R. K., Clark, I., Towrie, M., Greetham, G. M., Meech, S. R. and Tonge, P. J. (2011) *Journal of the American Chemistry Society 133*, 16893-900

[6] Scott, A. P. and Radom, L. (1996) *Journal of Physical Chemistry 100*, 16502.

[7] Pan, J., Byrdin, M., Aubert, C., Eker, A. P. M., Brettel, K. and Vos, M. H. (2004) *Journal of Physical Chemistry B 108*, 10160-10167.

[8] Eisenberg, A. S. and Schelvis, J. P. M. (2008) *Journal of Physical Chemistry A 112*, 6179-6189.

[9] Kao, Y. T., Saxena, C., He, T. F., Guo, L. J., Wang, L. J., Sancar, A., Zhong, D. P. (2008) *Journal of the American Chemical Society 130*, 13132-13139.

[10] Mataga, N., Chosrowjan, H., Taniguchi, S., Tanaka, F., Kido, N. and Kitamura, M. (2002) *Journal of Physical Chemistry B 106*, 8917-8920.

[11] Knight, JR E., and Hardy, R. W. F. (1967) *The Journal of Biological Chemistry 42(7)*, 1370-1374.

[12] Zhong, D. P. and Zewail, A. H. (2001) *Proceedings of the National Academy of Sciences of the* United *States of America 98 (25)*, 11867-11872.

[13] Johnson, C. R., Ludwig, M. and Asher, S. A. (1986) *Journal of the American Chemical Society 108*, 905-912.

Chapter 5 Excited State Dynamics and Temperature Dependence of Flavin Fluorescence in Different Redox States

5.1 Introduction

The physical and chemical properties of the isoalloxazine ring and the two most common flavin cofactors: flavin mononucleotide (FMN) and flavin adenine dinucleotide (FAD) have been extensively studied for several decades [1-3]. Following the previous descriptions of the photophysical properties of fully reduced flavins in Chapter 3 and radical flavins in Chapter 4, in this Chapter we will describe studies of the temperature dependence in all of these oxidation states. The objective is to provide further details on the nature of the radiationless relaxation.

There are some previous researches [4-9] about the temperature dependent fluorescence of flavins. Huppert *et al* [4] reported fluorescence measurements of both oxidized FMN and FAD dissolved in a 0.1% mole ratio methanol-doped ice solvent, which has a wide temperature range as a glass, from 79 K to 268 K. They found that both samples fluorescence much more strongly when they are in low temperature media indicating a temperature dependent non-radiative relaxation rate. They only reported the measurements on flavins in their oxidized state, so there is a need to further develop such measurements for other redox states. In this way we can extend our knowledge of reduced and radical states of flavin and thus better understand the BLUF domain protein photocycle (Chapter 2). In this chapter, we will describe systematic studies of temperature dependent fluorescence of oxidized, fully reduced and radical flavins dissolved in ethylene glycol/water mixed solvent, combined with some solvent dependent TRIR measurements of the rate of ground state recovery. The general principles underlying the analysis of the temperature dependence are introduced in the following paragraphs.

5.1.1 Temperature dependent fluorescence kinetics

The Arrhenius equation describes the temperature dependence of numerous rate constants. The equation was first proposed by the Van't Hoff in 1884 and five years later the Swedish chemist Svante Arrhenius provided a physical justification and interpretation for the behaviour [10]. Subsequently the Arrhenius equation was generalized in terms of transition state theory [11]. In our experiments, we applied Arrhenius analysis to calculate the activation energy for the temperature dependent radiationless decay. The exponential and logarithmic forms of the equations are shown in equations 5.1 and 5.2.

$$k_{rea} = A\exp(-E_a / RT) \qquad 5.1$$

$$\ln k_{rea} = \ln A - E_a / RT \qquad 5.2$$

Where k_{rea} is reaction rate constant, A is a constant known as the frequency factor (assumed temperature independent in Arrhenius equations, and shown by TST to be related to the entropy of activation) and E_a is the activation energy, which can be defined as the energy that must be overcome in order for a chemical reaction to occur (Illustrated in Fig. 5.1). Activation energy can be thought of as the height of the potential barrier separating the reactants from the products of a reaction. For a chemical reaction to proceed at a reasonable rate there should exist statistically an appreciable number of molecules with energy equal to or greater than the activation energy. The activation energy of a reaction can be determined if the rate constant is measured at a number of different temperatures from a plot of $\ln k_{\mathrm{rea}}$ against $1/T$ (Equation 5.2).

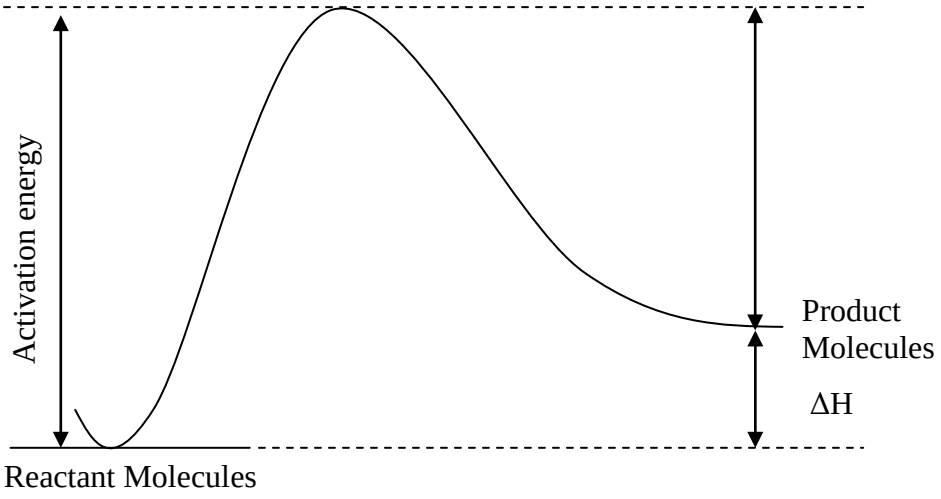

Fig. 5.1 Potential energy-reaction co-ordinate diagram

In measurements of the temperature dependent fluorescence, there was no chemical reaction involved, so the reaction rate constant k_{rea} can be replaced by the radiationless relaxation constant k_{nr} (the sum of all the non radiative rate constants, includes k_{rea} if there is any reaction but also, $k_{IC,}$ k_{ISC} and so on). k_r is the radiative relaxation rate constant. A diagram shown Fig. 5.2 can be used to explain this mechanism for our low temperature system followed by the steady state kinetic scheme.

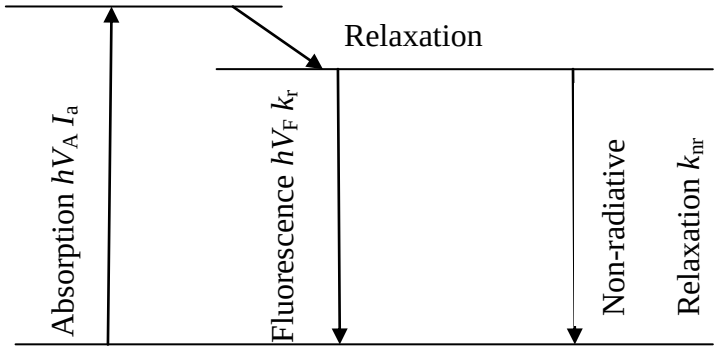

Fig. 5.2 Diagram of the steady state kinetic scheme

$$M \xrightarrow{h\nu_A} M^* \qquad I_a$$

$$M^* \xrightarrow{h\nu_F} M + h\nu \qquad k_r$$

$$M^* \longrightarrow M \qquad k_{nr}$$

So under steady state conditions,

$$\frac{d[M^*]}{dt} = I_a - k_r[M^*] - k_{nr}[M^*] = 0$$

Since the rate of emission is,

$$I_r = k_r[M^*]$$

And the fluorescence quantum yield is defined as,

$$\phi_f = \frac{I_r}{I_a}$$

So

$$\phi_f = \frac{k_r}{k_r + k_{nr}} \qquad 5.3$$

In case of 'high' temperatures (HT), it is often assumed that the radiative rate k_r is temperature independent and small compared to k_{nr}, ($k^{HT}_{nr} >> k_r$), if applying this into the above equation, then the fluorescence emission quantum yield (ϕ_f) is expressed as:

$$\phi_f = \frac{k_r}{k_{nr}^{HT}}$$

Then,

$$\phi_f \propto \frac{1}{k^{HT}_{nr}}$$

So we can conclude that under these conditions the inverse of the quantum yield is proportional to k_{nr}.

In the case of 'low' temperatures, we also assume the radiative rate k_r is temperature independent, but k_{nr} decreases as temperature decreases, and becomes comparable to k_r, so divided by $\frac{1}{1-\phi_f}$ from both sides of equation 5.3, we can obtain:

$$\frac{k_{nr}^{LT}}{k_r} = \frac{1-\phi_f}{\phi_f}$$

Then,

$$k_{nr}^{LT} \propto \frac{1-\phi_f}{\phi_f}$$

As a summary:

At high temperature: $k_{nr}^{HT} \propto \frac{1}{\phi_f}$ 5.4

At low temperature: $k_{nr}^{LT} \propto \frac{1-\phi_f}{\phi_f}$ 5.5

These equations 5.4 and 5.5 were applied to the T dependent data, the fluorescence emission quantum yield (ϕ_f) was normalized based on the lowest temperature (80K) data which was regarded as 1 (i.e. $k_{nr} \approx 0$ at 77 K), and then an Arrhenius plot yields the activation energy for both high and low temperature ranges respectively.

5.1.2 Temperature dependent spectral shift

The emission spectra as well as the emission intensity were found to be a function of temperature. To characterise this temperature dependence the mean frequency of the emission was calculated. The mean frequency of a spectrum is the sum of the product of the spectral intensity and the frequency, divided by the total sum of spectral intensities, effectively the first moment of the spectrum [12]. In other words:

$$f_{mean} = \frac{\sum_{i=0}^{n} I_i \bullet f_i}{\sum_{i=0}^{n} I_i} \qquad 5.6$$

where f_{mean} = mean frequency

n = number of frequency points in the spectrum

f_i = frequency of spectrum at frequency point i

I_i = Intensity of spectrum at frequency point i

This parameter is a more useful indicator of spectral frequency shifts than the maximum, especially when the shift is accompanied by a shape change.

5.2 Materials and Experimental Methods

Fig. 4.1 in Chapter 4 shows the chemical structure of flavin in its neutral radical state and synthetic (methylated) radical state, the free radical electron is at the same position for both cases (at C_{4a} position) [13]. Details on the low temperature fluorescence measurements used for flavins in different redox states were introduced in Section 2.2.2.

5.3 Results and Discussion

5.3.1 Low temperature fluorescence of oxidized FAD, FMN and GOx

Oxidized FAD, FMN and GOx samples were made with concentration of ~ 50 μM in a 50:50 by volume water: ethylene glycol mixed solvent. The use of ethylene glycol ensures the presence of FAD molecules in the bulk of a glassy solvent rather than at grain boundaries as was observed in the Huppert's experiments with 1% methanol [4]. The disadvantage is that we are no longer using the most biologically relevant solvent, water. The freezing temperature for the water: ethylene glycol mixed solvent system is 225 K (-45^{o}C), and the glass transition temperature T_g is 155 K [14]. The low temperature fluorescence measurements were made with excitation at 400 nm.

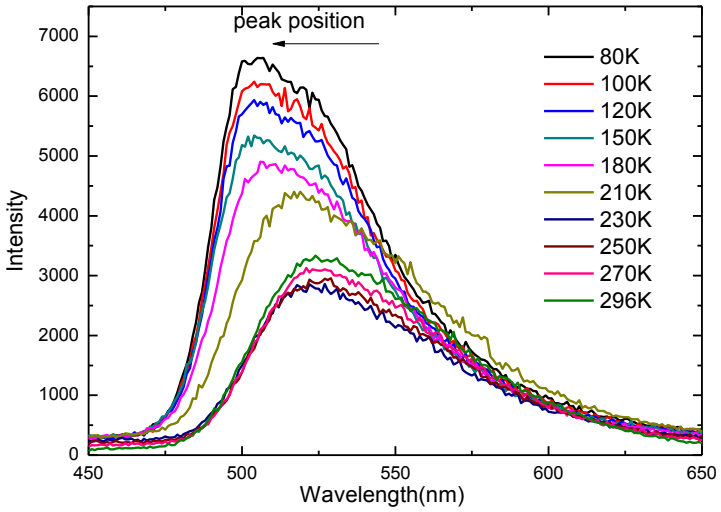

Fig. 5.4 Temperature dependent fluorescence emission spectra of FAD oxidized in H_2O/EG solvent

Fig. 5.4 shows the fluorescence spectra of the FAD oxidized sample at different temperatures ranging from ambient (296 K) to liquid nitrogen (80 K). The fluorescence intensity initially decreased with decreased in temperature, from 296 K to 230 K, and then turned around and started to increase from 210 K until the lowest temperature measured. The peak position was blue shifted for all the spectra with decreasing

temperature. In addition the spectral shape changed slightly, rising more steeply on the short wavelength side, and showing very weak vibronic structure (shoulder at 530 nm).

At room temperature, when FAD dissolves in water it exists in two conformations: approximately 80% in a 'closed' or 'stacked' form in which the isoalloxazine ring and adenine are close enough to give rise to quenching by electron transfer from the adenine to isoalloxazine ring. (Shown in Fig. 5.5); In contrast the ~20% 'open' form is fluorescent due to the distance between iosalloaxazine ring and the adenine group [3].

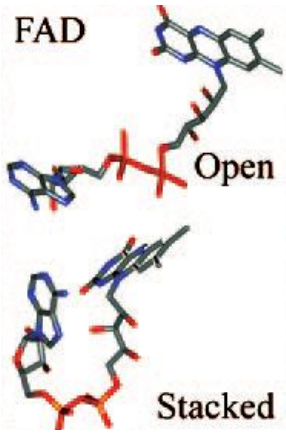

Fig. 5.5 Schematic representation of FAD in open and stacked conformations [3]

Returning to the spectra in Fig. 5.4, qualitatively we assign the decrease in fluorescence quantum yield from 296 K to 230 K, to an increase in the percentage of non-radiative 'closed' form, as was previously suggested by Huppert [4]. This assignment of quenching in the closed form is consistent with the low fluorescence intensity in FAD compared to FMN which we have shown (see below) does not show the initial decrease in fluorescence with decreasing temperature. For FAD from 210 K down to 80 K, the conformation ratio of the open/closed form in the sample system has apparently stabilised, so the large increase in intensity is due to the decrease of non-radiative relaxation rate for the sample. This may arise because of an intrinsic activation barrier to the radiationless decay or from the friction (viscosity) on the solvent (which may lead to a temperature dependence of the Arrhenius *A* factor) [15]. Also evident from Fig. 4 is that the emission band of FAD is blue shifted with decreasing temperature which indicates a change in the energy of the emissive (S_1) level. The shift happened on the change from

230 K to 210 K, which lies within the super cooled region for EG. We analyzed the data in two parts: low temperature and high temperature, thereby making the simplifying assumption that either the open-closed equilibrium or the temperature dependent radiationless rate dominates. Clearly in the intermediate region both may be significant.

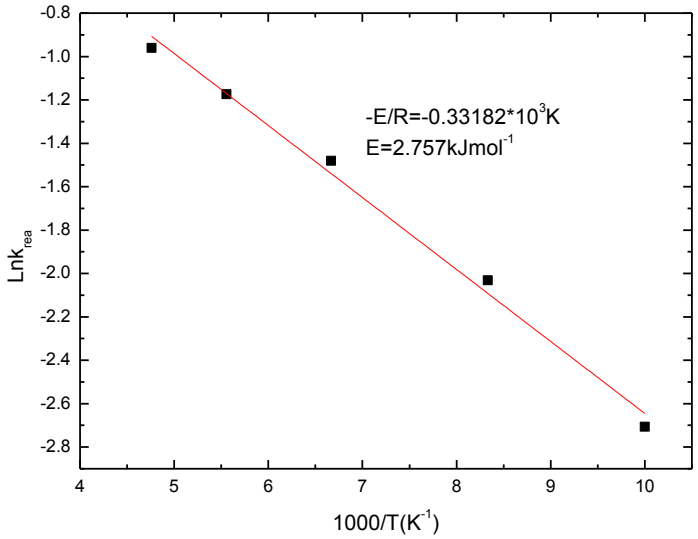

Fig. 5.6 Arrhenius analysis of FAD oxidized in low temperature range

First, the low temperature increase in fluorescence intensity is analyzed in Fig. 5.6 which shows the Arrhenius fitting of the FAD data in the low temperature range: from 80K to 210K. The non-radiative rate constant k_{nr} was calculated from the quantum yield according to equation 5. Then equation 2 was applied to calculate the activation energy within this temperature range as 2.8±0.13 kJmol^{-1}.

Turning to the high temperature range from 230 K to 294 K, the increase in fluorescence with increasing T was assigned to a conformation change involved between the fluorescent open form and non-(or weakly) fluorescent closed form; the temperature dependent equilibrium state can be expressed as follow:

$$[\text{Open}] \underset{k_{CO}}{\overset{k_{OC}}{\rightleftharpoons}} [\text{Closed}]$$

So the equilibrium constant can be written

$$K = \frac{k_{OC}}{k_{CO}} = \frac{[\text{Closed}]}{[\text{Open}]}$$

And if we make the approximation (justified by the ratio of open to closed decay times of ~5ns to ~5-10ps [16]) that only the open state fluoresces, then

$$[\text{Open}] \propto \phi_f$$

So

$$K \propto 1/\phi_f$$

Using,

$$\Delta G = -RT \ln K$$

Then,

$$\ln \frac{1}{\phi_f} \propto -\frac{\Delta G}{R}\left(\frac{1}{T}\right) \qquad 5.7$$

We applied equation 5.7 to the analysis of FAD data for the high temperature range (Fig. 5. 7). The Gibbs free energy ΔG was calculated as -4.6 kJ the negative value implying that the most stable state of FAD conformation is the closed form. In principle these data can be used to test simulations of the population of open and closed configurations of FAD, although this is beyond our current scope.

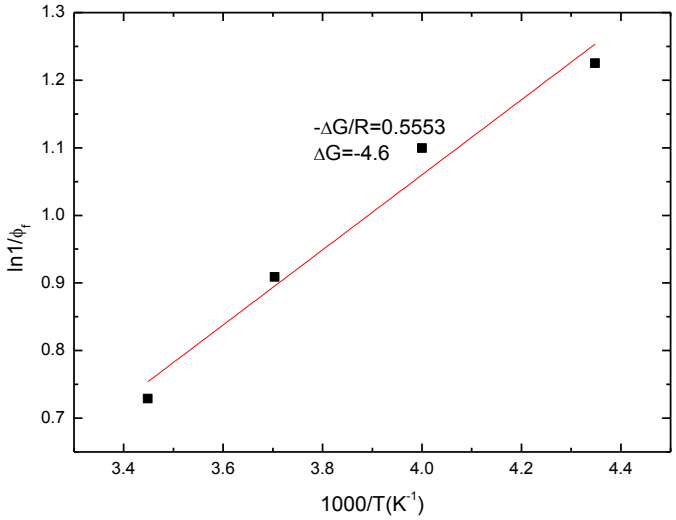

Fig. 5.7 $\ln \frac{1}{\phi_f}$ against 1000/Temperature (K) of FAD oxidized in high temperature range

We extended these measurements to FMN, which does not have the quenching adenine group. Fig. 5.8 shows the spectra of the temperature dependent fluorescence measurements of FMN, processed in the same way as for FAD. Because of the absence of a quenching closed form the FMN fluorescence intensity increases continuously with decreasing temperature. As for FAD the spectrum was blue shifted from 530 nm down to around 500 nm. The activation energy was calculated as 2.4±0.19 kJmol^{-1} with the Arrhenius analysis which is very similar to the FAD value (2.8±0.13 kJmol^{-1}), (Fig. 5.9).

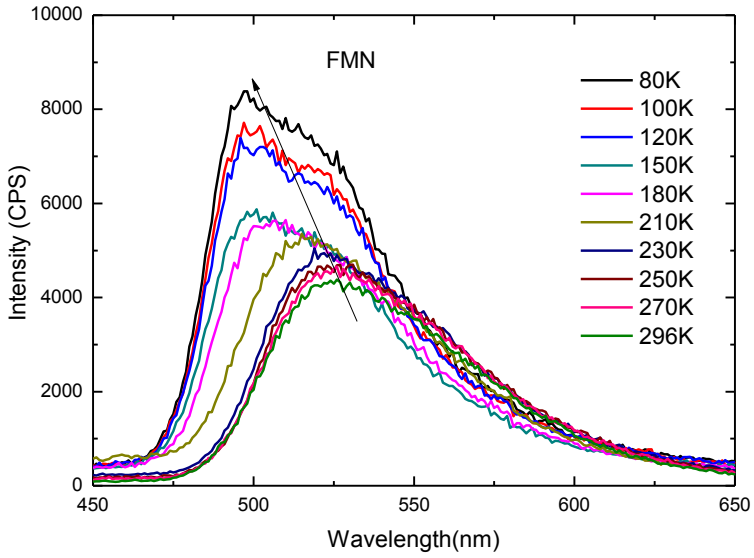

Fig. 5.8 Temperature dependent fluorescence emission spectra of FMN oxidized

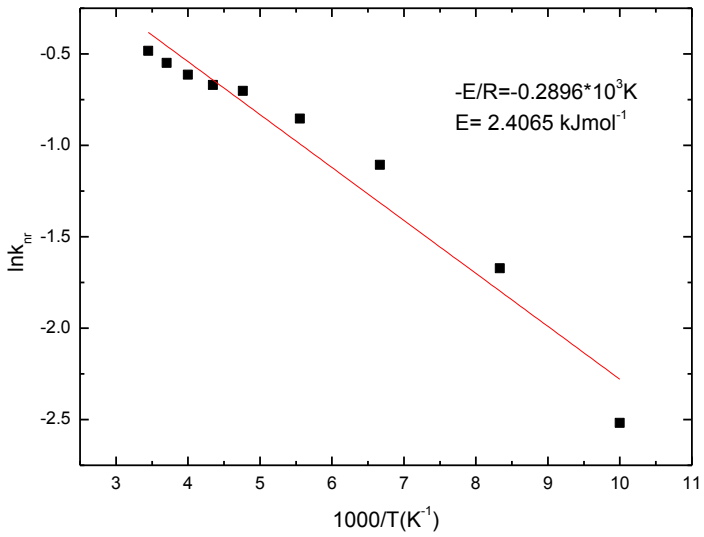

Fig. 5.9 Arrhenius analysis of FMN oxidized

Next we consider the temperature dependence of the mean frequency for both FAD and FMN emission. In the spectra shown in Fig. 5.4 and 5.8, the sample's emission band

position continuously blue shifted. The mean frequencies for spectra at different temperatures are plotted in Fig. 5.10. The frequency value increased significantly as the temperature decreased, possibly due to a solvation effect: the solvent molecules became less in order to align the dipole direction of either FAD or FMN in low temperature, then result in a higher energy emission shown as the band blue shifted. The extra emission band shift (higher the emission band frequency) of FMN compared to FAD was possibly due to the lack of the adenine which influences the environment of flavin in the case of FAD during measurements.

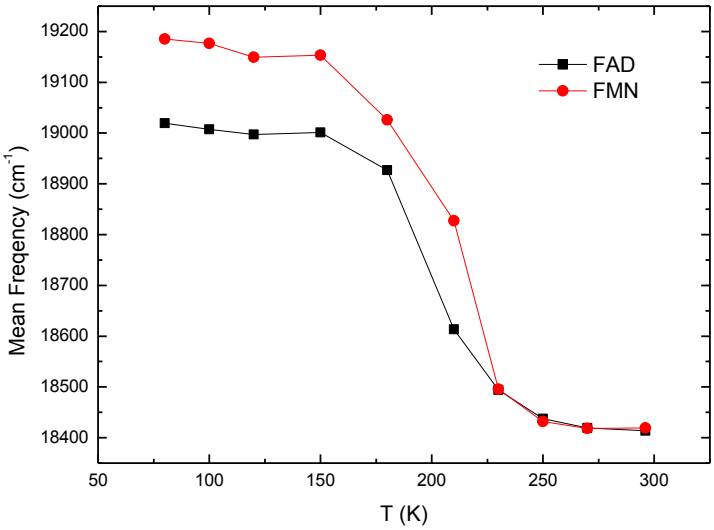

Fig. 5.10 Mean frequency against *T* for oxidized FMN sample compared to FAD in water/EG

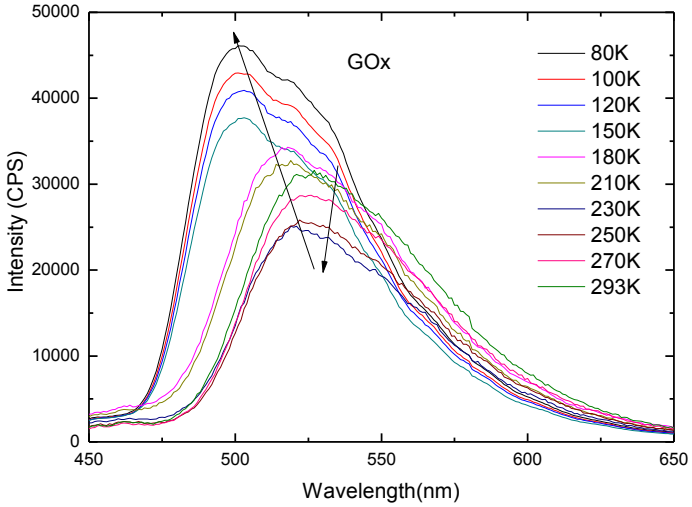

Fig. 5.11 Temperature dependent fluorescence emission spectra of GOx oxidized

Next we describe an ultimately unsuccessful attempt to study the temperature dependence of FAD in a protein environment, specifically GOx. Fig. 5.11 shows the fluorescence emission data of GOx dissolved in 50:50 Water/EG against temperature. As the sample was cooled down, the intensity of the spectra decreased first from 293 K to 230 K, then increased from 210 K to 80 K which is very similar to FAD. But in principle, according to the structure of GOx shown in Fig. 5.12, FAD as the chromophore is surrounded by protein residues, so it is expected to behave differently to the 'free' FAD. In particular the decrease in emission with decreasing temperature (assigned to the open – closed equilibrium) should not be seen in GOx as the binding environment appears quite rigid and FAD is in a more-or-less open form. Further, we already showed (Chapter 4) that GOx is strongly quenched by electron transfer from a Trp residue. These results (Fig. 5.11) raise the question, is the FAD really bound in GOx in this solvent? First we compared quantitatively the 'GOx' data with FAD in solution. The activation energy at low temperature was calculated to be 2.8 $kJmol^{-1}$ (Fig. 5.13). Further the high temperature data produced a free energy for the equilibrium of -2.8 $kJmol^{-1}$ (Fig. 5.14). These data are all effectively identical to FAD in solution.

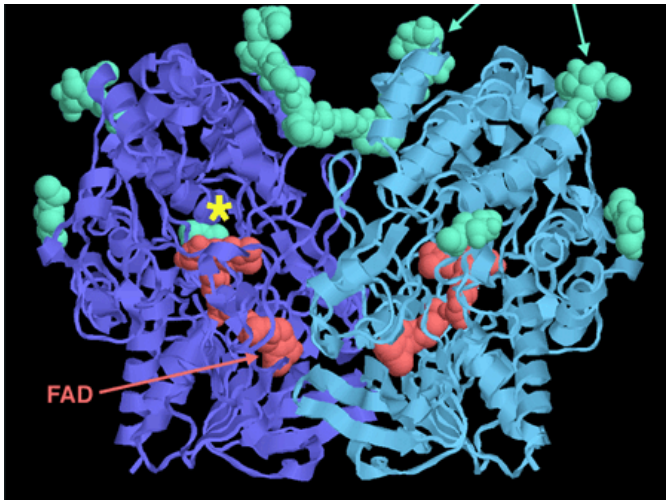

Fig. 5.12 Crystal structure of Glucose Oxidase with FAD as chromophore bound

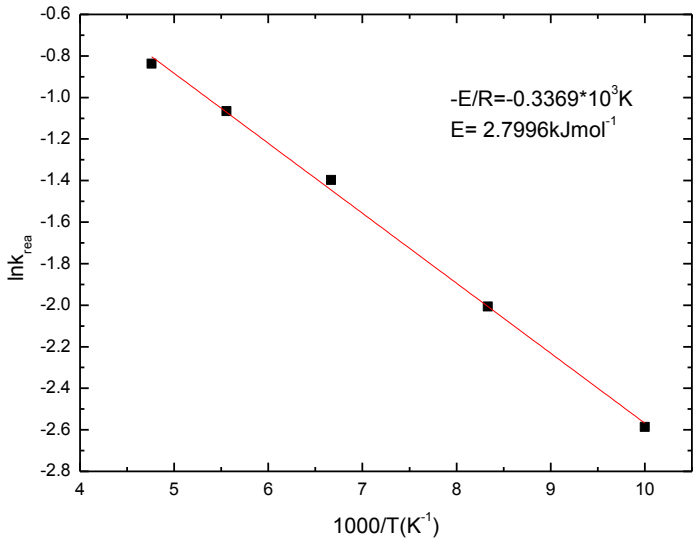

Fig. 5.13 Arrhenius analysis of GOx oxidized in low temperature range

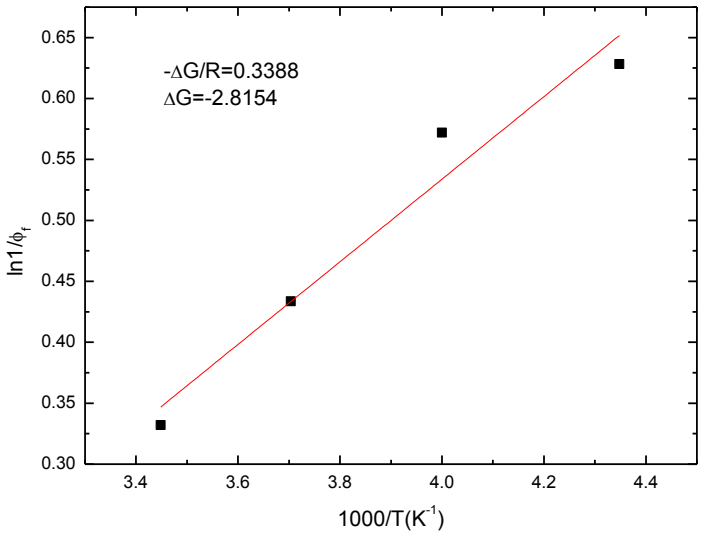

Fig. 5.14 $\ln\frac{1}{\phi_f}$ against temperature change of GOx in high temperature range

To check this result, we measured the fluorescence for a series of FAD and GOx samples dissolved in different solvents with the same concentration. As we show in Fig. 5.15 and 5.16, the UV spectra of GOx samples look very similar to FAD (shown in Fig. 5.15). In the emission spectra, the GOx dissolved in water is only weakly fluorescent (Blue line), but when the solvent was 50:50 ethylene glycol/water the sample became more fluorescent (Green line) though still less than the free FAD (Red line).

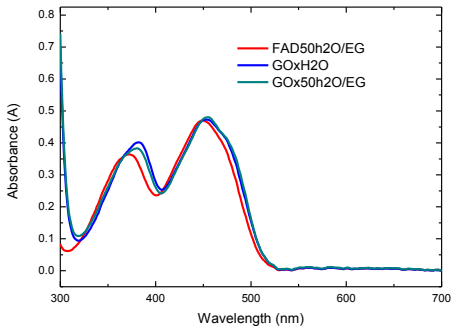

Fig. 5.15 UV-Visible spectra of GOx samples

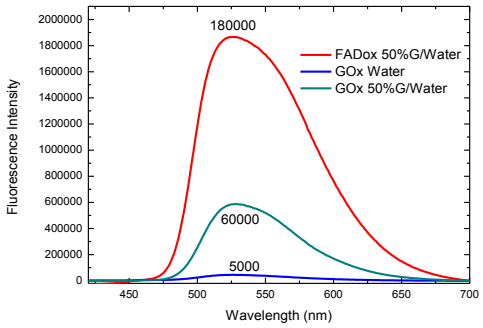

Fig. 5.16 Fluorescence emission spectra of GOx samples

According to those findings, we can conclude that ethylene glycol causes the release of a fraction of the FAD from GOx which makes the sample more fluorescent. GOx itself is essentially non fluorescent, due to the electron transfer quenching reaction described in Chapter 4. The 50% ethylene glycol is estimated to release about 1/3 FAD to become 'Free' FAD in GOx (i.e. the emission intensity of GOx sample dissolved in EG/Water solvent is about one third of the same concentration of FAD dissolved in the same solvent). Thus, what we measured here was actually the temperature dependence of 'released' FAD molecules. The present results suggest the protein-FAD interaction was disturbed by the solvent, even though FAD is quite well buried within the protein structure [17].

5.3.2 Low temperature fluorescence of methylated FAD & FMN radicals and $FADH^{\bullet}$ in GOx

The radical states of FAD and FMN were prepared to compare the data for radical samples in solution with that seen in the protein, to probe the possibility of electron transfer in the protein to form the radical state. This was discussed in Chapter 4. Here we extend these studies to characterise the temperature dependence of the radical states, which are actually the ground state in some flavoproteins [18, 19].

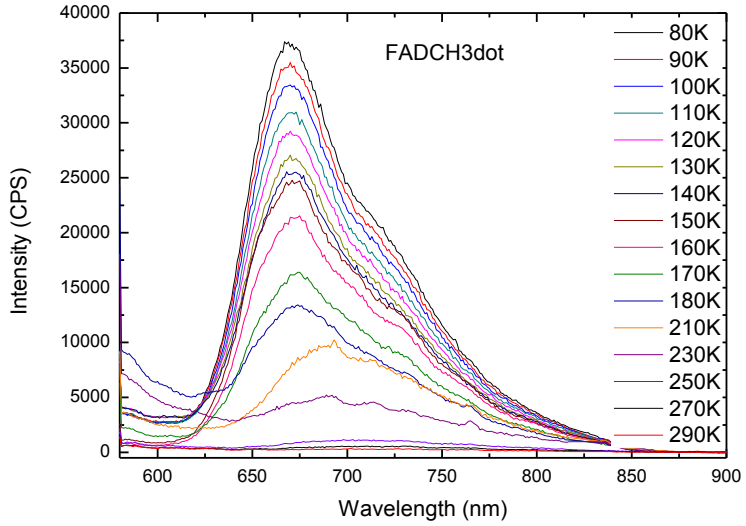

Fig. 5.17 Temperature dependent fluorescence emission spectra of methylated FAD radical in H_2O/EG mixed solvent

Fig. 5.17 shows the temperature dependent fluorescence for the sample of the methylated FAD radical in 50:50 water/ethylene glycol solvent. The sample was excited at 520 nm, and it fluoresced only very weakly at room temperature, consistent with a short lifetime and low oscillator strength (discussed in Chapter 4). However, the radical sample does become much more fluorescent at low temperature. The fluorescence emission intensity increased monotonically from ambient temperature 290 K down to 80 K. As was also seen for oxidised FAD the spectrum shifts to the blue and develops weak vibronic structure as the temperature decreased.

Fig. 5.18 shows the data of FAD methylated radical spectra fitted to the Arrhenius equation, equations 4 and 5. Interestingly, we again found that the data are best described by two Arrhenius plots with a transition between 160 K and 150 K. Above that (160 K to 296 K) the activation energy was calculated as 15.8±0.72 $kJmol^{-1}$, below (150 K to 80 K) it was calculated as 4.46±0.16 $kJmol^{-1}$. The glass transition temperature for the 50/50 ethylene/water system is 155 K, which correlates with the slope change in the data.

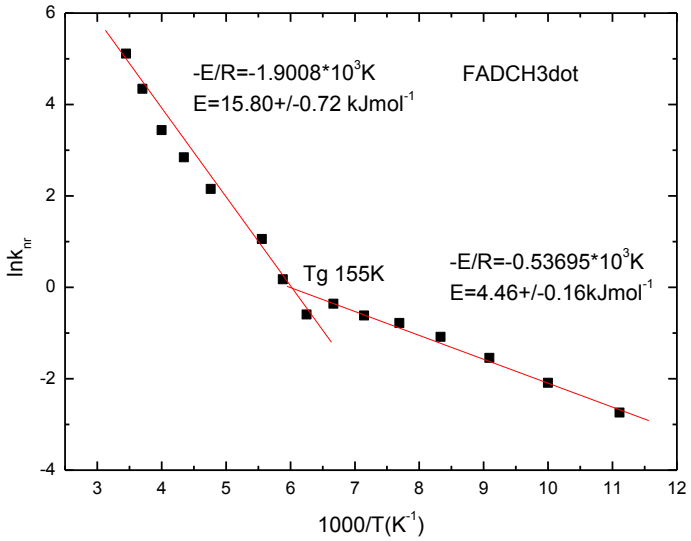

Fig. 5.18 Arrhenius analysis of methylated FAD radical

Fig. 5.19 shows the mean frequency of each spectrum against the temperature decrease. Because the radical sample is weakly fluorescent at high temperature and the emission band is very broad it is difficult to calculate the mean frequency very precisely, especially in the cryostat there is some solvent scattered/Raman signal on the blue edge of the spectrum. Thus in this case only the low temperature data are shown. As can be seen, the methylated FAD radical sample experienced an emission blue shift along with the temperature decrease which was also observed in the case of oxidized FAD (Fig. 5.4), the reason of that is the solvation effect as discussed for the case of FAD_{ox}.

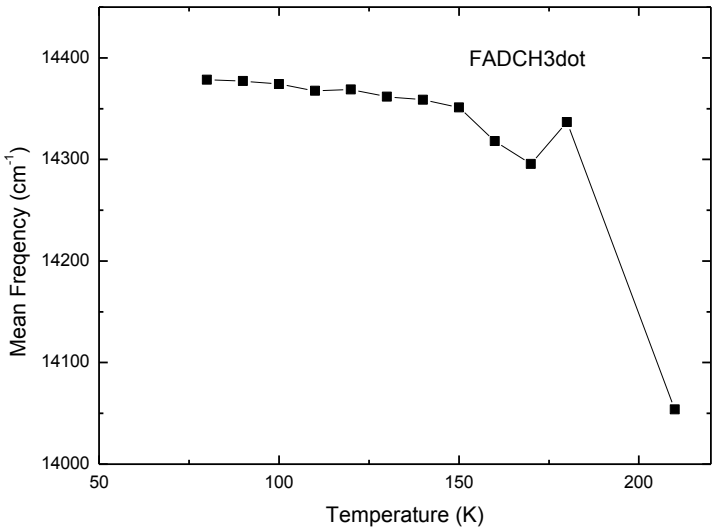

Fig. 5.19 Mean frequencies against T for methylated FAD radical

We now turn to investigate the temperature dependence of the radical state of FAD in the protein GOx. In principle we might be expected to meet the same problem as described above for the oxidised FAD. However, we established that the radical state of FAD is not stable in the EG: H_2O solvent so would revert to the oxidised form. This form is not excited by the excitation wavelength used (520 nm). Thus the data measured here refer to the steady state population of protein bound radical states, although the protein itself may be perturbed by the solvent. We assume that the FAD does not rebind to GOx at low temperature.

In Fig. 5.20 and 5.21, the temperature dependent fluorescence emission spectra of FAD radical state in GOx and the corresponding Arrhenius analysis are shown. The FAD radical GOx sample was excited at 520 nm. The intensity increases as the temperature decreases. The spectra blue shift and narrow appreciably as the intensity increases at low temperature. Again the Arrhenius plot is nonlinear but well fit by two processes at low and high temperature. The activation energy was calculated as 13.68±0.78 $kJmol^{-1}$ and 5.43±0.16 $kJmole^{-1}$ for high and low temperature respectively. Again the transition temperature point was found at T_g 155 K.

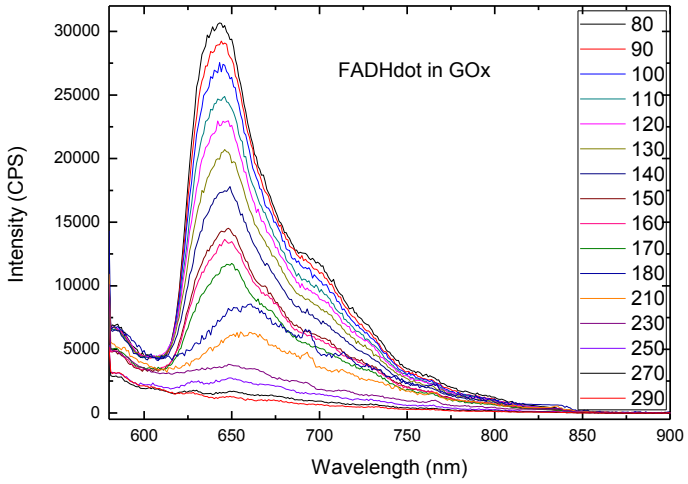

Fig. 5.20 Temperature dependent fluorescence emission spectra of FADH radical in GOx

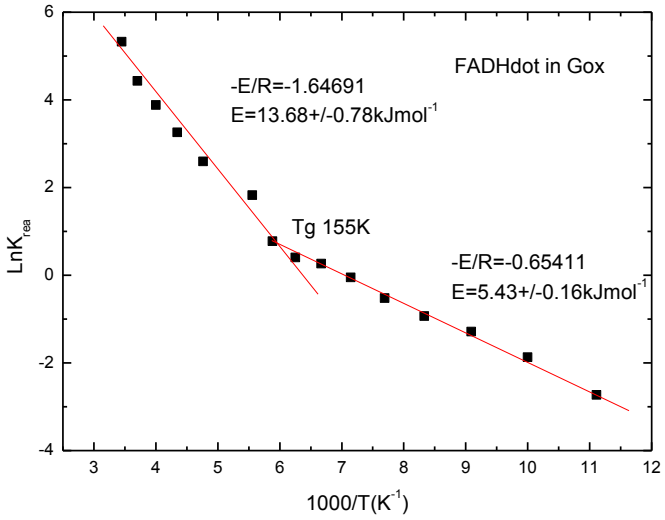

Fig. 5.21 Arrhenius analysis of FADH radical in GOx

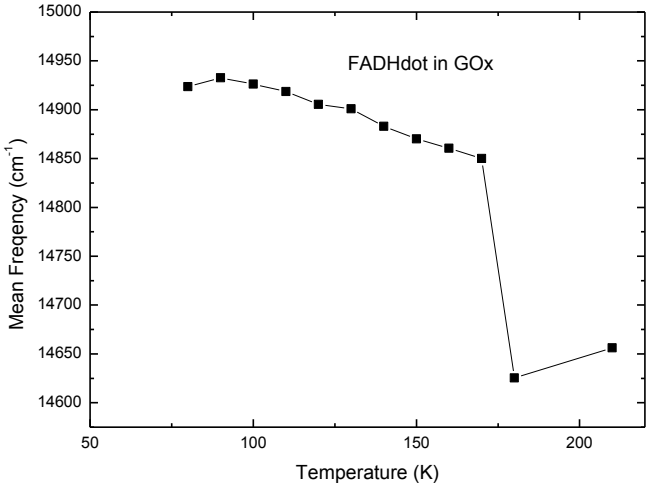

Fig. 5.22 Mean frequencies against *T* for FADH radical in GOx

In Fig. 5.22, the mean frequency value is plotted against the temperature decrease for FADH radical in GOx. The FAD radical in GOx also showed an emission band blue shift in low temperature which is very similar to the FAD methylated radical sample. For completeness, these measurements were extended to the synthetic methylated FMN radical.

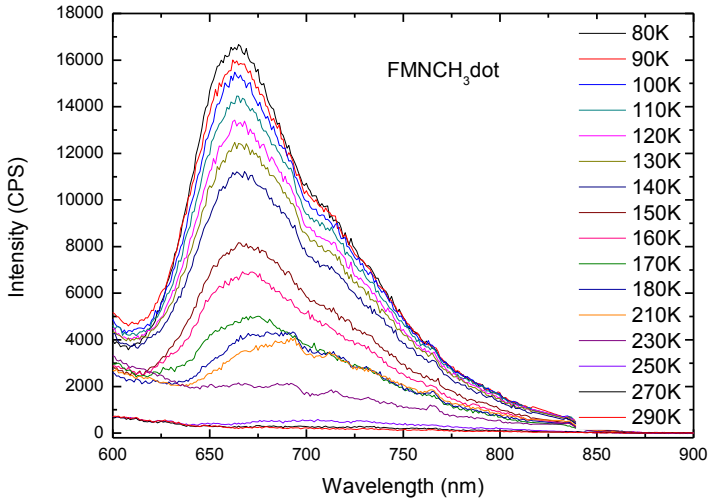

Fig. 5.23 Temperature dependent fluorescence emission spectra of methylated FMN radical

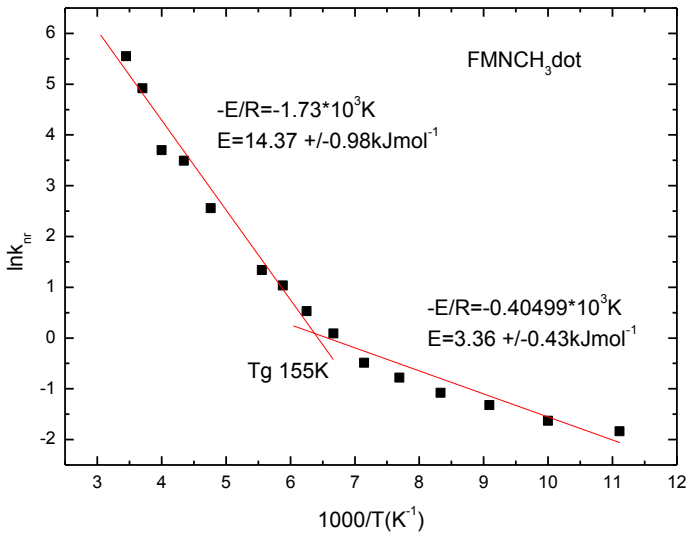

Fig. 5.24 Arrhenius analysis of methylated FMN radical

The FMN radical data are shown in Fig. 5.23 and 5.24. The activation energy was calculated as 14.37±0.98 kJ mol^{-1} for high temperature; and 3.36±0.43 kJ $mole^{-1}$ for low

temperature. The break point was at the T_g temperature 155 K, just as in the above two radical cases.

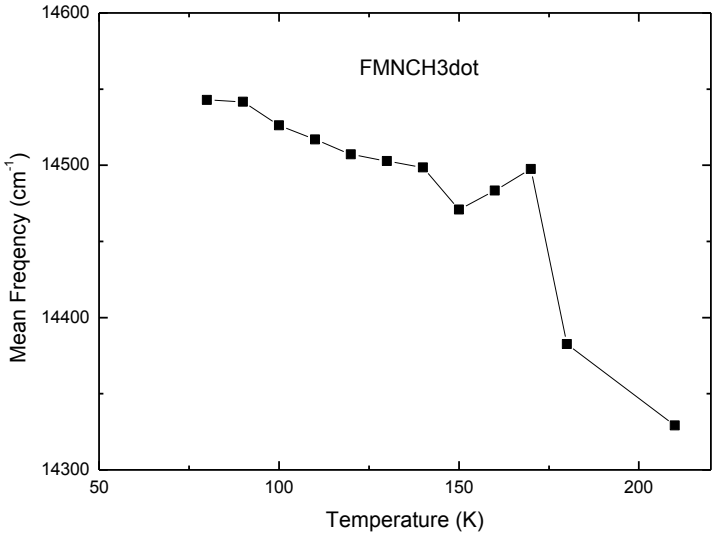

Fig. 5.25 Mean frequencies against *T* for methylated FMN radical

Fig. 5.25 shows the mean frequency value of each spectrum against the temperature decrease for the methylated FMN radical sample. As we see, the methylated FMN radical also has an emission band blue shift in the low temperature range which is very similar to the previous two examples. Essentially the radical FMN and FAD states behave in an identical fashion. The series of observations for each different radical state are summarized in table 5.1.

	Low T ($kJmol^{-1}$)	High T ($kJmol^{-1}$)	λ_{Ex}	λ_{Em}
$FAD(CH_3)^{\bullet}$	4.46±0.16	15.8±0.72	520 nm	680 nm
$FMN(CH_3)^{\bullet}$	3.36±0.43	14.37±0.98	520 nm	680 nm
$FADH^{\bullet}$ in GOx	5.43±0.16	13.68±0.78	520 nm	650 nm

Table 5.1. Summary of activation energy of methylated FAD and FMN radicals as well as $FADH^{\bullet}$ in GOx

In summary, all the radical states (methylated in solution, protonated in protein), do not fluorescence strongly at room temperature, where radiationless decay dominates. However, as the temperature decreases the emission yield increased markedly (more than 10 times, Fig. 5.17, 5.20 and 5.23), with the increase being accompanied by a blue shift. According to the data shown in table 5.1, the radical decay mechanism has significantly higher activation energy at high temperature than low temperature. One possible explanation is that there are two channels involved in these high and low temperature ranges, within each channel the pre-exponential constant A from Equation 1 and 2 (the intercept value from Arrhenius fitting, Fig. 5.18, 5.21 and 5.24) is higher in high temperature, so the k_{nr} is higher in high temperature, which derives a higher activation E_a from equation 1 or 2 as we observed from the data shown in table 5.1.

5.3.3 Excited State Dynamics of flavin radicals dissolved in water/ethylene glycol mixed solvent

As an extension, the time resolved IR data of different radicals, dissolved in solvents with different volume percentage of ethylene glycol were studied. This allows us to manipulate the viscosity of the medium. Fig. 5.26 shows the TRIR data of the radicals made in either solution (methylated FAD) or protein ($FADH^{\bullet}$). As we see, there is a remarkable transient band in each case peaked at 1549 cm^{-1} and 1568 cm^{-1} respectively. This positive transient indicates an excited state band, so can be used to monitor the excited state decay. A series of measurements with different percentage of EG were made. The spectra were independent of the solvent content and the same as the spectrum of each radical state shown in Fig. 5.26. The transient band was fit to find the kinetics as a function of the viscosity.

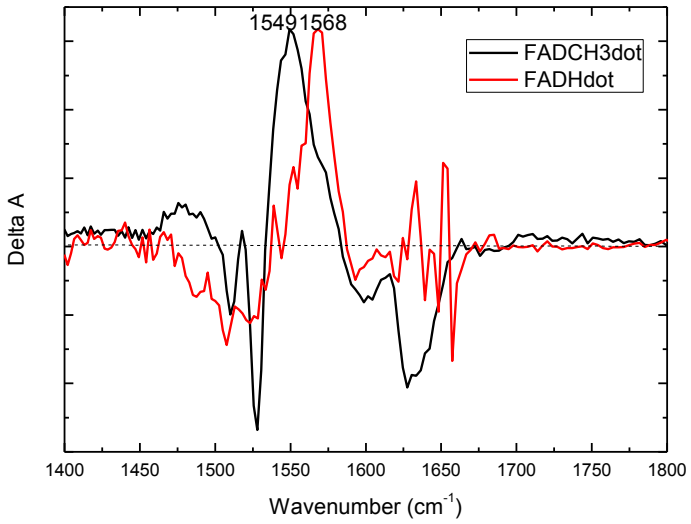

Fig. 5.26 TRIR spectra of $FADCH_3^{\bullet}$ and $FADH^{\bullet}$ in GOx

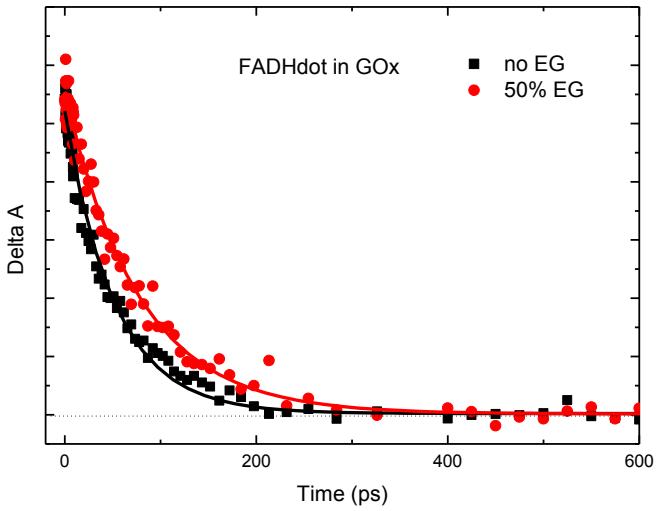

Fig. 5.27 Decay fittings of the transient bands at 1568 cm^{-1} of $FADH^{\bullet}$ in GOx samples

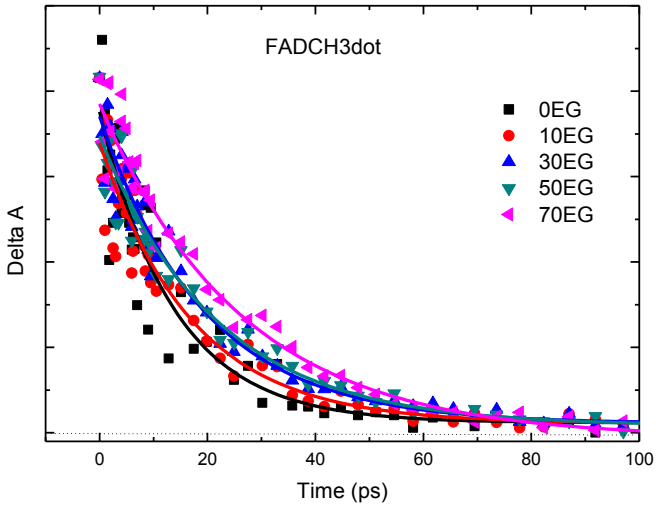

Fig. 5.28 Decay fitting of the transient bands at 1549 cm^{-1} $FADCH_3^{\bullet}$ sample dissolved in solvent with different EG%

Fig. 5.27 and 5.28 show the fitted data at the transient band of each radical state: 1568 cm^{-1} for $FADH^{\bullet}$ GOx and 1549 cm^{-1} for $FADCH_3^{\bullet}$. The data are tabulated in Table 5.2: in the case of $FADH^{\bullet}$ GOx sample, the one dissolved in 50 EG% has a longer relaxation time of 76ps than the one dissolved in pure water (51ps). This indicates that the solvent perturbs the protein matrix, as was found for FAD in GOx above. In the case of $FADCH_3^{\bullet}$ samples, the relaxation time becomes systematically longer when the EG% is increased; those values for the samples dissolved in pure water are consistent with the data presented in Chapter 4.

	$FADH^{\bullet}$ (GOx) 0%EG/D2O	$FADH^{\bullet}$ (GOx) 50%EG/D2O	$FADCH_3^{\bullet}$ 0%EG/D2O	$FADCH_3^{\bullet}$ in 10%EG/D2O	$FADCH_3^{\bullet}$ in 30%EG/D2O	$FADCH_3^{\bullet}$ in 50%EG/D2O	$FADCH_3^{\bullet}$ in 70%EG/D2O
τ	51±3.4ps	76±4.2 ps	14±1.9 ps	17±2.1 ps	21±1.8 ps	22±2.1 ps	25±2.6 ps

Table 5.2. Summary of relaxation time of methylated FAD as well as $FADH^{\bullet}$ in GOx

The relaxation time for the radical state increases as % EG increases. Two explanations are possible. First is because as the viscosity increases it slows the decay. This also seems

consistent with the observed *T* dependent data, since viscosity increases with decreasing temperature. Alternatively the open/closed conformation change is solvent dependent and has some influence on the radical kinetics, as it was shown to do for the oxidized state.

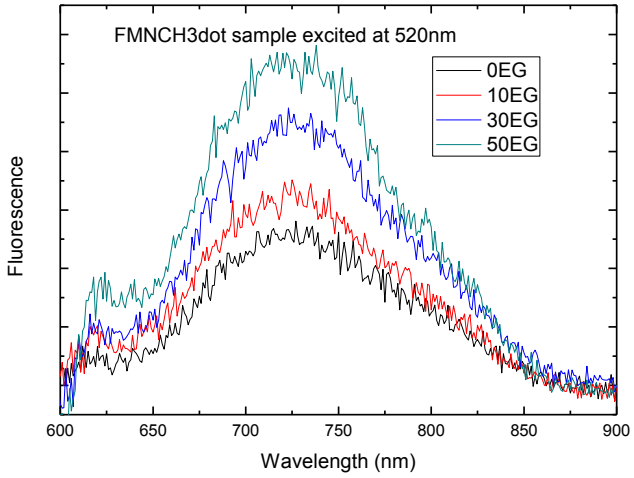

Fig. 5.29 EG% dependent steady-state fluorescence emission of FMN methyl radical

In Fig. 5.29 the steady-state fluorescence emission for FMN methylated radicals are shown as a function of percentage of EG in the solvent. As we see from the spectra, there is an intensity increase as the EG% increases. As the FMN has no adenine group the intensity increase has no relationship with the 'Open/closed conformation change. Then the increase of fluorescence can be assigned to a viscosity increase induced by adding more EG into the solvent system. This suggests that radiationless decay is reduced at higher viscosities. The mechanism here is quite similar to the 'cooling down' process that results in a fluorescence intensity increase.

5.3.4 Low temperature fluorescence measurements of fully reduced $FADH_2$ and $FADH^-$

In Chapter 3, we discussed the electronic and vibrational spectroscopy of fully reduced $FADH_2$ and $FADH^-$ revealed by ultrafast transient mid IR to visible spectroscopy. As an extension of that, we will describe the temperature dependent fluorescence measurements

of these two fully reduced states in the water/ethylene glycol 50:50 mixed solvent. The sample preparation details were introduced in section 2.1.1.

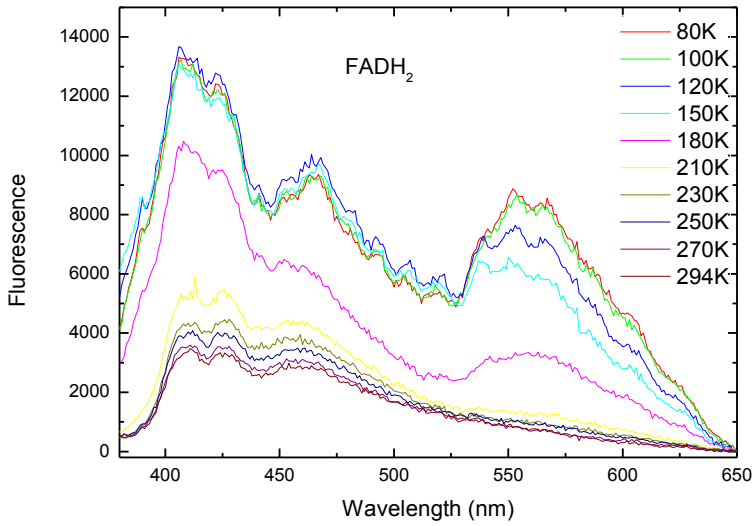

Fig. 5.30 Temperature dependent fluorescence emission spectra of $FADH_2$ dissolved in H_2O/EG mixed solvent (Raw data)

In Fig. 5.30, the raw spectra of low temperature fluorescence measurements of one of the fully reduced states, $FADH_2$, are shown. As can be seen from the data, as the temperature decreases, the intensity increases. However, qualitatively the intensity increase is much lower than was seen for the radical and oxidized states. Quantitatively the total integrated emission intensity increased by four times between room temperature and 80 K. It is also obvious that there are multiple contributions to these spectra, especially at low temperature. However it is also apparent that not every component in the spectrum behaves in the same way as temperature is decreased.

From left to right, the first two bands at 410 nm and 430 nm were shown to be Raman bands, by comparison with the mixed solvent in the absence of a chromophore (as shown by the red spectrum in Fig. 5.31). The increase with decreasing temperature is unexpected for Stokes Raman. Increasing solvent density at lower temperature may contribute to the observed increase, but it is possible that there is an underlying emission band around

420 nm which also increases with decreasing temperature. The band at 460 nm is probably the reduced sample emission band (as was shown in Fig. 3.2 of Chapter 3). We already know that both FAD oxidized and FADH• radical spectra blue shift at lower temperature, so the emission underlying the Raman may also be from the reduced state. Finally a band at 560 nm only appeared at low temperature.

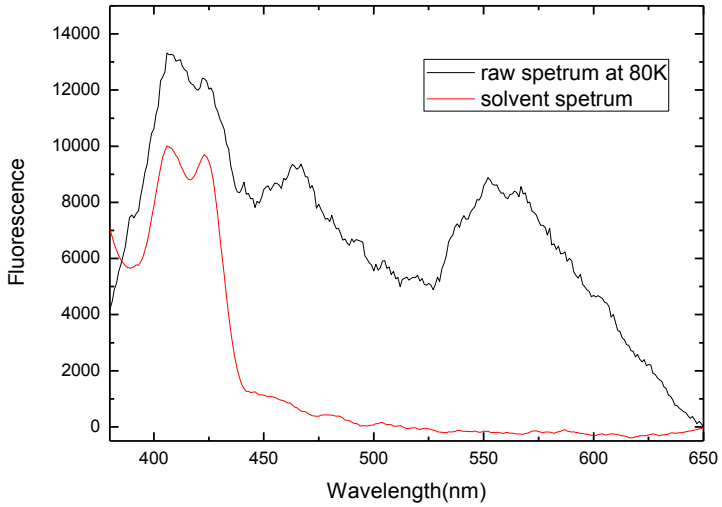

Fig. 5.31 Subtraction example of $FADH_2$ raw data from blank solvent spectrum

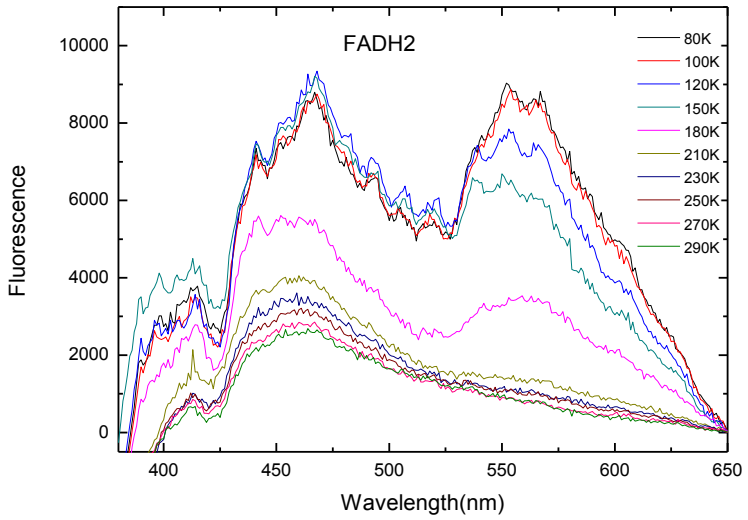

Fig. 5.32 Temperature dependent fluorescence emission spectra of $FADH_2$ (Processed data, solvent spectrum subtracted)

In an attempt to isolate the $FADH_2$ spectrum from Raman, a subtraction was done. The blank solvent spectrum is shown in Fig. 5.31, the processed (subtracted) data are show in Fig. 5.32. Although the subtraction is not very successful, probably because of the difficulty in normalising the two data sets, the spectra do approximately separate into a weakly *T* dependent reduced flavin band at 480 nm and the unknown low temperature band at 560 nm, One possible assignment for the long wavelength low temperature band is phosphorescence. However, Jorns *et al* [20] found the $FADH_2$ had phosphorescence at low temperature which peaked at 442 nm when sample was dissolved in pure water. That is rather far from 560 nm seen here, although it is possible that the band shown in our spectra at low temperature is also the phosphorescence, but red shifted due to differences in the solvent. Further resolution of this very complex spectrum will require time resolved experiments, with a slow decay being expected for phosphorescence.

The band at 480 nm is assigned to the reduced flavin fluorescence which is only slightly temperature dependent (allowing for density decreases and the underlying contribution of the 560 nm band). This weak dependence is in contrast to a proposal that the $FADH_2$ molecule should be strongly temperature dependent [3]. It is known that $FADH_2$ has a

bent ground state structure as shown in Fig. 5.33. It was suggested that the radiationless decay might involve the 'butterfly' motion in which the ring 1 and ring 3 wag about the axis of ring 2, just like a butterfly's flying. It was proposed that this can act as a coordinate promoting radiationless decay. Specifically a conical intersection between S_0 and S_1 was supposed to be accessed along this coordinate, inducing the quenching. However, it is expected that such a large scale intramolecular reorganisation as the butterfly motion would be suppressed when the solvent is cooed to the glass state. Thus the fluorescence intensity should go up steeply with decreasing temperature. However in our case we found that the intensity increase is only weak, suggesting that the radiationless decay pathway is not as proposed.

Fig. 5.33 Bent structure and proposed butterfly motion of reduced flavin

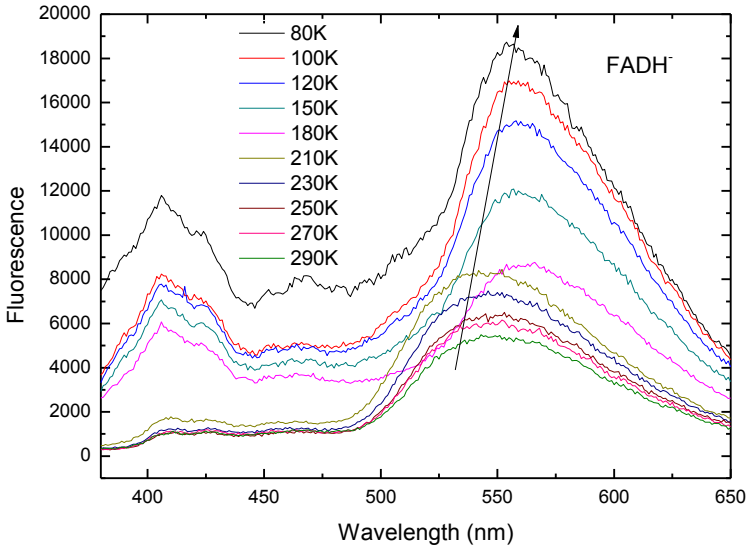

Fig. 5.34 Temperature dependent fluorescence emission spectra of $FADH^-$

Finally in this chapter we describe the data of another fully reduced flavin $FADH^-$, which also has the bent structure and is thus a potential candidate for 'butterfly motion' promoted radiationless decay. According to the observed spectra (Fig. 5.34), the fluorescence intensity at 455 nm does not increase very strongly at low temperatures, which is the same result as reported above for $FADH_2$. In addition we found a broad band peaked at 560 nm for both low and high temperature range. Its intensity was somewhat temperature dependent, but its presence in fluid media seems to rule out phosphorescence. We tried a series of measurements on $FADH^-$ samples with different concentrations to investigate the possibility of a dimerization or exciplex emission. No concentration dependence was found. We also checked for emission from impurities or reaction products of the reducing agent (dithionite), but none were found. These measurements were extended to study different volume percentages of ethylene glycol in solvent. In each case the 560 nm band persists whenever $FADH^-$ is formed. Thus the assignment of this band is not clear at this stage, other than it is formed along with $FADH^-$. However, once again no strong temperature dependence was resolved for this fully reduced state, seemingly in disagreement with the proposed butterfly mode promoted radiationless decay.

5.4 Conclusion

This chapter reports the studies of low temperature fluorescence measurements of flavin in its oxidised, radical and fully reduced states. For oxidised and radical states, we observed an emission intensity increase as temperature decreased, which is from the decreasing of non-radiative relaxation rate. The Arrhenius equation was applied to analyse the data further and derive the activation energy for the different redox states. Two activated processes were found, and qualitiatively ascribed to different processes accessed under different circumstances. The fully reduced samples do not experience a strongly temperature dependent fluorescence. The viscosity dependent time resolved infra-red measurements revealed a slow decay for the radical states as we increased the viscosity of the solvent system.

References

[1] van der Horst, M. A. and Hellingwerf, K. J. (2004) *Accounts of Chemistry Research 37*, 13-20.

[2] Gressel, J. (1979) *Photochemistry and Photobiology 30 (3)*, 749–754.

[3] Kao, Y. T., Saxena, C., He, T. F., Guo, L. J., Wang, L. J., Sancar, A. and Zhong, D. P. (2008) *Journal of the American Chemical Society 130*, 13132-13139.

[4] Presiado, I. and Huppert, D. (2009) *Journal of Physical Chemistry C 113 (9)*, 3835–3843.

[5] Song, P. S. (1970) *Israel Academy of Sciences and Humanities: Jerusalem, 358*.

[6] Leijonmarck, M. (1977) *Chemical Communications 8*, 1-70.

[7] Hall, L. H., Orchard, B. J. and Tripathy, S. K. (1987) *International Journal of Quantum Chemistry 31*, 217-242.

[8] Weber, G. (1950) *Biochemical Journal 47*, 114-121.

[9] Spencer, R. D. and Weber, G. (1972) *Structure and Function of Oxidation Reduction Enzymes*, Pergamon Press: Oxford, 393-399.

[10] Gomelsky M, K.G.(2002) *Trends in Biochemical Sciences 27(10)*, 497-500.

[11] Connors, K. (1990) *Chemical Kinetics: The Study of Reaction Rates in Solution*, Wiley-VCH.

[12] Lachlan, R.F. (2007) *Luscinia: a bioacoustics analysis computer program*. Version 1.0 [Computer program]. Retrieved from www.lusciniasound.org.

[13] Eisenberg, A. S., Schelvis, J. P. M. (2008) *Journal of Physical Chemistry A 112*, 6179-6189.

[14] Mayer, D. and Rebsdat, S. (2002) *Ethylene Glycol In Ullmann's Encyclopedia of Industrial Chemistry*, 6th ed, Wiley-VCH.

[15] Bagchi, B., Fleming, G.R. and Oxtoby, D.W. (1983) *Journal of Chemical Physics 78*,7375–7385.

[16] Li, G. F. and Glusac, K. D. (2009) *Journal of Physical Chemistry B 113(27)*, 9059-9061.

[17] Newman, J. D. and Turner A. P. F. (2005) *Biosensors and Bioelectronics 20*, 2435-2453.

[18] Massey, V. (2000) *Biochemical Society Transactions 28(4)*, 283-296.

[19] Theorell, H. (1935) *Biochemische Zeitschrift 275*, 344-346.

[20] Chanderkar, L. P and Jorns, M. S. (1991) *Biochemistry 30*, 745-754.

Chapter 6 Conclusion and Future Perspective

6.1 Conclusion

For understanding the BLUF domain photocycle, we characterized the different flavin intermediates in solution also in protein for radical states. A series of steady-state UV-Vis, fluorescence and Infra-red measurements as well as the time resolved UV-Vis and Infra-red measurements were attempted. Low temperature fluorescence measurements were carried out with the cryostat for all the different redox states. From which we found that:

● The oxidized FAD and FMN exhibit temperature dependent fluorescence, which in case of FAD, there was a Open/Closed conformation change during the cooling down process, while they both show a significant intensity increase as temperature decrease which can be referred to the mechanism of decreasing non-radiative relaxation rate.

● Both the two fully reduced forms of FAD ($FADH^-$ and $FADH_2$) have excited state decay times on the tens of picoseconds timescale obtained from their transient IR and electronic spectra. Measurements of the ground state recovery show that the mechanism of radiationless decay is internal conversion. There is a short lived bottleneck in the ground state recovery cycle, possibly a vibrationally hot state of the ground state. The protonated form $FADH_2$ has a faster excited state decay than $FADH^-$. The latter exhibits an unexpected inverse deuterium isotope effect. Neither of them show a strong temperature dependent florescence.

● The photophysical properties of N5-methyl FAD and N5-methyl FMN radicals in solution were characterized by means of steady state and ultrafast transient visible and infrared spectroscopy. The bleach transitions were assigned with the aid of DFT calculations. The transient infrared spectra of flavodoxin and GOX were also measured when the flavin cofactor was in its neutral radical state ($FADH^{\bullet}$). It was found that the decay kinetics are a sensitive function of the protein binding site, a fact that could be ascribed to electron transfer quenching reactions and environment dependent suppression

of internal conversion. All of the radical states show a significant temperature dependent fluorescence: intensity increases as temperature decreases.

●Based on the measurements of AppA BLUF domain protein, there was no radical state formation observed thus we did not see any evidence to support the BLUF photocycle proposal (Fig. 1.2). However we did find the radicals formed for the flavoprotein GOx when excited along with the electron transfer and proton transfer between flavin and relative residual protein molecules.

6.2 Future Perspective

Further TRIR experiments on AppA and its mutants are needed. At this stage, the infra-red spectra of the flavin and their different redox states have been thoroughly analyzed and the vibrations assigned. Those information can be utilized to assign the BLUF photocycle, especially the radical state intermediates. We can also include Raman spectroscopy to further investigate the atoms which are important in any given flavoprotein system. Studies of flavin systems with Raman spectroscopy would be interesting.

The transient UV to mid IR spectroscopic analysis can be used for other flavin containing enzyme studies, such as cryptochromes or photolyase, whose exact function is not well understood. A spectroscopic study of these enzymes may reveal specific structural features and flavin-protein interactions which might be able to be used to elucidate their working mechanism.

Chapter 7 Publications and Conferences

7.1 Publications

[1] Zhao, R. K., Lukacs, A., Haigney, A., Brust, R., Greetham, G.M., Towrie, M., Tonge, P.J and Meech, S. R. (2011) *Physical Chemistry Chemical Physics 13*, 17642–17648.

[2] Zhao, R. K., Lukacs, A. and Meech, S. R. 'Low Temperature Property of Flavin Chromophore in Different Redox States Revealed by Fluorescence Measurement', *manuscript in preparation*

[3] Lukacs, A., Zhao R. K., Haigney, A., Brust, R., Greetham, G. M., Towrie, M., Tonge, P. J. and Meech, S. R. (2012) *Journal of Physical Chemistry B 116*, 5810−5818

[4] Lukacs, A., Zhao R. K., and Meech, S. R. (2012) 'Probing the Mechanism of Blue Light Sensing BLUF Domain Proteins: A Study through Transient Infra-red Spectroscopy, Isotope Editing and Mutagenesis'

http://www.clf.stfc.ac.uk/resources/PDF/ar10-11_full_biology.pdf

[5] Haigney, A., Zhao R. K., and Meech, S. R. (2011) 'Time Resolved Infrared Analysis of $AppA_{BLUF}$ using Isotopic Labelling at Mutant Studies' *http://www.clf.rl.ac.uk/resources/PDF/ar09-10_lsf_full_chemistry.pdf*

[6] Haigney, A., Lukacs, A., Zhao, R. K., Stelling, A. L., Brust, R., Kim, R. R., Kondo, M., Clark, I., Towrie, M., Greetham, G. M., Illarionov, B., Bacher, A., Romisch-Margl, W., Fischer, M., Meech, S. R. and Tonge, P. J. (2011) *Biochemistry 50*, 1321-1328.

[7] Lukacs, A., Haigney, A., Brust, R., Zhao, R. K., Stelling, A. L., Clark, I., Towrie, M., Greetham, G. M., Meech, S. R. and Tonge, P. J. (2011) *Journal of the American Chemical Society 133 (42),* 16893–16900.

7.2 Conferences and Presentations

[1] 1st May 2009, School of Chemistry and Pharmacy research colloquium, *School of Chemistry, UEA* Presentation 'Photochemistry and photophysics of BLUF domain proteins'

[2] 27th June 2010, Chemistry Research day, *School of Chemistry, UEA*

Poster 'Ultrafast Vibrational Spectroscopy of the Flavin Chromophore in H_2O/D_2O'

[3] 14th July 2010, Physical Chemistry Research Day, *School of Chemistry, UEA*

Presentation 'Ultrafast Vibrational Spectroscopy of the Flavin Chromophore'

[4] 10th-15th July 2011, FEMTO-10 Madrid Conference, *Madrid, SPAIN*

Poster 'Ultrafast Vibrational Spectroscopy of Flavin Chromophore in different redox states'

[5] 14th -16th Dec 2011, Ultrafast Chemical Physics (UCP 2011), *University of Strathclyde, Glasgow*, Poster 'Excited State Dynamics and Low Temperature Property of Flavin Radical Revealed by Ultrafast Transient Mid IR and Fluorescence Spectroscopy'